

Disturbance Attenuation in Mass Chains with Passive Interconnection



Kaoru Yamamoto

Department of Engineering

University of Cambridge

This dissertation is submitted for the degree of
Doctor of Philosophy

Gonville and Caius College

August 2015

(Revised October 2015)

DECLARATION

I hereby declare that except where specific reference is made to the work of others, the contents of this dissertation are original and have not been submitted in whole or in part for consideration for any other degree or qualification in this, or any other university. This dissertation is my own work and contains nothing which is the outcome of work done in collaboration with others, except as specified in the text and Acknowledgements. This dissertation contains fewer than 65,000 words including appendices, bibliography, footnotes, tables and equations and has fewer than 150 figures.

Kaoru Yamamoto

August 2015

(Revised October 2015)

ACKNOWLEDGEMENTS

First of all, I would like to express my sincere gratitude to my supervisor, Professor Malcolm C. Smith, for his support and guidance during my years of research in Cambridge. I have been very lucky to have a supervisor who has immense knowledge and great passion for science and who cared so much about my work. It has been an honour to work with him as his student.

I would also like to thank my thesis examiners, Dr. Glenn Vinnicombe and Professor Alessandro Astolfi for their insightful suggestions and comments. It has been my pleasure to have had an opportunity to discuss my work and learn from them.

Completing this dissertation would not have been possible without the financial support from the Funai Foundation for Information Technology. I am extremely privileged to be a recipient of their scholarship.

My gratitude also goes to the member of the Control Group for providing a stimulating research environment and to my fellow students and my housemates for their friendship and company. A special thanks goes to Richard Pates for his insightful advice on my work, our fruitful discussions, and his continued support and encouragement. I would also like to thank his family, especially Alan and Ruth, for always welcoming me and making me feel at home while far away from home.

Most of all, I would like to thank my father, mother, brother and grandmother for caring me all the time and being always supportive. Their unconditional love and support have encouraged me throughout the last four years and I am deeply indebted to them.

ABSTRACT

DISTURBANCE ATTENUATION IN MASS CHAINS WITH PASSIVE INTER-CONNECTION

This thesis is concerned with disturbance amplification in interconnected systems which may consist of a large number of elements. The main focus is on passive control of a chain of interconnected masses where a single point is subject to an external disturbance. The problem arises in the design of multi-storey buildings subjected to earthquake disturbances, but applies in other situations such as bidirectional control of vehicle platoons. It is shown that the scalar transfer functions from the disturbance to a given intermass displacement can be represented as a complex iterative map. This description is used to establish uniform boundedness of the \mathcal{H}_∞ -norm of these transfer functions for certain choices of interconnection impedance. A graphical method for selecting an impedance such that the \mathcal{H}_∞ -norm is no greater than a prescribed value for an arbitrary length of the mass chain is given. A design methodology for a fixed length of the mass chain is also provided. A case study for a 10-storey building model demonstrates the validity of this method.

Kaoru Yamamoto

TABLE OF CONTENTS

Table of contents	ix
List of figures	xi
List of tables	xv
Nomenclature	xix
1 Introduction	1
1.1 Outline	2
2 Background	5
2.1 Overview of Passive Mechanical Networks	5
2.1.1 Multi-port networks	5
2.1.2 Passive mechanical networks and mechanical elements	6
2.2 Overview of Vibration Control in Buildings	8
2.2.1 Basic principles and classification of control systems	8
2.2.2 Passive vibration control devices	10
2.2.3 Characteristics of earthquake ground motions	12
2.3 Overview of Vehicle Platooning	15
2.3.1 Automated highway system	17
2.3.2 Vehicle platooning specification	17
2.3.3 Control schemes and string stability	18
3 Homogeneous Mass Chains with Passive Interconnection	21
3.1 Overview	21
3.2 A Lumped Mass System with Base Excitation	22
3.3 Problem Formulation	23
3.4 Stability of Passive Interconnection	25

3.5	Bidirectional Control in Vehicle Platoons	26
4	Recursive Features and Uniform Boundedness in Homogeneous Mass Chains	29
4.1	Overview	29
4.2	Möbius Transformation	30
4.3	Intermass Displacements	31
4.3.1	Convergence to Fixed Points	32
4.4	Bounds on Iterative Maps	35
4.4.1	Examples	36
Appendix 4.A	Proof of Theorem 4.1	42
Appendix 4.B	Proof of (4.10b) and (4.10d)	44
Appendix 4.C	Proof of (4.14)	45
Appendix 4.D	Proof of Theorem 4.5	45
5	Design of Passive Interconnection	51
5.1	Overview	51
5.2	Disturbance Rejection and Design Objectives	51
5.2.1	Graphical design method	52
5.2.2	Frequency content of ground displacements	53
5.3	Case Study	54
5.3.1	Multi-storey homogeneous building model	54
5.3.2	Interconnection design	56
5.3.3	Time response	57
5.3.4	Heterogeneous mass chain model	57
Appendix 5.A	Heterogeneous Mass Chains	66
Appendix 5.B	Recursions in Heterogeneous Mass Chains	67
6	Towards Exact Computation of Supremal Bounds and Conjectures	71
6.1	Introduction	71
6.2	Description of the Problem and Motivations	72
6.3	Possible Solution Paths	75
6.4	Conjectures on Higher Intermass Displacements	80
7	Conclusions	83
7.1	Contributions	83
7.2	Future Research Directions	84
	References	87

LIST OF FIGURES

2.1	A free-body diagram of a one-port (two-terminal) mechanical network. . . .	6
2.2	Typical configurations of interstorey-installment type control devices in a building frame.	9
2.3	Constitutive models of viscoelastic dampers.	11
2.4	Ground acceleration of historical earthquakes.	13
2.5	Fourier amplitude spectra of ground acceleration of historical earthquakes. NS represents North-South component and EW represents East-West component.	14
2.6	Frequency responses of Kanai-Tajimi filter W_{KT} and Clough-Penzien-Kanai-Tajimi filter $W_{CP}W_{KT}$ for rock or stiff soil conditions.	16
2.7	Platoon of N vehicles.	17
3.1	Multi-storey building models.	22
3.2	Chain of N masses m connected by a passive mechanical impedance $Z(s)$ (admittance $Y(s) = Z(s)^{-1}$), and connected to a movable point x_0	23
3.3	Platoon of N vehicles.	27
4.1	Contour plot of $ \zeta(h) $ where $h = g^{-1}$	37
4.2	Contour plot of $ \mu_+^{(1)}(h) $ where $h = g^{-1}$	38
4.3	Contour plot of $\max_N F_N^{(1)}(h) = \gamma$ for $\ln(\gamma) = 0, 0.2, 0.4, \dots$ where $h = g^{-1}$	38
4.4	Nyquist diagrams of $g(s) = Y(s)/(sm)$ for the vibration control devices in Table 4.1b and contour plot of $\max_i \max_N F_N^{(i)}(h) = \gamma$ for $\ln(\gamma) = 0, 0.2, 0.4, \dots$ where $h = g^{-1}$	40
4.5	$\max_i F_N^{(i)}(j\omega) $ using Device 2 for $N = 1, 20, 50, 100$	40
4.6	$\max_i F_N^{(i)}(j\omega) $ using Device 3 for $N = 1, 20, 50, 100$	41
4.7	Curves representing $\max_N F_N^{(i)}(h) = 1$ for $i = 1, 2, \dots, 5$ where $h = g^{-1}$	41
4.8	The ellipse defined by $h = \zeta + \zeta^{-1} - 2$ for $ \zeta $ fixed and $\arg(\zeta)$ varying.	46

5.1	Chain of N masses m connected by a passive mechanical impedance $Z(s)$ (admittance $Y(s) = Z(s)^{-1}$), and connected to a movable point x_0 . Each interconnection is depicted in (b) where its admittance $Y(s) = k_s/s + c_s + Y_a(s)$ ($Y_a(s) = Z_a(s)^{-1}$).	52
5.2	Contour plot of $\max_i F_{10}^{(i)}(h) $ where $h = g^{-1}$	53
5.3	A log-log plot of weighting functions $W(j\omega)$ for three different soil conditions: rock or stiff soil conditions, deep cohesionless soils and soft to medium clays and sands.	54
5.4	A log-log plot of $\max_i F_{10}^{(i)}(j\omega)W(j\omega) $ for the uncontrolled homogeneous building model, i.e., $Y_a(s) = 0$	55
5.5	Design of layout L1. The parameters are: $-- c = 1.12 \times 10^4$ kNs/m, $b = 0$ kg, $— c = 1.12 \times 10^4$ kNs/m, $b = 1.0 \times 10^6$ kg, $-\cdot-\cdot c = 1.12 \times 10^4$ kNs/m, $b = 5.0 \times 10^6$ kg. (a) Nyquist diagrams of $g(s) = (k_s/s + c_s + Y_a(s))/(sm)$ and the contour plot of $\max_i F_{10}^{(i)}(h) $. The black and white markers \bullet, \circ indicate $g(4j)$ and $g(10j)$. (b) A log-log plot of $\max_i F_{10}^{(i)}(j\omega)W(j\omega) $	58
5.6	Design of layout L2. The parameters are: $-- c = 1.12 \times 10^4$ kNs/m, $b = 1.0 \times 10^6$ kg, $k = 3.93 \times 10^4$ kN/m, $— c = 1.12 \times 10^4$ kNs/m, $b = 3.0 \times 10^6$ kg, $k = 1.18 \times 10^5$ kN/m, $-\cdot-\cdot c = 1.12 \times 10^4$ kNs/m, $b = 5.0 \times 10^6$ kg, $k = 1.97 \times 10^5$ kN/m. (a) Nyquist diagrams of $g(s) = (k_s/s + c_s + Y_a(s))/(sm)$ and the contour plot of $\max_i F_{10}^{(i)}(h) $. The black and white markers \bullet, \circ indicate $g(4.7j)$ and $g(10j)$. (b) A log-log plot of $\max_i F_{10}^{(i)}(j\omega)W(j\omega) $	59
5.7	The design of L1 – L4 in Table 5.2. The parameters are given in Table 5.3. (a) Nyquist diagrams of $g(s) = (k_s/s + c_s + Y_a(s))/(sm)$ and the contour plot of $\max_i F_{10}^{(i)}(h) $. (b) A log-log plot of $\max_i F_{10}^{(i)}(j\omega)W(j\omega) $ for the uncontrolled homogeneous building model of and the model controlled by the vibration control devices L1 – L4.	60
5.8	Time response of the first interstorey drift against JMA Kobe 1995 NS earthquake.	61
5.9	Maximum interstorey drifts against historical earthquakes for the uncontrolled homogeneous building model and the model controlled by the vibration control devices L1 – L4.	62
5.10	Chain of N masses m_i and a movable point x_0 with passive interconnections corresponding to the admittance $\frac{k_{si}}{s} + c_{si} + Y_{ai}(s)$	63

5.11	A log-log plot of $\max_i F_{10}^{(i)}(j\omega)W(j\omega) $ for the uncontrolled heterogenous building model and the model controlled by the vibration control devices L1 – L4.	64
5.12	Maximum interstorey drift against JMA Kobe 1995 NS earthquake for the uncontrolled heterogenous building model and the model controlled by the vibration control devices L1 – L4.	65
5.13	Feedback configuration of the system of Fig. 5.10.	67
5.14	Chain of N masses m_i connected by a passive mechanical impedance $Z_i(s)$ and connected to a movable point x_0	67
6.1	Chain of N masses m connected by a passive mechanical impedance $Z(s)$ (admittance $Y(s) = Z(s)^{-1}$), and connected to a movable point x_0	72
6.2	Nyquist diagram of $g(s) = (\sqrt{2}s+1)/s^2$ on a contour plot of $\max_N F_N^{(1)}(h) $ where $h = g^{-1}$	73
6.3	Nyquist diagrams of $F_N^{(1)}(j\omega)$ for $N = 1, 2, \dots, 100$ and a unit circle.	73
6.4	A mass-spring-damper system.	74
6.5	Values of $\sup_N \ F_N^{(1)}(s)\ _\infty$ with respect to the damping coefficient c in the system of Fig. 6.4.	74
6.6	The locus $\zeta(j\omega)$ where $h(s) = s^2/(\sqrt{2}s+1)$	77
6.7	A spiral ζ^p and its closest point to $(-1, 0)$	77
6.8	Values of the upper bound (6.4).	78
6.9	A log-log plot of $ F_N^{(1)}(j\omega) $ for $N = 1, 20, 50, 100$	78
6.10	A lower linear fractional transformation in Redheffer's lemma.	79
6.11	Frequency plot of the largest singular values of P defined in (6.5) with $P_{12} = P_{21} = 1/(h+1)$ where $h = s^2/(\sqrt{2}s+1)$	80

LIST OF TABLES

2.1	Parameters for the Kanai-Tajimi filter and the Clough-Penzien filter.	15
4.1	Interconnection layouts and their parameters.	39
5.1	Structural parameters of the homogeneous building model.	55
5.2	Interconnection configuration and corresponding admittance $Y_a(s)$	56
5.3	Parameters of vibration control devices.	57
5.4	Structural parameters of the heterogeneous building model.	64
6.1	Values of $\ F_{10}^{(i)}(h(s))\ _\infty$	81

NOMENCLATURE

Symbols

\square end of conjecture

\diamond end of definition

\blacksquare end of proof

\heartsuit end of remark

Constants, Variables & Functions

j the imaginary unit $\sqrt{-1}$

Y admittance

Z impedance

Operators

I_N $N \times N$ identity matrix

$|z|$ absolute value of z

$f \circ g$ the composition of f and g

$\det(A)$ determinant of A

\Leftrightarrow if and only if

\Rightarrow implies

\mapsto maps to

\in belongs to

$:=$ defined as

\subset subset

\cup union

$\sigma(A)$ spectrum of A

$\bar{\sigma}(A)$ the largest singular value of A

$\|f\|_{\infty}$ \mathcal{H}_{∞} -norm of f

$\|f\|_p$ p -norm of f

$\operatorname{Re}(z)$, $\operatorname{Im}(z)$ the real and imaginary parts of z , respectively

\prod product

Sets

\mathcal{H}_{∞} the Hardy ∞ -space

l^{∞} the space of bounded sequences

l^p the space of sequences whose p -powers are summable ($p < \infty$)

\mathbb{C} the set of complex numbers

\mathbb{N} the set of natural numbers

\mathbb{R} the set of real numbers

\mathbb{R}_+ the set of non-negative real numbers

$\mathbb{R}^{m \times n}$ the set of m by n real matrices

Acronyms

ADAS added damping and stiffness

AHS Automated Highway System

BRB buckling restrained brace

EW east-west

LQR linear quadratic regulator

MDOF multiple degree of freedom

NS north-south

TID tuned-inerter-damper

TMDI tuned-mass-damper-inerter

TMD tuned mass damper

TVMD tuned viscous mass damper

CHAPTER 1

INTRODUCTION

This thesis studies disturbance amplification in mechanical systems. In particular, it is concerned with interconnections which may have a large number of elements. Such systems include, for example, vehicle platoons, electrical power grids, the Internet, gene regulatory networks and financial markets. In such a system, one problem is ensuring the ability to control a system behaviour independent of the size of the interconnections. This can be characterised as a “scalability” property.

A particular focus in this thesis is passive interconnections in a chain of masses where a single point is subject to an external disturbance. The primary motivating example is the vibration control problem in multi-storey buildings subjected to earthquake disturbances. One of the main objectives for seismic design is to limit the interstorey displacements in response to disturbances. For this purpose, the installation of passive control devices between floors is widely accepted, e.g., [Constantinou et al., 1998; Soong and Dargush, 1997; Takewaki, 2009]. The thesis considers passive interconnections of the most general type, which may require the use of inerters [Smith, 2002] in addition to springs and dampers.

Another example is bidirectional control of vehicle platoons albeit with the passivity constraint. An example of such a system is an automated highway system (AHS) which is a transportation system in which vehicles are fully automated so that they travel together tightly [Rajamani, 2005]. Bidirectional control schemes are one of the decentralised control strategies for vehicle platooning in which the control action for each vehicle is dependent on the spacing errors with the preceding vehicle and the following vehicle. Such a scheme has an advantage that the necessary information can be obtained by on-board sensors alone and it does not require sophisticated inter-vehicular communication [Barooah et al., 2009; Seiler et al., 2004]. However, some literature has reported that platoons using symmetric bidirectional control schemes are not scalable in the sense of l_p string stability which has been proposed in [Swaroop and Hedrick, 1996] and widely accepted as a measure of scalability

in this field. In [Barooah and Hespanha, 2005] a general result has been shown that, using symmetric bidirectional control, the infinity norm of the transfer function vector from lead vehicle trajectory to spacing error grows without bound as the number of vehicles increases, if the combined vehicle-controller dynamics contains a double integrator. This corresponds to a positive static (spring) stiffness in the case of a mass chain with passive interconnection, which is the usual case. However, it is a central point in this thesis to draw attention to the fact that this measure may be too restrictive in general in the sense that the increasing length of the error vector with the string length is playing a role in the unboundedness property.

Accordingly, this thesis proposes to employ the \mathcal{H}_∞ -norm of individual entries of the error vector as a scalability measure. The thesis will go on to show that this measure is uniformly bounded with a suitable interconnection. The approach to prove uniform boundedness makes use of complex iterative maps. In particular, it is shown that the error transfer functions can be defined recursively in N and these recursions can be interpreted as complex iterative maps, more specifically, iterated Möbius transformations. It will be seen that the properties of Möbius transformations provide additional insight into the asymptotic behaviours of the transfer functions beyond the uniform boundedness property. A graphical means to design a suitable interconnection impedance is also provided so that the supremum of the \mathcal{H}_∞ -norm over N is no greater than a prescribed value. This can be thought of as an \mathcal{H}_∞ control design for an infinite family of plants in which the interconnection impedance is the controller.

The thesis goes further to build a design methodology for a fixed length of the mass chain. For seismic design of a multi-storey building, it is important to ensure that the interstorey drifts are well suppressed during an earthquake. A case study is presented to demonstrate the effect of the techniques using a benchmark model of a 10-storey building.

1.1 Outline

This thesis is structured as follows:

Chapter 2 provides an overview of the theory and facts on passive mechanical networks and vibration control in buildings. It begins with terminologies and definitions in the field of passive mechanical network and introduces some significant achievements in this field. The chapter then continues to give a comprehensive review on basic principles and techniques for vibration control in buildings, in particular against earthquakes. Devices that interconnects neighbouring storeys (interstorey devices) are mainly discussed as a control technique. Several types of dampers are introduced and some recent works on inerters for a building application are also presented. Charac-

teristics of earthquake ground motions are then discussed introducing some historical earthquakes, mainly in the context of frequency domain analysis. The chapter concludes with an overview of vehicle platooning, including a comprehensive review of relevant literature in this field.

Chapter 3 introduces a mass chain model with passive interconnections. The chapter starts with describing how a multi-storey building with base excitation is modelled as a proposed mass chain model. Identical masses and identical interconnections are considered, i.e., a homogeneous mass chain. Then the transfer functions from a movable point to a given intermass displacements are described as a function of a dimensionless parameter depending on the interconnection impedance and mass. The stability of the system is then studied in this chapter. The connection to a symmetric bidirectional control problem of a vehicle platoon is also discussed.

Chapter 4 studies the transfer functions defined in Chapter 3. They are described in the form of iterated Möbius transformations. The asymptotic behaviours of them are first discussed. Then it is shown that the \mathcal{H}_∞ -norm of these transfer functions are uniformly bounded with respect to the number of masses N for a suitable choice of the interconnection impedance. These results are also illustrated graphically in this chapter.

Chapter 5 proposes a design methodology for a specific length of the mass chain in the context of seismic design of a multi-storey building. A graphical technique is introduced to choose a suitable interconnection. Several interconnection designs are studied using a homogeneous 10-storey building model. The vibration suppression performance of these designs is numerically tested for a 10-storey building model which has a non-identical stiffness distribution. Weighting functions are introduced based on the well-known Clough-Penzien and Kanai-Tajimi acceleration filter to represent the characteristics of earthquakes. Vibration suppression performance of these designs is compared with respect to the frequency response and the time response against some historical earthquakes.

Chapter 6 introduces some open problems related to the thesis. A conjecture on the uniform boundedness of disturbance amplification by the value one is discussed for the transfer functions introduced in Chapter 4. Although an analytical proof has not been obtained, heuristic justifications are given for the first intermass case. The techniques introduced in this chapter is possibly useful for the exact computation of uniform bound. The chapter continues to pose conjectures on higher intermass displacements

with respect to uniform boundedness.

Chapter 7 summarises the conclusions and contributions of the thesis. Future research directions are also discussed.

BACKGROUND

This chapter provides an overview of background theory that underlies the contributions in this thesis. For this purpose, it presents a comprehensive review of relevant background literature.

2.1 Overview of Passive Mechanical Networks

This section introduces some terminologies and definitions in passive mechanical networks.

2.1.1 Multi-port networks

A multi-port network is a physical device consisting of a collection of elements that are connected according to some scheme. A *port* is a pair of access points called *terminals* or *nodes*. At each port of the network, other elements or the port of another network may be connected. A fixed reference point in an inertial frame is called the *ground* [Anderson and Vongpanitlerd, 2006; Smith and Walker, 2000]. Each port has a pair of port variables, which may be classified as a through-variable and an across variable. The concept of through- and across-variables is the basis of the force-current analogy [Firestone, 1933]. A *through-variable* has the same value at the two terminals or ends of the element, and to make the measurement, the system must be severed at a measurement point. On the other hand, an *across-variable* is specified in terms of a relative value or difference between the terminals and can be measured without breaking into the system. The *impedance* is then defined by the ratio of the across variable to the through variable and *admittance* is defined as the reciprocal of impedance.

2.1.2 Passive mechanical networks and mechanical elements

In mechanical networks, an equal and opposite force F is applied to a port and the port experiences a relative velocity v [Shearer et al., 1971]. Figure 2.1 is a free body diagram of a one-port mechanical network showing a positive $v = v_2 - v_1$ and a compressive force F . The force F is the through-variable and the relative velocity v is the across-variable.

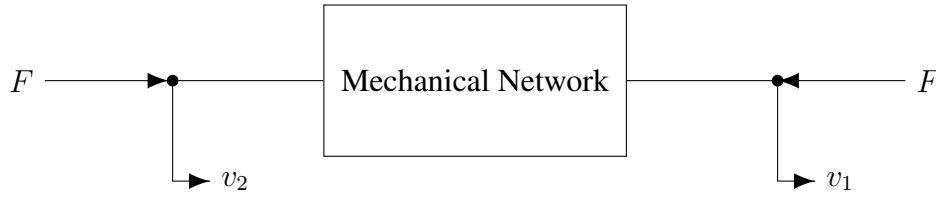


Fig. 2.1 A free-body diagram of a one-port (two-terminal) mechanical network.

In the sequel only mechanical elements with nonnegative constant element values are concerned. The class of all such elements is linear, lumped, time-invariant and passive. Passivity of a mechanical one-port network is defined as follows:

Definition 2.1 (Passivity). A mechanical one-port network with force-velocity pair (F, v) is *passive* if for all square integrable pairs $F(t)$ and $v(t)$ on $(-\infty, T]$,

$$\int_{-\infty}^T F(t)v(t)dt \geq 0. \quad (2.1)$$

◇

For a multi-port network, (2.1) is replaced by

$$\int_{-\infty}^T F(t)'v(t)dt \geq 0 \quad (2.2)$$

where $F(t)'v(t) = \sum_j F_j(t)v_j(t)$. The left hand side of (2.2) can be interpreted as the total energy delivered to the network up to time T . Therefore, a passive network cannot deliver energy to the environment. Furthermore, a passive network is *lossless* if it satisfies the condition

$$\int_{-\infty}^T F(t)v(t)dt = 0$$

or, for a multiport network,

$$\int_{-\infty}^T F(t)'v(t)dt = 0.$$

It can be interpreted that a passive mechanical network is lossless if all the energy which are put into the network can be extracted again. The spring and inerter (see Remark 2.1) are lossless elements. Any network which is not passive is termed active.

It can be shown that a linear time-invariant network is passive if and only if the impedance $Z(s)$ or the admittance $Y(s) = Z(s)^{-1}$ is positive real.

Definition 2.2 (Positive realness). A real-rational function $G(s)$ is *positive real* if (i) $G(s)$ has no poles in $\text{Re}(s) > 0$ (i.e., $G(s)$ is analytic in the open right half plane) and (ii) $\text{Re}(G(s)) \geq 0$ in $\text{Re}(s) > 0$. \diamond

In the aforementioned definition, (ii) is equivalent to (ii'): $\text{Re}(G(j\omega)) \geq 0$ for all ω at which $G(j\omega)$ is finite, and any poles of $G(j\omega)$ on the imaginary axis or at infinity are simple and have a positive residue. A pole is said to be *simple* if it has multiplicity one. The residue of a simple pole of $G(s)$ at p_0 is equal to $\lim_{s \rightarrow p_0} (s - p_0)G(s)$. Poles and zeros of $G(s)$ at $s = \infty$ can be defined as the poles and zeros of $G(s^{-1})$ at $s = 0$. Thus, the residue of a simple pole at $s = \infty$ is equal to $\lim_{s \rightarrow \infty} G(s)/s$.

The following two theorems are key results on classical electrical network theory.

Theorem 2.1 ([Anderson and Vongpanitlerd, 2006]). *Consider a network with real-rational impedance $Z(s)$ (or admittance $Y(s)$). The network is passive if and only if $Z(s)$ (or $Y(s)$) is positive real.*

Theorem 2.2 ([Bott and Duffin, 1949; Brune, 1931]). *Any real-rational positive-real functions can be realized as the impedance or admittance of a network with inductors, capacitors, and resistors only.*

Historically, Brune first showed in [Brune, 1931] that any real-rational positive-real function can be realized as the driving-point impedance of an electrical network consisting of resistors, capacitors, inductors, and transformers, and later, Bott and Duffin established the possibility of achieving the synthesis without the use of transformers in [Bott and Duffin, 1949]. Theorem 2.2 can now be restated in mechanical terms:

Theorem 2.3 ([Smith, 2002]). *Any real-rational positive-real functions can be realized as the impedance or admittance of a network with springs, inerters, and dampers only.*

Remark 2.1. The *inert*er is a mechanical two-terminal, one-port device with the property that the applied force at the terminals is proportional to the relative acceleration between the terminals, i.e., $F = b(\ddot{v}_2 - \ddot{v}_1)$ where b is the constant of proportionality called the *inertance* which has units of kilograms [Smith, 2002] and v_1, v_2 are the terminal velocities. The inerter completes a standard analogy between mechanical and electrical networks which allows classical results from electrical network synthesis to be translated over exactly to mechanical systems. \heartsuit

2.2 Overview of Vibration Control in Buildings

This section provides an introduction to vibration control in building structures.

2.2.1 Basic principles and classification of control systems

In addition to gravity loads, buildings are often subjected to dynamic loads caused by winds, earthquakes, road traffic etc. Although the characteristics of these types of loads are very different from gravity loads which are static, the traditional approach treats such loads in the same way for gravity loads. For example, winds and earthquake forces are often idealised as lateral static loads of suitable magnitude and buildings are designed to resist such loads by elastic action of the structure. This is based on the philosophy that for winds and small earthquakes the building remains elastic and it is permitted to be damaged but not collapsed by moderate or severe earthquakes. Although this approach has been reasonably successful, more improvements can be achieved by considering the dynamic nature of these loads.

Various vibration control devices have been developed for this purpose. These devices may be classified as passive, active or semi-active in terms of the external energy supply to the device. Semi-active and active control devices control the motion of a structure through external energy supply. However, semi-active control devices normally require only a little amount of energy to adjust their mechanical properties. Active control devices require more energy but can add energy to the structure using actuators. On the other hand, passive control devices consist of passive mechanical components only and do not require an external supply of power. For seismic design, passive or semi-active control systems are normally employed since it is not realistic to store huge amount of energy for severe earthquakes which may happen in every decades.

Another classification of those control devices is based on how the device is implemented in a structure. In this classification, the control systems may be classified broadly into three categories [Takewaki, 2009]: base-isolation type, tuned mass damper (TMD) type and interstorey type.

A base-isolation system is typically placed at the foundation of structure. The idea of base isolation is to partially reflect and partially absorb the earthquake input energy before this can be transmitted to the superstructure by means of its flexibility and energy absorption capability. Elastomeric bearings, lead rubber bearings, sliding friction pendulum are the examples of this type. They are normally designed to be effective for moderate to severe earthquakes but not for winds or small earthquakes.

The simplest form of TMD consists of an auxiliary mass-spring-dashpot system anchored or attached to the main structure. There are also active type in which an actuator is

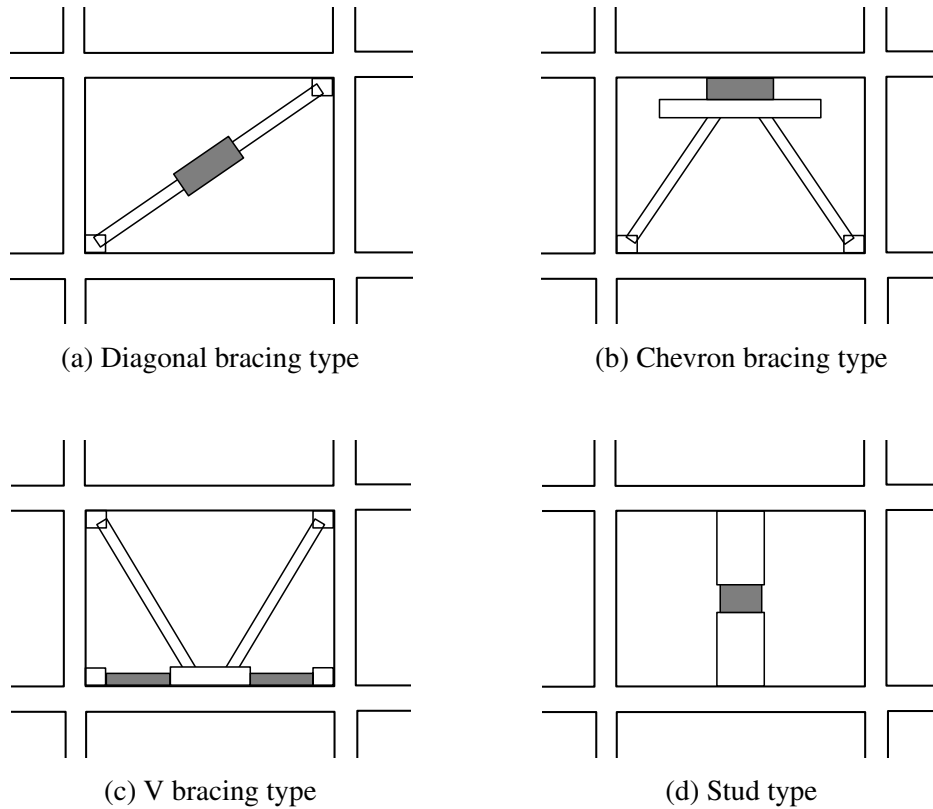


Fig. 2.2 Typical configurations of interstorey-installment type control devices in a building frame.

used to move the auxiliary mass and semi-active type in which the mechanical parameters of TMD are adjustable. A TMD is typically placed at the top of a building. They are mainly used to suppress the vibration caused by winds.

The basic principle of control using interstorey devices, i.e., devices interconnecting neighbouring storeys, is to add energy dissipation capability to the structure by installing additional devices to reduce the damage of a structure. Therefore main components of this type of control are energy dissipation devices such as various type of dampers. The other devices such as the inerter may be incorporated to enhance the performance. The devices are normally incorporated in a brace or a stud. Typical configurations are illustrated in Fig. 2.2. The focus of this thesis is on this type of passive control systems. In the next section, some examples of passive energy dissipation devices used in this control system are reviewed as well as the inerter.

2.2.2 Passive vibration control devices

This section gives a brief introduction to the typical passive energy dissipation devices and the inerter and its similar devices for building vibration control.

Passive energy dissipation devices

The major types of passive energy dissipation devices can be classified into viscous fluid dampers, viscoelastic dampers, metallic dampers and friction dampers. Note that there are so many configurations of these devices that only some basic ones are introduced here. More detailed reviews can be found in, for example, [Constantinou et al., 1998; Soong and Dargush, 1997; Symans et al., 2008].

Viscous fluid dampers consist of a cylinder filled with viscous fluid. The piston head has small orifices and as the damper piston rod and piston are stroked, fluid is forced to flow through orifices either around or through the piston head causing friction. Properties are typically frequency and temperature independent. The idealised constitutive model is a dashpot.

Viscoelastic dampers generally consist of viscoelastic materials bonded to steel plates. Copolymers or glassy substances are typically used as viscoelastic materials. Properties are normally frequency and temperature dependent. Constitutive models of viscoelastic dampers include the Maxwell model, the Kelvin-Voigt model (Fig. 2.2.2) and complex combination of these elementary models. The suitable models depend on the materials used for a damper. However, each model has drawbacks in terms of its accuracy. More detailed discussion can be found in the literature, e.g., [Soong and Dargush, 1997].

Metallic dampers dissipate energy due to the inelastic deformation of a metal. Usually that metal is mild steel. Two major types of metallic dampers are buckling-restrained brace (BRB) dampers and added damping and stiffness (ADAS) dampers. A BRB damper consists of a steel core usually having a low-yield strength supported by a concrete casing in order to prevent buckling. An ADAS damper consists of a series of steel plates made of mild steel. The bottom of the plates are attached to the top of a chevron bracing and the top of the plates are attached to the floor level above the bracing (see Fig. 2.2b). They have a stable hysteretic behaviour. However, devices are damaged after a severe earthquake and may need to be replaced.

Friction dampers employ solid sliding friction as their basic dissipative mechanism. There are two solid bodies and they slide over each other during an earthquake. There is a

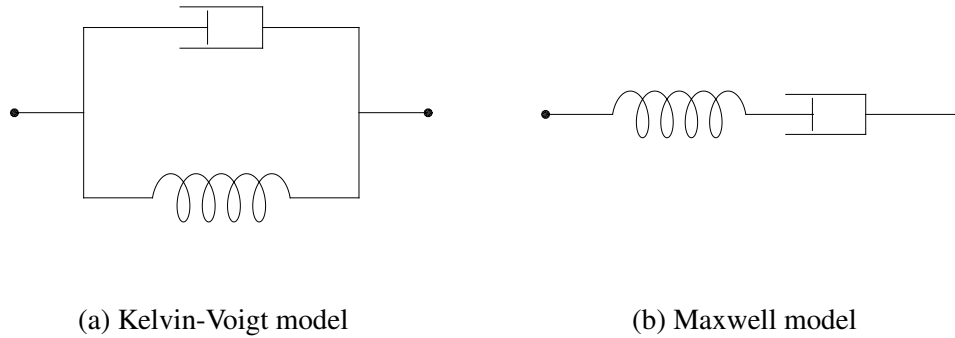


Fig. 2.3 Constitutive models of viscoelastic dampers.

reliability concern since the sliding interface conditions may change during the cycle. The device needs some sort of restoring force mechanism since it leaves permanent displacements otherwise.

Note that metallic dampers and friction dampers both show highly nonlinear behaviour and are out of scope of this thesis.

Inerter

As introduced in Section 2.1.2, the inerter is a mechanical device with the property that the applied force at the terminals is proportional to the relative acceleration between the terminals. Various physical realisations of an inerter are proposed in [Smith, 2002] and [Smith, 2005]. Laboratory experimental testing of two types of inerter devices has been reported in [Papageorgiou et al., 2009; Papageorgiou and Smith, 2005]. The first type is the rack-and-pinion inerter and the second is the ball-screw inerter. Testing of a hydraulic inerter was reported in [Wang et al., 2011].

Some successful applications of the inerter have been reported on vehicle suspensions [Papageorgiou and Smith, 2006; Smith and Wang, 2004], mechanical steering compensators of high-performance motorcycles [Evangelou et al., 2007; Papageorgiou and Smith, 2007], vibration absorption [Smith, 2002] and rail suspensions [Jiang et al., 2012; Wang et al., 2009].

Applications of inerters for building vibration suppression have been also extensively studied in the recent years. Some early arrangements in the literature can be interpreted as acting like inerters in combination with other elements, e.g., [Arakaki et al., 1999a,b; Okumura, 1997; Pradono et al., 2008]. These devices are sometimes referred to as “inertia mass”, “inertial dampers”, “dynamic mass”, “angular mass damper” etc. Throughout the thesis, the term “inerter” is used.

Following the development of such devices, effective ways to use the inerter have been investigated. A mode isolation method has been proposed in [Furuhashi and Ishimaru, 2004, 2006] in which inerters are placed in parallel to the storey stiffness in a multi-storey building so that the higher modes of vibration disappear. Also for a parallel inerter arrangement, [Takewaki et al., 2012] has introduced an “influence vector”, though this is not clearly related to disturbance transmission paths. Enhancing the performance of the inerter has also been considered by combining it with properly tuned springs and dampers, e.g., a tuned viscous mass damper (TVMD) [Ikago et al., 2012a,b; Saito et al., 2007, 2008], a tuned-inerter-damper (TID) [Lazar et al., 2014] and a tuned-mass-damper-inerter (TMDI) [Giaralis and Taflanidis, 2015; Marian and Giaralis, 2014]. Those ideas have been mainly inspired by TMDs and the fixed-point theory of Hartog [Hartog, 1985], which is an optimal tuning method for TMDs employed for selecting the device parameters. A tuning method for TVMDs in a multiple-degree-of-freedom (MDOF) building has also been proposed in [Ikago et al., 2012a] based on a modal analysis.

These design methods, however, may only be applicable to a specific device. Although the problem setup considered in [Wang et al., 2007, 2010] is applicable to more general classes, the optimisation algorithms used in these articles resulted in a design which gives a large resonance peak outside of the frequency range considered. This suggests that more careful analysis will be required for incorporating inerters in buildings. This thesis proposes a systematic and an intuitive design methodology which covers any layouts consisting of springs, dampers and inerters in Chapter 5.

2.2.3 Characteristics of earthquake ground motions

Dynamic loads such as winds and earthquakes are dominant over certain frequency range. The motion produced during an earthquake is complex and the dominant frequency range varies. Loosely speaking, a rapid movement or a slip of a fault within the Earth’s crust due to a sudden release of energy in its interior generates seismic waves and the characteristics of these waves are not unique. Furthermore, these seismic waves are modified by the soil and rock on the path before reaching the Earth’s surface, and also by the soil condition of the ground beneath a building.

The acceleration records of historical earthquakes of (a) the 1940 Imperial Valley earthquake, El Centro record, north-south component (El Centro 1940 NS), (b) the 1952 Kern County earthquake, Taft Lincoln School record, east-west component (Taft 1952 EW), (c) the 1968 Tokachi-oki earthquake, Hachinohe record, north-south component (Hachinohe 1968 NS) and the 1995 Kobe earthquake, Kobe JMA station record, north-south component (JMA Kobe 1995 NS) are shown in Fig. 2.4. It may be observed that these seismic

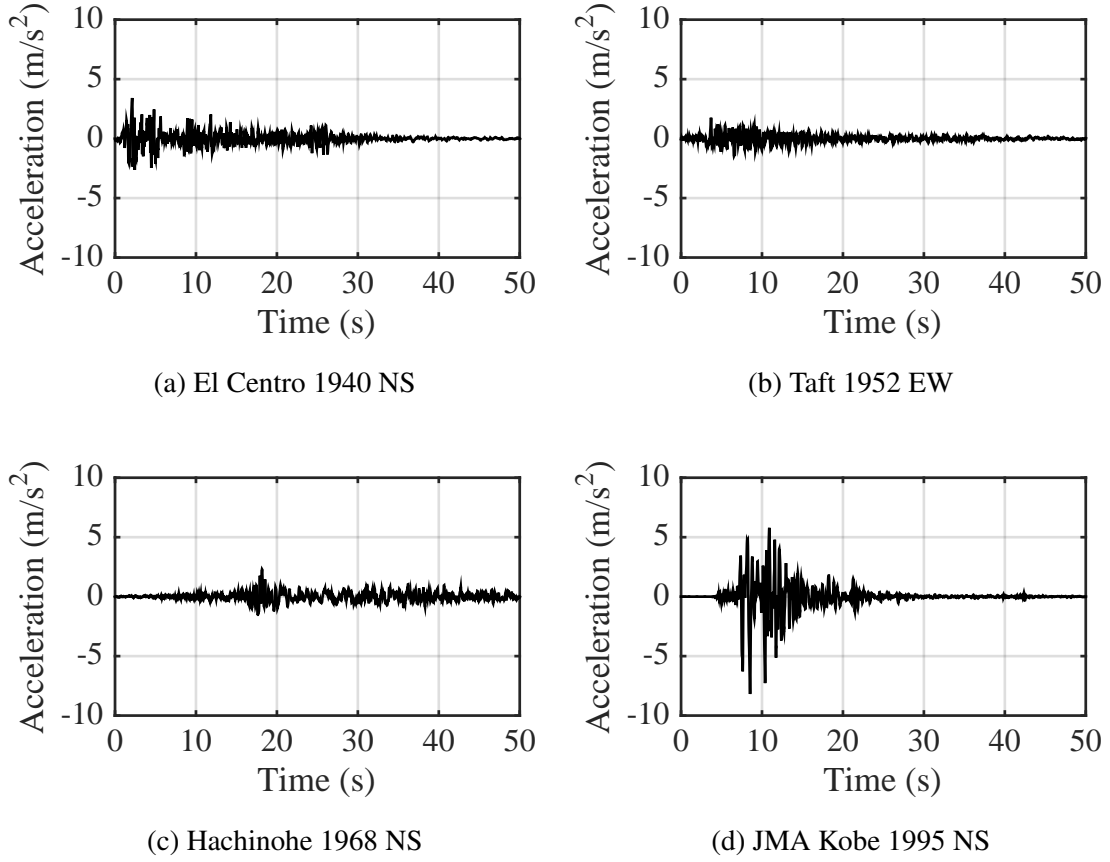


Fig. 2.4 Ground acceleration of historical earthquakes.

waves have quite different characteristics. Their Fourier amplitude spectra are also shown in Fig. 2.5.

Instead of these recorded earthquakes, simulated earthquakes taking account of the soil condition at the site are often used to design or analyse a building. One of the most well-used methods is to describe the ground acceleration wave as a product of a sample function $z(t)$ which has a stationary power spectral density and an envelope function $g(t)$. As a power spectral density function $S(\omega)$, a band-limited white noise model or the *Kanai-Tajimi model* are often employed.

Definition 2.3 (Kanai-Tajimi Power Spectrum, [Kanai, 1957; Tajimi, 1960]).

$$S_{KT}(\omega) = |W_{KT}(\omega)|^2 S_0 = \frac{1 + 4\eta_g^2 \frac{\omega^2}{\omega_g^2}}{\left(1 - \frac{\omega^2}{\omega_g^2}\right)^2 + 4\eta_g^2 \frac{\omega^2}{\omega_g^2}} S_0$$

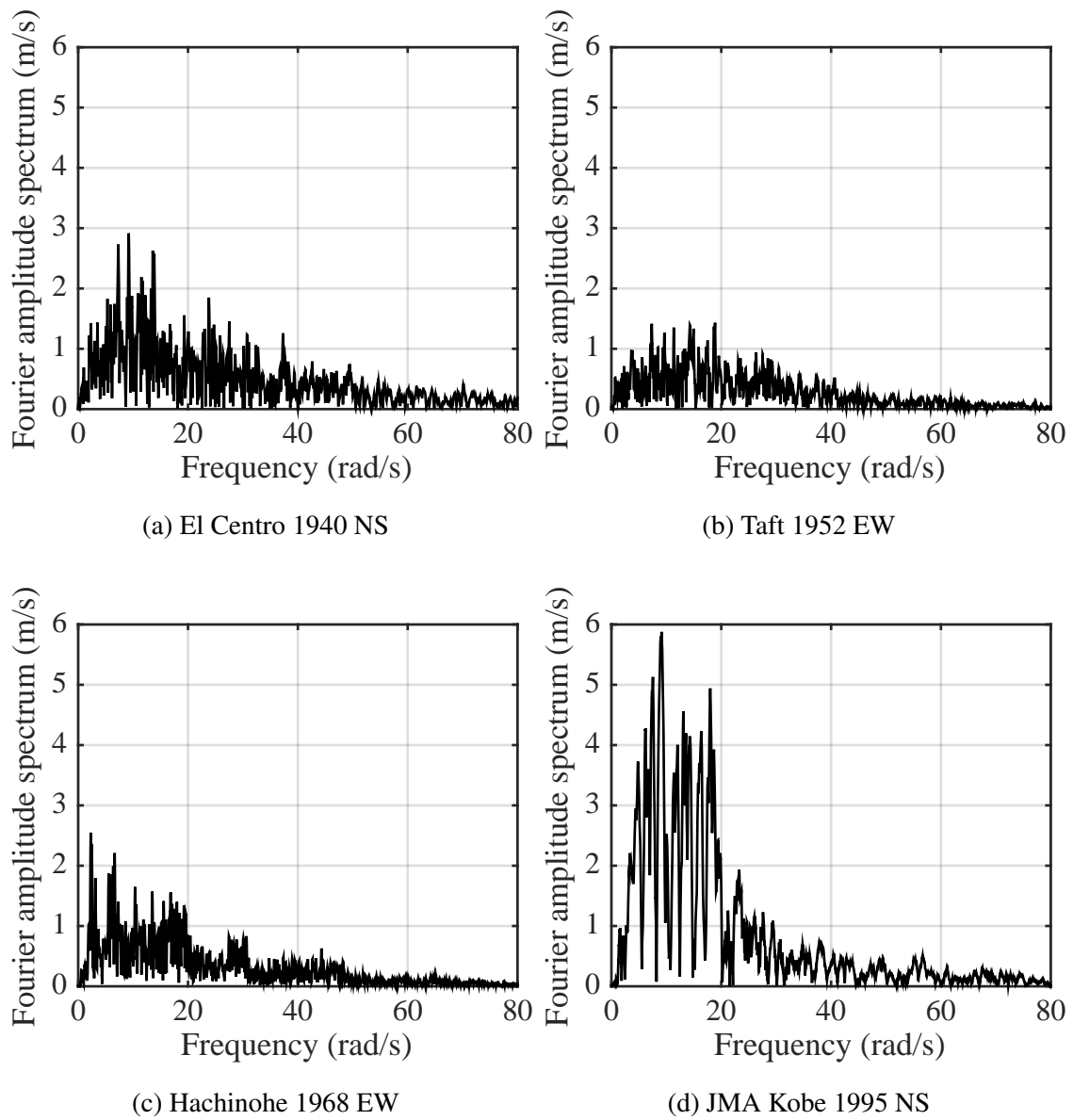


Fig. 2.5 Fourier amplitude spectra of ground acceleration of historical earthquakes. NS represents North-South component and EW represents East-West component.

Table 2.1 Parameters for the Kanai-Tajimi filter and the Clough-Penzien filter.

Soil condition	Kanai-Tajimi W_{KT}		Clough-Penzien W_{CP}	
	ω_g (rad/s)	η_g	ω_f (rad/s)	η_f
Rock or stiff soil conditions	8π	0.60	0.8π	0.60
Deep cohesion-less soils	5π	0.60	0.5π	0.60
Soft to medium clays and sands	2.4π	0.85	0.24π	0.85

where S_0 is a constant determining the intensity of the ground acceleration at a site. Parameters ω_g and η_g may be thought of as some characteristic ground frequency and characteristic damping ratio, respectively. \diamond

The function

$$W_{KT}(\omega) = \frac{1 + 2j\eta_g \frac{\omega}{\omega_g}}{\left(1 - \frac{\omega^2}{\omega_g^2}\right) + 2j\eta_g \frac{\omega}{\omega_g}} \quad (2.3)$$

is sometimes referred as the *Kanai-Tajimi filter*. Note that the Kanai-Tajimi power spectrum takes non-zero value at zero frequency. Clough and Penzien has proposed an additional filter multiplied by the Kanai-Tajimi filter to deal with this [Clough and Penzien, 1975]:

$$W(\omega) = W_{CP}(\omega)W_{KT}(\omega) = \frac{\left(\frac{\omega}{\omega_f}\right)^2}{\left(1 - \frac{\omega^2}{\omega_f^2}\right) + 2j\eta_f \frac{\omega}{\omega_f}} W_{KT}(\omega). \quad (2.4)$$

In this thesis, the filter $W_{CP}(\omega)$ is called the *Clough-Penzien filter* and the filter $W_{CP}(\omega)W_{KT}(\omega)$ is called the *Clough-Penzien-Kanai-Tajimi filter*. Some suggested values for parameters $\omega_g, \eta_g, \omega_f, \eta_f$ in (2.3) and (2.4) for three different soil conditions are shown in Table 2.1 [Deodatis, 1996]. Figure 2.6 shows the frequency response of $W_{KT}(\omega)$ and $W_{CP}(\omega)W_{KT}(\omega)$ using the parameters for rock or stiff soil conditions in Table 2.1.

2.3 Overview of Vehicle Platooning

As the control problem in this thesis is closely related to the bidirectional control of a string of vehicles, this section provides an introduction to vehicle platooning. Vehicle platoons

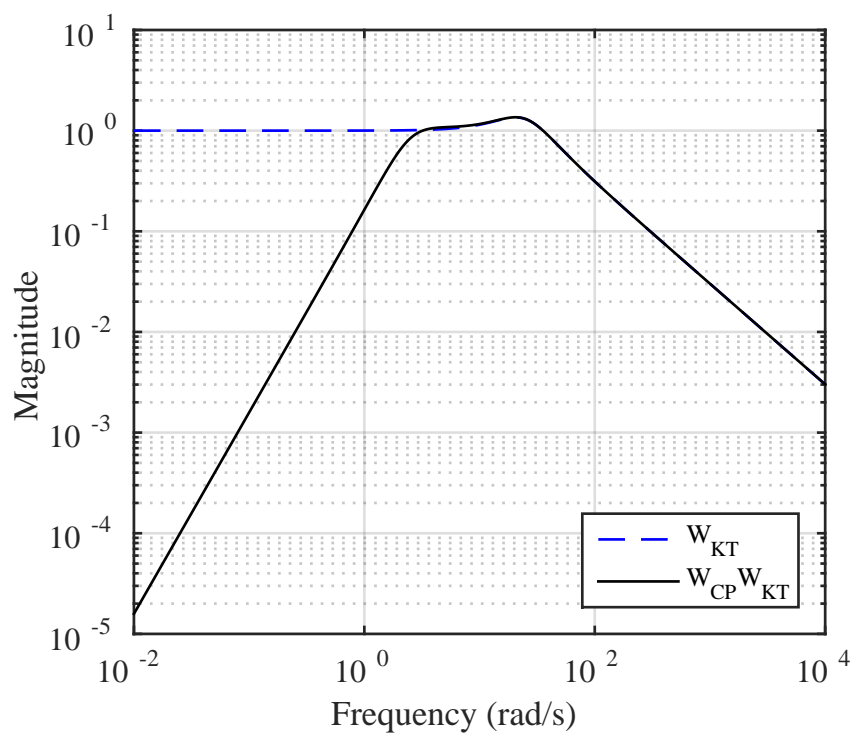


Fig. 2.6 Frequency responses of Kanai-Tajimi filter W_{KT} and Clough-Penzien-Kanai-Tajimi filter $W_{CP}W_{KT}$ for rock or stiff soil conditions.

refer to groups of tightly spaced vehicles moving together in the same direction. A proposed application of such systems is automated highway systems (AHS) where the vehicles are fully automated. This section first introduces the basic idea of AHSs. An important concept so-called “string stability” to control such a system is then discussed. The section finishes with introducing some significant works in this field.

2.3.1 Automated highway system

In an AHS, the vehicles are fully automated to travel together in a tightly spaced platoon as depicted in Fig. 2.7. The principal motivation is to increase the traffic capacity on a highway by operating the vehicles at a closer spacing than human drivers can operate. As data suggest [Varaiya, 1993] that 90% of highway accidents are caused by human error, the AHS is also expected to improve the safety. An additional benefit is also pointed out that the tightly spaced vehicles reduce aerodynamic drag which results in lower fuel consumption and vehicle emissions. This effect is more significant for heavy-duty vehicles such as trucks (e.g., [Alam, 2014]). More detailed reviews for AHSs including the technology used in the systems can be found in, for example, [Hedrick et al., 1994; Horowitz and Varaiya, 2000; Varaiya, 1993].

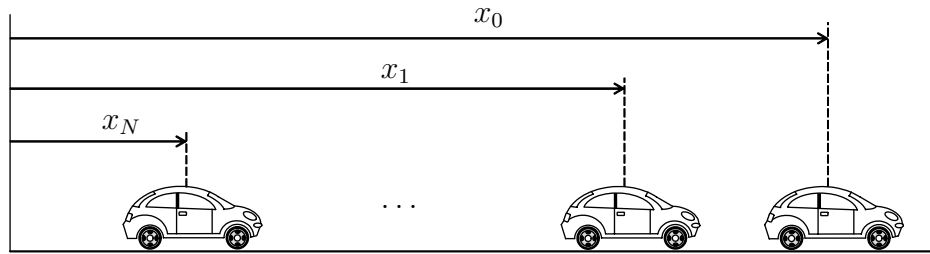


Fig. 2.7 Platoon of N vehicles.

2.3.2 Vehicle platooning specification

A major objective for vehicle platooning is that each vehicle maintains a desired spacing from the preceding vehicle while satisfying individual vehicle stability and *string stability*. There are two spacing policies; a constant spacing policy which requires a desired spacing to be fixed and a constant time headway policy in which a desired spacing is proportional to the vehicle velocity. Individual vehicle stability refers to the specification of the spacing error of a vehicle converging to zero when the preceding vehicle is operating at a constant speed [Rajamani, 2005]. Spacing error here refers to the difference between the actual and the

desired inter-vehicle spacing. If the preceding vehicle accelerates or decelerates, a spacing error will appear and may propagate from vehicle to vehicle in a string. The concept of string stability is to ensure that spacing errors are not amplified downstream in a platoon. This property is often described as uniform boundedness of the response to disturbances with respect to the size of a platoon. Although it has not always been referred to as string stability, such a problem has been considered as early as [Chien and Ioannou, 1992; Ioannou et al., 1993; Levine and Athans, 1966; Melzer and Kuo, 1971; Peppard, 1974] for example. The following definitions of string stability proposed in [Swaroop and Hedrick, 1996] have now been widely accepted.

Definition 2.4 (l_∞ string stability). Consider the following interconnected system:

$$\dot{x}_i = f(x_i, x_{i-1}, \dots, x_{i-r+1}) \quad (2.5)$$

where $i \in \mathbb{N}$, $x_{i-j} \equiv 0 \forall i \leq j$, $x \in \mathbb{R}^n$, $f : \underbrace{\mathbb{R}^n \times \dots \times \mathbb{R}^n}_{r \text{ times}} \rightarrow \mathbb{R}^n$ and $f(0, \dots, 0) = 0$.

Then the origin $x_i = 0, i \in \mathbb{N}$ of (2.5) is string stable, if given any $\epsilon > 0$, there exists a $\delta > 0$ such that

$$\|x_i(0)\|_\infty < \delta \Rightarrow \sup_i \|x_i(\cdot)\|_\infty < \epsilon.$$

◇

Definition 2.5 (l_p string stability). The origin $x_i = 0, i \in \mathbb{N}$ of (2.5) is l_p string stable if given any $\epsilon > 0$, there exists a $\delta > 0$ such that

$$\|x_i(0)\|_p < \delta \iff \sup_t \left(\sum_1^\infty |x_i(t)|^p \right)^{\frac{1}{p}} < \epsilon.$$

◇

2.3.3 Control schemes and string stability

The control strategies for vehicle platooning can be classified into two broad categories: *centralised* and *decentralised*. In the present context, centralised control schemes need the inter-vehicle communication between all the vehicles in a platoon while decentralised control schemes only require the information obtained by on-board sensors and possibly wireless communication with a limited number of vehicles.

There are two typical decentralised control schemes. One is a predecessor-following scheme which is a control law based only on relative spacing error from the preceding vehi-

cle (predecessor). The other is a bidirectional scheme where the control action on each vehicle is based on the relative spacing with respect to its immediate neighbours. On the other hand, a predecessor-leader-following scheme is an example of centralised control schemes. In this scheme, the information of the first vehicle in a platoon (leader) is communicated to all the following vehicles in addition to a predecessor-following scheme. Optimal linear quadratic regulator (LQR) methods considered in [Levine and Athans, 1966; Melzer and Kuo, 1971] also typically result in centralised controllers.

Most of the control schemes, however, often experiences string instability under a constant spacing policy. The difficulty is mainly due to the fact that the combined vehicle-controller dynamics normally contains a double integrator. In particular, [Seiler et al., 2004] has shown that for any linear controller disturbances are amplified as they propagate along the string using a predecessor-following scheme. In [Barooah and Hespanha, 2005] it has been shown that, using symmetric bidirectional control, the infinity norm of a spacing error vector due to deviation of lead vehicle trajectory grows without bound as the number of vehicles increases. The term “symmetric” here implies that the control law is equally dependent on the spacing errors with the predecessor and the following vehicle (follower). It has also pointed out in [Jovanovic and Bamieh, 2005] that the solutions to the LQR methods in [Levine and Athans, 1966; Melzer and Kuo, 1971] are not scalable and that the least stable eigenvalue of the closed loop tends to the imaginary axis as the size of the platoon increases. The least stable closed-loop eigenvalue also tends to zero using a bidirectional control scheme. The speed of the eigenvalue tending to zero can be made slower using asymmetric bidirectional control than using symmetric one [Barooah et al., 2009].

Several ways to avoid string instability have been proposed. For example, [Seiler et al., 2004] has shown that spacing errors can attenuate using a predecessor-leader-following scheme. It has also been shown in [Lestas and Vinnicombe, 2007] that arbitrarily weak coupling with the leader information makes symmetric bidirectional control schemes scalable, though this cannot be achieved with no leader information with respect to uniform boundedness of the infinity norm. However, these centralised control schemes require a global communication in a platoon and may encounter technical difficulties especially for a large platoon. Indeed, it has been pointed out in [Middleton and Braslavsky, 2010] that limited forward communication range does not avoid string instability although it can reduce the rate of disturbance amplification. Another way of avoiding string instability is using a constant time headway policy [Swaroop and Rajagopal, 2001]. However, [Middleton and Braslavsky, 2010] has reported that a small time headway is not much of help with respect to string stability and a sufficiently large time headway is necessary.

Although some difficulties seem to exist to apply these decentralised control schemes

for vehicle platooning as above, it may be noted that the results for symmetric bidirectional control in [Barooah and Hespanha, 2005; Lestas and Vinnicombe, 2007] are based on an analysis for uniform boundedness of the infinity norm of the transfer function vector and the increasing length of the vector with the string length is playing a role in the unboundedness property. In Chapter 4, it is shown that individual entries of the error vector is uniformly bounded for a suitable choice of the interconnection when the system is subject to deviating leader trajectory. This result could be viewed as a relaxation of the definition of string stability. Note that [Knorn et al., 2014] has considered a different alternative to string stability, formulated in the time domain, and shown that this may be satisfied by a vehicle platoon with integral action.

It is, however, worth noting that, in [Bamieh et al., 2012] it is observed that slow accordion-like motion of the entire formation in a large vehicular platoon may not be inconsistent with the spacing between each vehicle being well regulated.

CHAPTER 3

HOMOGENEOUS MASS CHAINS WITH PASSIVE INTERCONNECTION

3.1 Overview

A mass chain model with passive interconnection is introduced in this chapter. A lumped mass system with base excitation is an elementary model to analyse the dynamical behaviour of a multi-storey building during earthquakes. The interconnection of masses is often modelled as a spring or other passive components in parallel to a spring i.e., a fixed-structure admittance. In this thesis, a general passive admittance is employed as the interconnection to capture common characteristics over the whole class of positive real functions. This chapter first introduces how buildings are modelled as multi-degree-of-freedom lumped mass systems with the interconnection of general admittances. The chapter continues to pose the control problem of a chain of N identical masses in which there is an identical passive interconnection between neighbouring masses and a similar connection to a movable point.

The transfer functions from a movable point displacement to a given intermass displacements are studied. They correspond to inter-storey displacements of a building which should be well suppressed to prevent damage to buildings, not only the structural components but also utilities like water or gas pipes. They are described as a function of a dimensionless parameter h depending on the impedance and mass. Then an explicit condition for stability of the system is provided.

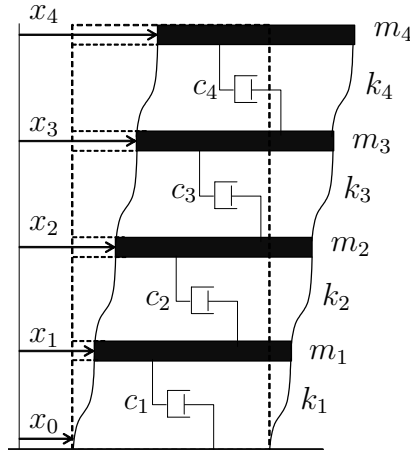
The problem is closely related to the spacing control of a vehicle string. The final section in this chapter discusses this point further.

3.2 A Lumped Mass System with Base Excitation

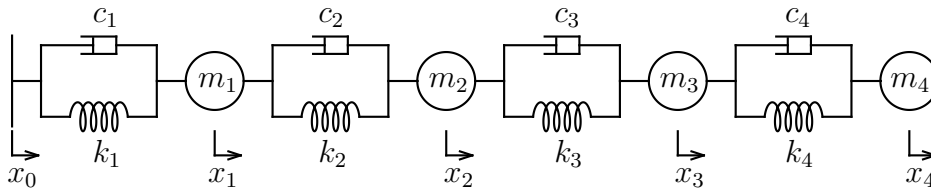
The shear-type building model of Fig. 3.1a is an idealised model for analysing the seismic response of a building. It is assumed that:

1. The distributed mass of the structure is lumped at equidistant floor levels.
2. The floor slabs are infinitely rigid and do not rotate during deformation.
3. The columns or the walls are axially inextensible but laterally flexible so that the entire shear stiffness at any column level is concentrated in one linear elastic shear spring.
4. There is no foundation rotation.

It is also assumed that the ground motion is essentially horizontal. There are several ways of approximating the shear stiffness, which are reviewed in [Schultz, 1992]. A shear-type building model is equivalent to the multi-degree-of-freedom (MDOF) lumped mass system of Fig. 3.1b.



(a) A damped shear-type building model.



(b) A damped MDOF lumped mass model.

Fig. 3.1 Multi-storey building models.

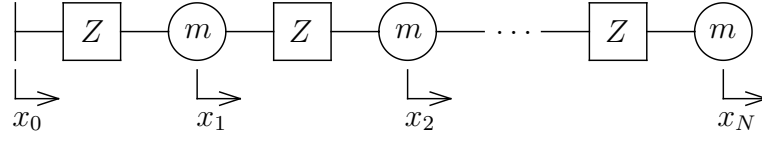


Fig. 3.2 Chain of N masses m connected by a passive mechanical impedance $Z(s)$ (admittance $Y(s) = Z(s)^{-1}$), and connected to a movable point x_0 .

3.3 Problem Formulation

In the previous section, an MDOF lumped mass system has been introduced. In the sequel, the interconnection of the masses is modelled as a general passive mechanical admittance instead of a fixed structure to capture common characteristics over the whole class of positive real functions. As the simplest case, a homogeneous mass chain is considered, i.e., a chain of N identical masses m connected by identical passive mechanical networks (Fig. 3.2). Each passive mechanical network provides an equal and opposite force on each mass and is assumed here to have negligible mass. The system is excited by a movable point $x_0(t)$ and the displacement of the i th mass is denoted by $x_i(t)$, $i \in \{1, 2, \dots, N\}$. Assume that the initial conditions of the movable point and the mass displacements are all zero. The equations of motion in the Laplace transformed domain are

$$\begin{aligned} ms^2\hat{x}_i &= sY(s)(\hat{x}_{i-1} - \hat{x}_i) + sY(s)(\hat{x}_{i+1} - \hat{x}_i) \quad \text{for } i = 1, \dots, N-1, \\ ms^2\hat{x}_N &= sY(s)(\hat{x}_{N-1} - \hat{x}_N) \end{aligned}$$

where $\hat{\cdot}$ denotes the Laplace transform. In matrix form this can be written as

$$ms^2\hat{x} = sY(s)H_N\hat{x} + sY(s)e_1\hat{x}_0$$

and hence

$$\hat{x} = (h(s)I_N - H_N)^{-1}e_1\hat{x}_0 \quad (3.1)$$

where I_N is the $N \times N$ identity matrix,

$$\begin{aligned}
 h(s) &= sZ(s)m, \quad Z = Y^{-1}, \\
 \hat{x} &= [\hat{x}_1, \dots, \hat{x}_N]^T, \\
 e_1 &\in \mathbb{R}^N, \quad e_1 = [1, 0, \dots, 0]^T, \\
 H_N &\in \mathbb{R}^{N \times N}, \\
 H_N &= \begin{bmatrix} -2 & 1 & 0 & \dots & 0 \\ 1 & -2 & 1 & \ddots & \vdots \\ 0 & \ddots & \ddots & \ddots & 0 \\ \vdots & \ddots & 1 & -2 & 1 \\ 0 & \dots & 0 & 1 & -1 \end{bmatrix}.
 \end{aligned}$$

Consider the characteristic polynomials d_i of $H_i \in \mathbb{R}^{i \times i}$ in the variable h given by

$$\begin{aligned}
 d_i &= \det(hI_i - H_i) \\
 &= \begin{vmatrix} h+2 & -1 & 0 & \dots & 0 \\ -1 & h+2 & -1 & \ddots & \vdots \\ 0 & \ddots & \ddots & \ddots & 0 \\ \vdots & \ddots & -1 & h+2 & -1 \\ 0 & \dots & 0 & -1 & h+1 \end{vmatrix} \quad (3.2)
 \end{aligned}$$

for $i = 1, \dots, N$. Then $d_1 = h + 1$. Suppose also $d_{-1} = 1$ and $d_0 = 1$. Using the Laplace expansion of (3.2), we find that

$$d_i(h) = (h + 2)d_{i-1}(h) - d_{i-2}(h) \quad \text{for } i = 1, \dots, N. \quad (3.3)$$

Equation (3.1) can be written using d_i as

$$\begin{aligned}
 \hat{x} &= \frac{\text{adj}(h(s)I_N - H_N)}{\det(h(s)I_N - H_N)} e_1 \hat{x}_0 \\
 &= \frac{1}{d_N} \begin{bmatrix} d_{N-1} & * & \cdots \\ \vdots & \vdots & \\ d_0 & * & \cdots \end{bmatrix} \begin{bmatrix} 1 \\ 0 \\ \vdots \\ 0 \end{bmatrix} \hat{x}_0 \\
 &= \begin{bmatrix} d_{N-1}/d_N \\ \vdots \\ d_0/d_N \end{bmatrix} \hat{x}_0.
 \end{aligned} \tag{3.4}$$

Then the intermass displacement of the i th mass defined by $\delta_i = x_i - x_{i-1}$ in the Laplace domain is given by

$$\hat{\delta}_i = \frac{d_{N-i} - d_{N-i+1}}{d_N} \hat{x}_0 =: T_{\hat{x}_0 \rightarrow \hat{\delta}_i} \hat{x}_0 \tag{3.5}$$

for $i = 1, \dots, N$.

3.4 Stability of Passive Interconnection

The stability of the system of Fig. 3.2 is discussed in this section. It is firstly shown that, treating h as the independent variable, the sequence $d_i(h)$ defined by (3.2) are Hurwitz with real distinct roots in the interval $(-4, 0)$ for $i = 1, 2, \dots$ and form a Sturm sequence.

Theorem 3.1.

1. $d_i(h)$ has negative real distinct roots which interlace the roots of $d_{i+1}(h)$ for $i = 1, 2, \dots$
2. The roots of $d_i(h)$ lie in the interval $(-4, 0)$ for $i = 1, 2, \dots$

Proof.

1. It is evident that $d_i(0) = 1$ and $d_i(h)$ are continuous and monic for all i . Let a_m for $m = 1, \dots, n+1$ denote the roots of $d_{n+1}(h)$ and b_m the roots of $d_n(h)$ for $m = 1, \dots, n$. Suppose the result holds for $i = n$, namely, $0 > a_1 > b_1 > a_2 >$

$b_2 > \dots > a_n > b_n > a_{n+1}$. Since $d_{n+1}(0) = 1$ and $d_{n+2}(a_1) = -d_n(a_1) < 0$, $d_{n+2}(h)$ has at least one root in $(a_1, 0)$. Similarly, $d_{n+2}(h)$ has at least one root in each interval (a_m, a_{m-1}) for $m = 2, \dots, n+1$ since $d_{n+2}(a_{m-1})d_{n+2}(a_m) = (-d_n(a_{m-1}))(-d_n(a_m)) < 0$ using (6.2). Further $d_n(h)$ and $d_{n+2}(h)$ have the same sign in the limit as $h \rightarrow -\infty$, which is opposite to that of $d_{n+1}(h)$. This implies there exists at least one root of $d_{n+2}(h)$ in $(-\infty, a_{n+1})$. Since $d_{n+2}(h)$ has at most $n+2$ roots, it has exactly one root in each interval. Hence the result holds for $i = n+1$. It is straightforward to check the case of $i = 1$, and the proof then follows by induction.

2. Let $\mathbb{P} = \cup_N \sigma(H_N)$ where $\sigma(\cdot)$ denotes the spectrum. Note that a Gershgorin disc bound on the eigenvalues of H_N [Baroah and Hespanha, 2005; Horn and Johnson, 1999; Lestas and Vinnicombe, 2007] (this holds for all N) implies $\mathbb{P} \subset [-4, 0]$. It is straightforward to check that $d_i(0) = 1$ and $d_i(-4) = (-1)^i(2i+1)$. Hence, the roots of $d_i(h)$ lie in the interval $(-4, 0)$.

■

Note that here the stability of the system of Fig. 3.2 implies that all poles in the transfer functions $T_{\hat{x}_0 \rightarrow \hat{\delta}_i}$ have negative real parts (in the s -domain). Note that [Hara et al., 2014] has investigated the stability of systems which are a generalised version of our model using the notion of “generalized frequency variables.” Here we provide an explicit condition for stability for a general N .

Theorem 3.2. *For $0 \neq Z(s)$ positive real, the system of Fig. 3.2 is stable if $sZ(s)m$ does not take values in the interval $(-4, 0)$ for any s with $\text{Re}(s) = 0$.*

Proof. From (3.4), poles in $T_{\hat{x}_0 \rightarrow \hat{\delta}_i}$ can only occur at an s for which $d_N(h(s)) = 0$. From [Brune, 1931] (Theorem VI) $\text{Re}(Z(s)) > 0$ for $\text{Re}(s) > 0$. The result now follows from Theorem 3.1. ■

3.5 Bidirectional Control in Vehicle Platoons

The control problem introduced in the previous section is similar to the problem of symmetric bidirectional control of a vehicle string, albeit with a passivity constraint. This is one of the longitudinal control schemes for vehicles to travel together in a tightly spaced platoon in an automated highway systems (AHS).

In the constant spacing policy, the aim of the control is to keep a desired spacing between successive vehicles when each vehicle in a platoon follows a lead vehicle that moves

independently (Fig. 3.3). The position of the leader is denoted by $x_0(t)$ and the i th following vehicle is denoted by $x_i(t)$, $i \in \{1, 2, \dots, N\}$. The spacing error of the i th vehicle is then defined by $x_{i-1}(t) - x_i(t) - L$ where L is a desired spacing. Symmetric bidirectional control schemes use only the local spacing information from the immediate neighbours (the predecessor and the follower) and the control law is equally dependent on the spacing errors with the predecessor and the follower. The following assumptions or similar are often made to consider this problem [Barooah and Hespanha, 2005; Barooah et al., 2009; Lestas and Vinnicombe, 2007; Seiler et al., 2004]:

1. All vehicles have the same dynamical model.
2. This dynamical model is linear, single-input-single-output and the combined vehicle-controller dynamics has two integrators.
3. All vehicles use the same control law.
4. The desired spacing is a constant.
5. The string of vehicles start with zero spacing errors and the lead vehicle starts at $x_0(0) = 0$.

With these assumptions, the mass chain model of Fig. 3.2 applies to a platoon of vehicles.

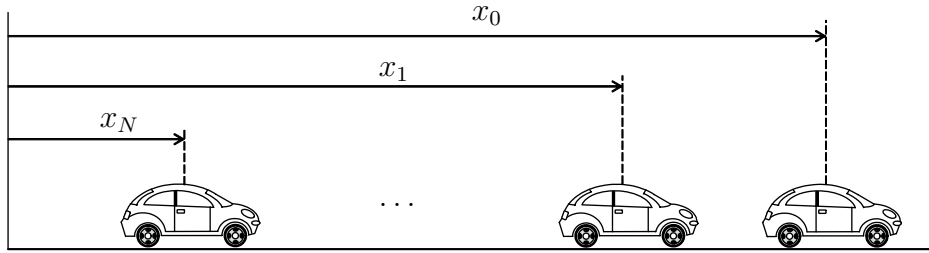


Fig. 3.3 Platoon of N vehicles.

CHAPTER 4

RECURSIVE FEATURES AND UNIFORM BOUNDEDNESS IN HOMOGENEOUS MASS CHAINS

4.1 Overview

In the previous chapter, the transfer functions from the ground displacement to a given inter-mass displacement in a chain of N identical masses are introduced as a function of a complex dimensionless parameter h . It is shown in this chapter that these transfer functions are given recursively in N and therefore interpreted as a complex iterative map, i.e., a sequence of complex numbers for a given fixed h . In particular, each map takes the form of a Möbius transformation which has a rich mathematical background. To understand the behaviour of these transfer functions against the change of system size, this chapter investigates the dynamics of these iterated Möbius transformation. The conditions on h for the convergence to fixed points are firstly derived. These fixed points determine the asymptotic behaviours of the transfer functions. Subsequently these functions are shown to be uniformly bounded with respect to N for a suitable choice of h . As mentioned in the introduction, in [Barooah and Hespanha, 2005] it has been shown that, in the context of automatic control of vehicles, the infinity norm of the vector of these transfer functions grows without bound as the number of vehicles increases, if the combined vehicle-controller dynamics contains a double integrator. This chapter focuses on the scalar transfer functions since well-regulated individual intermass displacements may be a satisfactory performance objective for buildings. The results are also illustrated graphically which are useful to design a suitable interconnection impedance so that the supremum of the \mathcal{H}_∞ -norm over N is no greater than a prescribed value.

4.2 Möbius Transformation

This section gives mathematical preliminaries which are used in this chapter.

Definition 4.1 ([Needham, 1997]). A Möbius transformation is a mapping of the form

$$f(z) = \frac{az + b}{cz + d}$$

where $a, b, c, d \in \mathbb{C}$ and $ad - bc \neq 0$. When $ad - bc = 1$, the Möbius transformation is said to be *normalised*. \diamond

Definition 4.2 ([Beardon, 2001; Needham, 1997]). For a normalised Möbius transformation

$$f(z) = \frac{az + b}{cz + d}, \quad ad - bc = 1,$$

$\text{trace}^2(f) = (a + d)^2$. Now suppose f is not the identity map. Then

1. f is parabolic if and only if $(a + d)^2 = 4$.
2. f is elliptic if and only if $(a + d)^2 \in [0, 4)$.
3. f is loxodromic if and only if $(a + d)^2 \notin [0, 4]$.

\diamond

Note that the above definition uses the terminology of [Beardon, 2001] in which hyperbolic maps are a subclass of loxodromic maps. The class of loxodromic maps divides into two subclasses: a loxodromic map is *hyperbolic* if and only if $(a + d)^2 \in (4, +\infty)$, and it is *strictly loxodromic* if and only if $(a + d)^2 \notin [0, +\infty)$.

Taking *conjugation* is one of the most important technique in studying Möbius transformations [Beardon, 2001].

Definition 4.3 (Conjugation). Let f_1 and f_2 be two Möbius transformations. Then f_1 and f_2 are called *conjugate* if there exists a Möbius transformation φ with $f_1 = \varphi^{-1} \circ f_2 \circ \varphi$. \diamond The transformation $f_1 = \varphi^{-1} \circ f_2 \circ \varphi$ is called a *conjugacy transformation*. The classification given in Definition 4.2 is now characterised in terms of the geometric action of the transformations as follows: A Möbius transformation f is

1. parabolic if it is conjugate to $z \mapsto z + 1$;
2. elliptic if it is conjugate to $z \mapsto \kappa z$ for some κ with $|\kappa| = 1, \kappa \neq 1$;
3. hyperbolic if it is conjugate to $z \mapsto \kappa z$ for some κ with $\kappa > 0$ and $\kappa \neq 1$;
4. loxodromic if it is conjugate to $z \mapsto \kappa z$ for some κ with $|\kappa| \neq 0, 1$.

4.3 Inter-mass Displacements

In the previous chapter, the transfer functions $T_{\hat{x}_0 \rightarrow \hat{\delta}_i}$ from the movable point displacement x_0 to the i th inter-mass displacement δ_i in a homogenous mass chain are introduced as

$$T_{\hat{x}_0 \rightarrow \hat{\delta}_i} = \frac{d_{N-i} - d_{N-i+1}}{d_N} \quad \text{for } i = 1, \dots, N,$$

where

$$d_i = \det(hI_i - H_i) \quad \text{for } i = 1, \dots, N, \quad (4.1)$$

$$H_i = \begin{bmatrix} -2 & 1 & 0 & \cdots & 0 \\ 1 & -2 & 1 & \ddots & \vdots \\ 0 & \ddots & \ddots & \ddots & 0 \\ \vdots & \ddots & 1 & -2 & 1 \\ 0 & \cdots & 0 & 1 & -1 \end{bmatrix} \in \mathbb{R}^{i \times i}$$

which satisfies the following recursion

$$d_i(h) = (h + 2)d_{i-1}(h) - d_{i-2}(h) \quad \text{for } i = 1, \dots, N \quad (4.2)$$

supposing $d_{-1} = 1$ and $d_0 = 1$. In the following theorem $T_{\hat{x}_0 \rightarrow \hat{\delta}_i}$ is represented in the form of complex iterative maps.

Theorem 4.1. *For any $i = 1, 2, \dots$, inter-mass displacements in a chain of N masses satisfy the recursion:*

$$-T_{\hat{x}_0 \rightarrow \hat{\delta}_i} =: F_N^{(i)} = \frac{d_{i-2}F_{N-1}^{(i)} + h}{F_{N-1}^{(i)} + d_i} \quad (4.3)$$

for $N = i, i + 1, \dots$, where $T_{\hat{x}_0 \rightarrow \hat{\delta}_i}$ is the transfer function from the disturbance x_0 to the i th inter-mass displacement δ_i , $F_{i-1}^{(i)} = 0$, $h(s) = sZ(s)m$ and d_i is as defined in (4.1).

Proof. See Appendix 4.A. ■

The above recursion describes a sequence of transfer functions in the complex variable s . It can also be interpreted as a complex iterative map [Devaney, 1989] for a given fixed

$s \in \mathbb{C}$, or equivalently a fixed $h \in \mathbb{C}$. In particular, writing

$$f_i(z) = \frac{d_{i-2}z + h}{z + d_i} \quad (4.4)$$

the sequence $F_N^{(i)}$ for $N = i-1, i, i+1, \dots$ is the same as $0, f_i(0), f_i(f_i(0)), \dots$ for a given $h \in \mathbb{C}$. This is called the orbit of 0 for the recursion (complex iterative map) defined by (4.4).

4.3.1 Convergence to Fixed Points

A complex number μ is called a fixed point of a mapping f if $f(\mu) = \mu$. For a fixed $h \in \mathbb{C}$, the sequence $F_N^{(i)}$ in (4.3) has at most two fixed points $\mu = \mu_{\pm}^{(i)}$ which satisfy

$$\mu^2 + (d_i - d_{i-2})\mu - h = 0. \quad (4.5)$$

It may be observed that (4.4) takes the form of a Möbius transformation which has the normalised form

$$f_i(z) = \frac{az + b}{cz + d} \quad (4.6)$$

where $a = d_{i-2}/d_{i-1}$, $b = h/d_{i-1}$, $c = 1/d_{i-1}$, $d = d_i/d_{i-1}$ and $ad - bc = 1$ since

$$d_{i-2}d_i - d_{i-1}^2 = h \quad (4.7)$$

which is easily shown by induction using (4.2).

The properties of the recursion (4.3) are then determined by $\text{trace}^2(f_i) = (a + d)^2 = (h + 2)^2$ with f_i in (4.6) as follows: f_i is (i) parabolic when $h = 0$ or -4 , (ii) elliptic when $h \in (-4, 0)$ and (iii) loxodromic when $h \notin [-4, 0]$. The following theorem can be shown by the use of a conjugacy transformation.

Theorem 4.2.

1. When $h = 0$ or -4 , there is a unique fixed point, in this case $\mu_+^{(i)}$, and the sequence $\{F_N^{(i)}\}$ defined by (4.3) converges pointwise for any initial condition.
2. When $h \in (-4, 0)$, $\{F_N^{(i)}\}$ fails to converge for any initial condition other than the fixed points.
3. When $h \notin [-4, 0]$, there are two fixed points, an attractive fixed point and a repulsive fixed point, in this case $\mu_+^{(i)}$ and $\mu_-^{(i)}$ respectively, and $\{F_N^{(i)}\}$ converges pointwise to $\mu_+^{(i)}$ for any initial condition other than $\mu_-^{(i)}$.

□

For the specific case of the orbit of 0, Theorem 4.2 specialises to: $\{F_N^{(i)}\}$ converges to $\mu_+^{(i)}$ when $h \notin (-4, 0)$ but fails to converge otherwise. Hence, if $h(s) \notin (-4, 0)$ for all $s \in \mathbb{C}_+$, $\sup_\omega \lim_{N \rightarrow \infty} |F_N^{(i)}(h(j\omega))| = \sup_\omega |\mu_+^{(i)}(h(j\omega))|$. Furthermore, $\sup_\omega |\mu_+^{(i)}(h(j\omega))| \leq \sup_N \|F_N^{(i)}(h(s))\|_\infty$ (since $|\mu_+^{(i)}(h(j\omega))| = \lim_{N \rightarrow \infty} |F_N^{(i)}(h(j\omega))|$). In Theorem 4.4 it is shown that $|\mu_+^{(i)}(h)| < 2$ for any $h \notin [-4, 0]$. However, it is not clear whether $\sup_N \|F_N^{(i)}\|_\infty$ can be suitably bounded or indeed whether it is finite. This result will be shown in Theorem 4.5. The proof relies on the conjugacy transformation of $f_i(z)$ which is explicitly described in the next theorem.

Theorem 4.3. For $h \notin [-4, 0]$

$$f_i(z) = \frac{d_{i-2}z + h}{z + d_i} = \varphi_i^{-1} \circ \lambda_i \circ \varphi_i(z) \quad (4.8)$$

with

$$\begin{aligned} \varphi_i(z) &= \frac{z - \mu_+^{(i)}}{z - \mu_-^{(i)}}, \\ \varphi_i^{-1}(z) &= \frac{\mu_+^{(i)} - z\mu_-^{(i)}}{1 - z}, \\ \lambda_i(z) &= \frac{d_{i-2} - \mu_+^{(i)}}{d_{i-2} - \mu_-^{(i)}}z \end{aligned} \quad (4.10a)$$

$$= \zeta^2 z \quad (4.10b)$$

where

$$\zeta = \frac{d_{i-2} - \mu_+^{(i)}}{d_{i-1}}. \quad (4.10c)$$

Moreover, ζ is independent of i and is the root of

$$\zeta^2 - (h + 2)\zeta + 1 = 0 \quad (4.10d)$$

satisfying $|\zeta| < 1$.

Proof. (4.8) with (4.10a) follows by direct algebraic computation. In Appendix 4.B it is shown that (4.10b) and (4.10d) hold for ζ as defined in (4.10c). One can check directly that (4.10d) has roots ζ_+ , ζ_- satisfying $|\zeta_+| < 1 < |\zeta_-|$ if and only if $h \notin [-4, 0]$. In this case (4.10c) holds with $\zeta = \zeta_+$. ■

Remark 4.1. For $h \notin [-4, 0]$, the labelling of the roots $\mu_+^{(i)}, \mu_-^{(i)}$ of (4.5) can be determined by finding the root ζ_+ of (4.10d) which satisfies $\zeta_+ < 1$ and then solving (4.10c) for $\mu_+^{(i)}$. ♡

Theorem 4.4. For $h \notin [-4, 0]$

$$\mu_+^{(i+1)} = \zeta \mu_+^{(i)} \quad (4.11)$$

and

$$|\mu_+^{(i)}| < |\mu_+^{(i-1)}| < \dots < |\mu_+^{(1)}| < 2 \quad (4.12)$$

where ζ is as defined in (4.10c).

Proof. Since ζ is independent of i ,

$$\zeta = \frac{d_{i-2} - \mu_+^{(i)}}{d_{i-1}} = \frac{d_{i-1} - \mu_+^{(i+1)}}{d_i}.$$

Therefore,

$$\begin{aligned} \mu_+^{(i+1)} &= \frac{d_i \mu_+^{(i)} + d_{i-1}^2 - d_{i-2} d_i}{d_{i-1}} \\ &= \frac{d_i \mu_+^{(i)} - h}{d_{i-1}} \quad (\text{see (4.7)}) \\ &= \frac{d_i \mu_+^{(i)} - (\mu_+^{(i)})^2 + (d_i - d_{i-2}) \mu_+^{(i)}}{d_{i-1}} \quad (\text{see (4.5)}) \\ &= \frac{d_{i-2} - \mu_+^{(i)}}{d_{i-1}} \mu_+^{(i)} \\ &= \zeta \mu_+^{(i)}. \end{aligned}$$

Since $|\zeta| < 1$ if $h \notin [-4, 0]$ and $\mu_+^{(1)} = 1 - \zeta$ given by substituting $i = 1$ in (4.10c),

$$|\mu_+^{(i)}| < |\mu_+^{(i-1)}| < \dots < |\mu_+^{(1)}| = |1 - \zeta| < 2.$$

■

Remark 4.2. Equation (4.11) holds also for $h \in [-4, 0]$. In particular, if $h = 0$ or -4 , (4.10d) has a multiple root and (4.10c) determines a unique fixed point. If $h \in (-4, 0)$, two roots of (4.10d) ζ_+ and ζ_- satisfy $|\zeta_+| = |\zeta_-| = 1$, and either root may be selected for ζ_+ with $\mu_+^{(i)}$ then determined by (4.10c). Consequently, if $h \in [-4, 0]$, $|\mu_+^{(i)}| = |\mu_+^{(i-1)}| = \dots = |\mu_+^{(1)}| \leq 2$. The equality $|\mu_+^{(1)}| = 2$ holds only when $\zeta = -1$ corresponding to $h = -4$. ♡

4.4 Bounds on Iterative Maps

Considering the orbit of 0 for (4.8), for $N = i - 1, i, \dots$,

$$\begin{aligned}
 F_N^{(i)} &= f_i^{N-i+1}(0) = \varphi_i^{-1} \circ \lambda_i^{N-i+1} \circ \varphi_i(0) \\
 &= \mu_+^{(i)} \frac{1 - \zeta^{2(N-i+1)}}{1 - \frac{\mu_+^{(i)}}{\mu_-^{(i)}} \zeta^{2(N-i+1)}} \\
 &= \mu_+^{(i)} \frac{1 - \zeta^{2(N-i+1)}}{1 + \zeta^{2N+1}}
 \end{aligned} \tag{4.13}$$

since

$$\varphi_i(0) = \mu_+^{(i)} / \mu_-^{(i)} = -\zeta^{2i-1} \tag{4.14}$$

(see Appendix 4.C).

Now upper bounds on $|F_N^{(i)}|$ are established for suitable choices of $h(s)$ making use of (4.13).

Theorem 4.5. *Suppose $Z(s) = (k/s + Y_a(s))^{-1}$ where k is a positive constant and $Y_a(s)$ is a positive-real admittance satisfying $Y_a(0) > 0$. Suppose $h(j\omega) = mj\omega Z(j\omega)$ does not intersect the interval $[-4, 0)$ for any $\omega \geq 0$. Then*

$$\sup_{N \geq i} \left\| F_N^{(i)}(h(s)) \right\|_\infty$$

is finite for any $i = 1, 2, \dots$

Proof. See Appendix 4.D. ■

Note that the condition that $h(s)$ does not intersect $[-4, 0)$ is equivalent to $m\omega Z(j\omega)$ not touching the imaginary axis between $(0, j4]$ since $Z(s)$ is positive real ($\text{Re}(Z(j\omega)) \geq 0$ for all ω). This essentially means that the mechanical impedance does not behave in a purely lossless manner for any frequencies for which $m\omega Z(j\omega) \in (0, j4]$, which is a very mild condition that is easy to satisfy (and hard to violate) in practice. The condition $Y_a(0) > 0$ can be interpreted in the same manner.

Theorem 4.5 shows that the individual transfer functions from x_0 to a given intermass displacement are uniformly bounded with respect to the size of the chain of masses for a suitable choice of h . It is evident that the increasing length of the error vector as $N \rightarrow \infty$ is playing a role in the unboundedness property of [Barooah and Hespanha, 2005], and that the unboundedness of the vector need not imply that the \mathcal{H}_∞ -norm of individual entries is

unbounded with N . In this sense our result could be viewed as a relaxation of the definition of string stability.

Remark 4.3. The proposed measure satisfies basic properties of norms:

$$\begin{aligned} \sup_j \|x_j\|_\infty &= 0 \quad \text{if and only if } x_j = 0 \text{ for all } j, \\ \sup_j \|\alpha x_j\|_\infty &= |\alpha| \sup_j \|x_j\|_\infty \quad \forall \alpha \in \mathbb{C}, \\ \sup_j \|x_j + y_j\|_\infty &\leq \sup_j (\|x_j\|_\infty + \|y_j\|_\infty) \leq \sup_j \|x_j\|_\infty + \sup_j \|y_j\|_\infty. \end{aligned}$$

♡

4.4.1 Examples

For the purpose of graphical representations the inverse of h is now introduced:

$$g(s) = h^{-1}(s) = Y(s)/(sm). \quad (4.15)$$

From (4.13) the speed of convergence of $F_N^{(i)}$ to $\mu_+^{(i)}$ is determined by $|\zeta|$, with the slowest convergence occurring for $|\zeta|$ close to 1. Fig. 4.1 shows a contour plot of $|\zeta|$ where $h = g^{-1}$ which shows that the speed of convergence will be slower when g is closer to the real axis between $(-\infty, -1/4)$ (corresponding to $h \in (-4, 0)$).

A contour plot of the magnitude of $\mu_+^{(1)}$ in the g -plane is shown in Fig. 4.2. The outermost boundary represents $\ln |\mu_+^{(1)}| = -1.5$ and the spacing of the contour is 0.1. As stated in Remark 4.2, $|\mu_+^{(1)}|$ takes its maximum value 2 ($\approx \ln(0.693)$) when $g = -1/4$. The figure shows that the asymptotic value of $F_N^{(1)}(j\omega)$ as $N \rightarrow \infty$ is directly related to the proximity of $h(j\omega)^{-1}$ to the point $-1/4$.

The boundedness result of Theorem 4.5 is now illustrated graphically. Figure 4.3 shows the region of the complex values of $g (= h^{-1})$ for which $\max_N |F_N^{(1)}(h)| \leq \gamma$ with $1 \leq N \leq 200$ for a positive constant γ . The spacing of the contours is 0.2 where $\ln(\gamma)$ takes the value 0, 0.2, 0.4, \dots . The outermost boundary represents $\gamma = 1$ and \mathcal{G}_1 denotes the set $\{g \in \mathbb{C} : \max_N |F_N^{(1)}(g^{-1})| \leq 1\}$. This means that $\max_N \|F_N^{(1)}(h(s))\|_\infty \leq 1$ if and only if $g(s) \in \mathcal{G}_1$ for $s \in \mathbb{C}_+$. Note that from Fig. 4.1 the sequence $\{F_N^{(1)}\}$ converges to the fixed point $\mu_+^{(1)}$ quickly when $g \in \mathcal{G}_1$ so the choice of $N = 200$ is large enough to accurately determine the shape of the boundary in the figure. Figure 4.4 is a similar figure to Fig. 4.3 but shows a contours of $\max_i \max_N |F_N^{(i)}(h)| = \gamma \in \mathbb{R}_+$ for $i = 1, 2, \dots, N, i \leq N \leq 200$ with the Nyquist diagrams of $g(s)$ of three passive vibration control devices. The layouts of these devices are shown in Table 4.1a and their structural parameters are given in Table 4.1b. The

parameters of the building model are fixed as $m = 1.0 \times 10^5$ kg, $k = 1.7 \times 10^5$ kN/m (based on values given in [Léger and Dussault, 1992]). The outermost boundary of the contours again represents $\gamma = 1$ so $\max_i \max_N \|F_N^{(i)}(h(s))\|_\infty \leq 1$ if the Nyquist diagram $g(j\omega)$ lies outside this boundary. It can be seen that devices 2 and 3 achieve this. It is also observed that the use of the inerters improves the high frequency performance (corresponding to the origin in the g -plane). The frequency domain plots of $\max_i |F_N^{(i)}(j\omega)|$ (Figs. 4.5 and 4.6) confirm these observations. Figure 4.7 shows the curves which represent $\max_N |F_N^{(i)}| = 1$ where $i = 1, 2, \dots, 5$ with $1 \leq N \leq 200$. It is observed that the set $\{g \in \mathbb{C} : \max_N |F_N^{(1)}(g^{-1})| \leq 1\}$ contains the sets $\{g \in \mathbb{C} : \max_N |F_N^{(i)}(g^{-1})| \leq 1\}$, $i = 2, \dots, 5$.

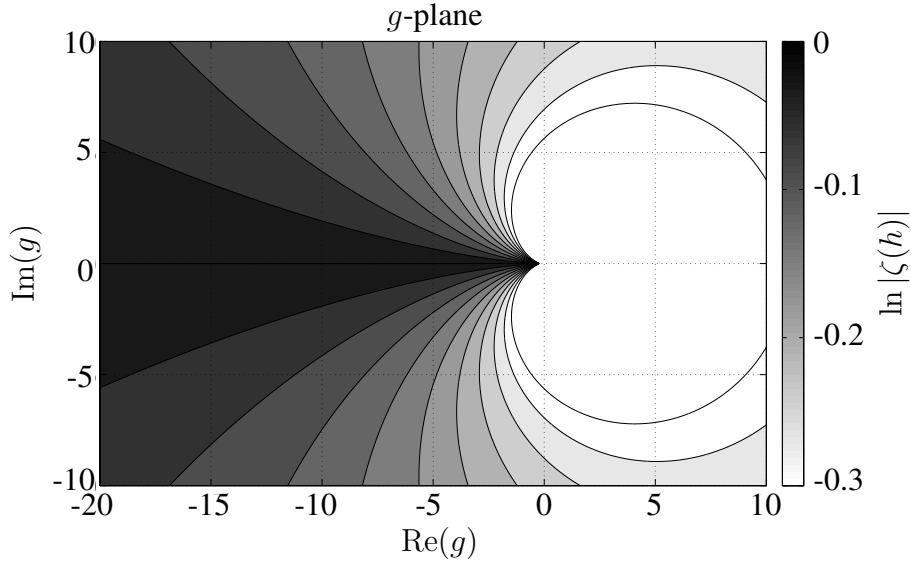


Fig. 4.1 Contour plot of $|\zeta(h)|$ where $h = g^{-1}$.

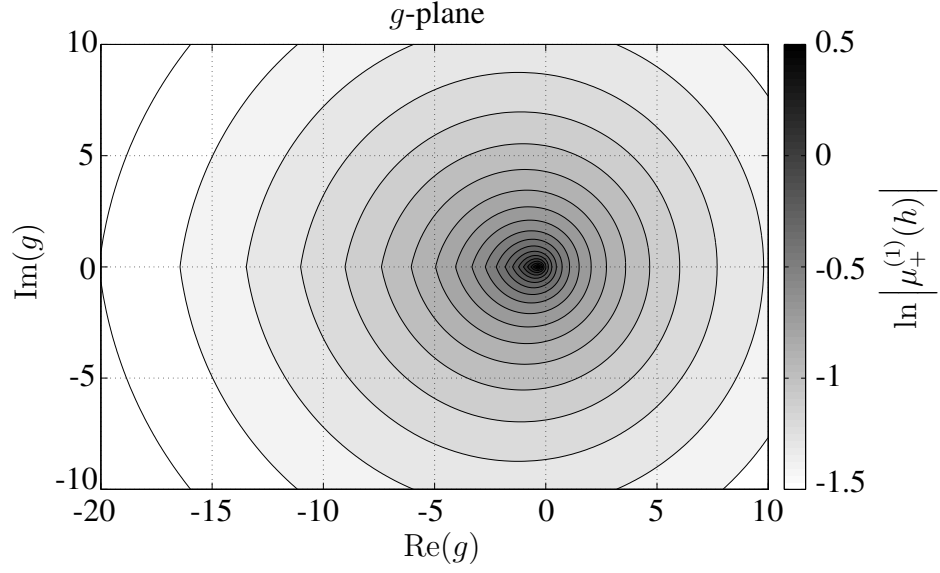


Fig. 4.2 Contour plot of $|\mu_+^{(1)}(h)|$ where $h = g^{-1}$.

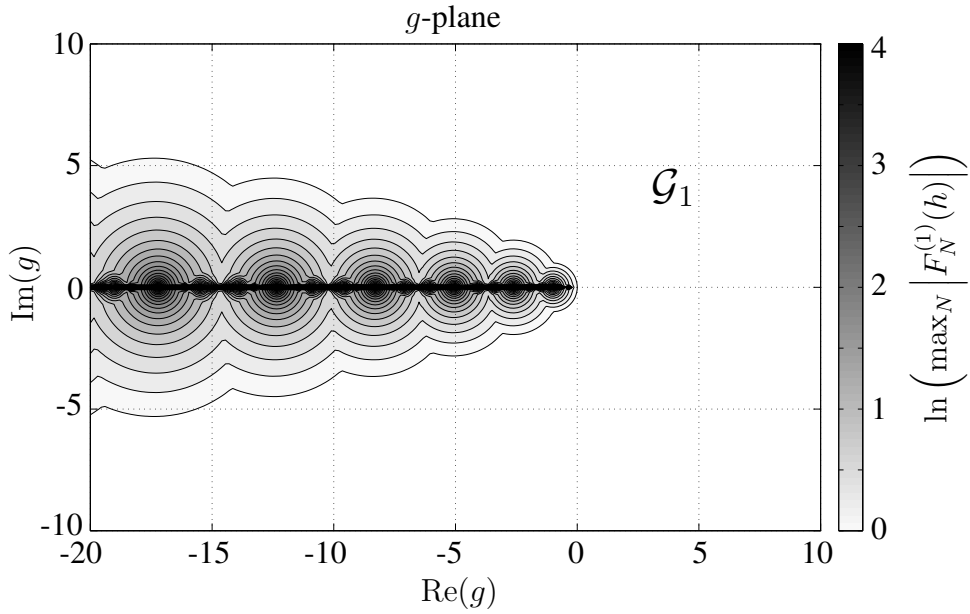
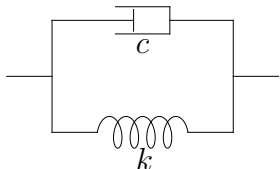
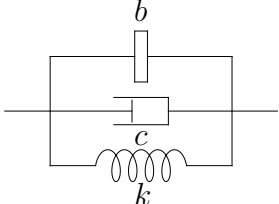


Fig. 4.3 Contour plot of $\max_N |F_N^{(1)}(h)| = \gamma$ for $\ln(\gamma) = 0, 0.2, 0.4, \dots$ where $h = g^{-1}$.

(a) Interconnection layouts and the corresponding admittances.

L1	L2
$Y(s) = c + \frac{k}{s}$	$Y(s) = bs + c + \frac{k}{s}$
	

(b) Parameters of vibration control devices.

	Layout	c (kNs/m)	b (kg)
Device 1	L1	4.0×10^3	—
Device 2	L1	6.0×10^3	—
Device 3	L2	6.0×10^3	1.0×10^5

Table 4.1 Interconnection layouts and their parameters.

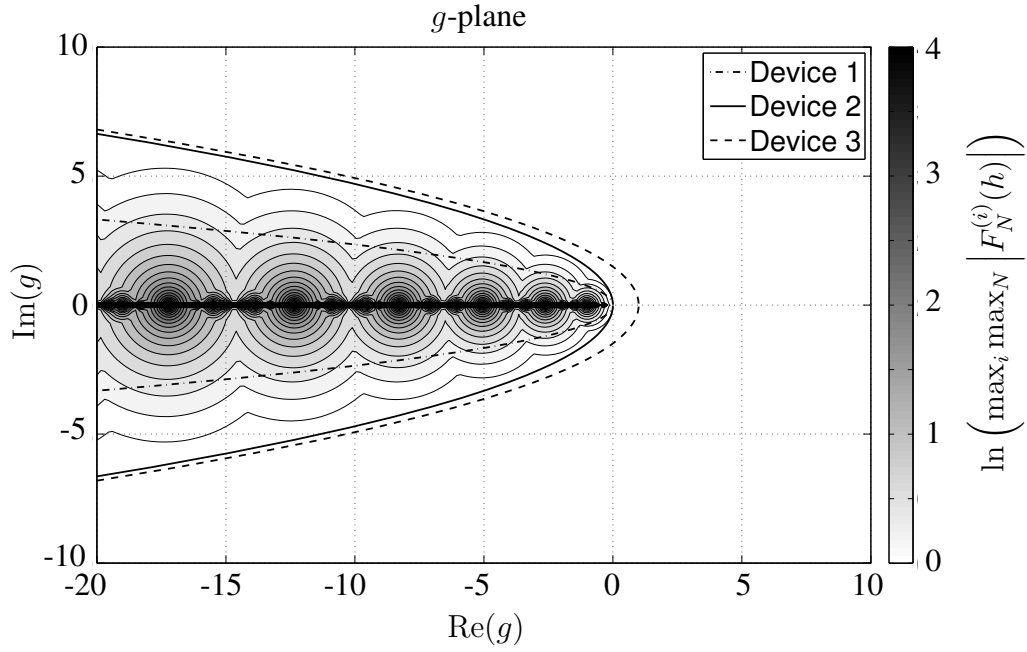


Fig. 4.4 Nyquist diagrams of $g(s) = Y(s)/(sm)$ for the vibration control devices in Table 4.1b and contour plot of $\max_i \max_N |F_N^{(i)}(h)| = \gamma$ for $\ln(\gamma) = 0, 0.2, 0.4, \dots$ where $h = g^{-1}$.

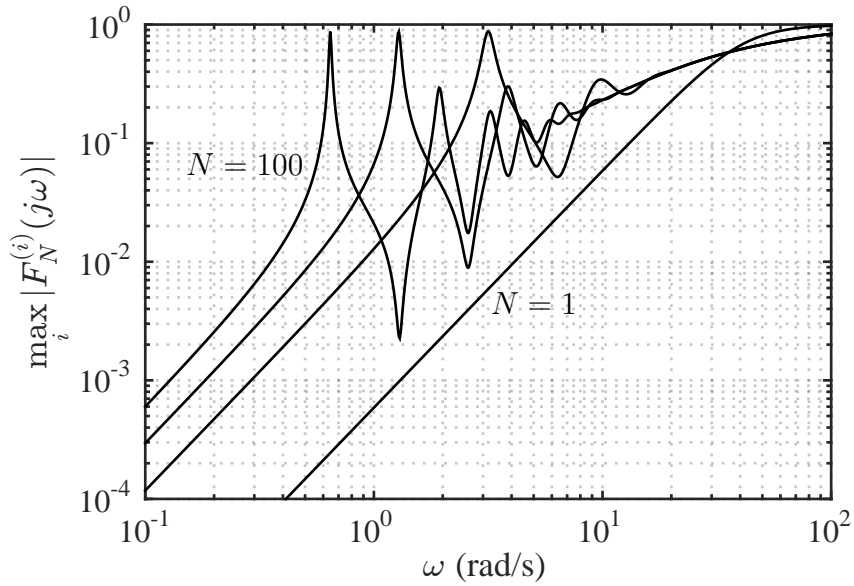


Fig. 4.5 $\max_i |F_N^{(i)}(j\omega)|$ using Device 2 for $N = 1, 20, 50, 100$.

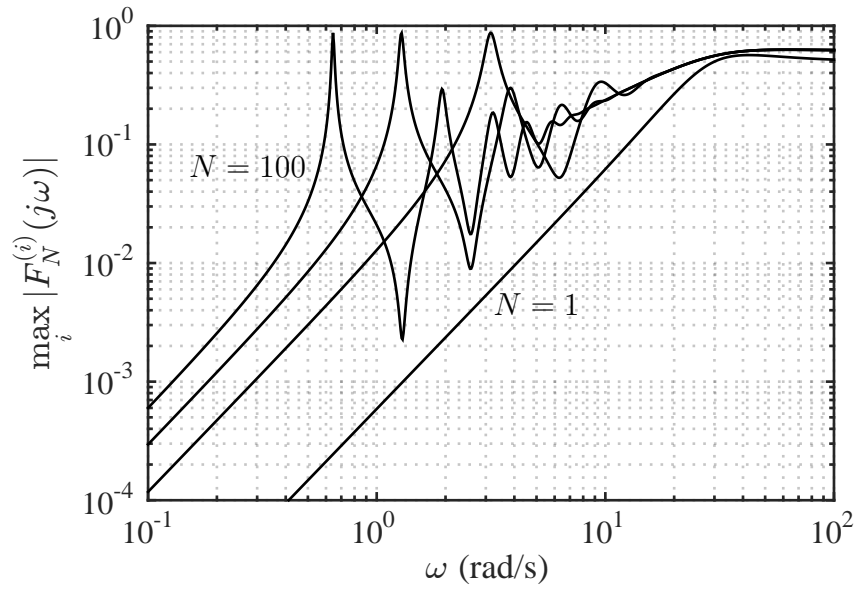


Fig. 4.6 $\max_i |F_N^{(i)}(j\omega)|$ using Device 3 for $N = 1, 20, 50, 100$.

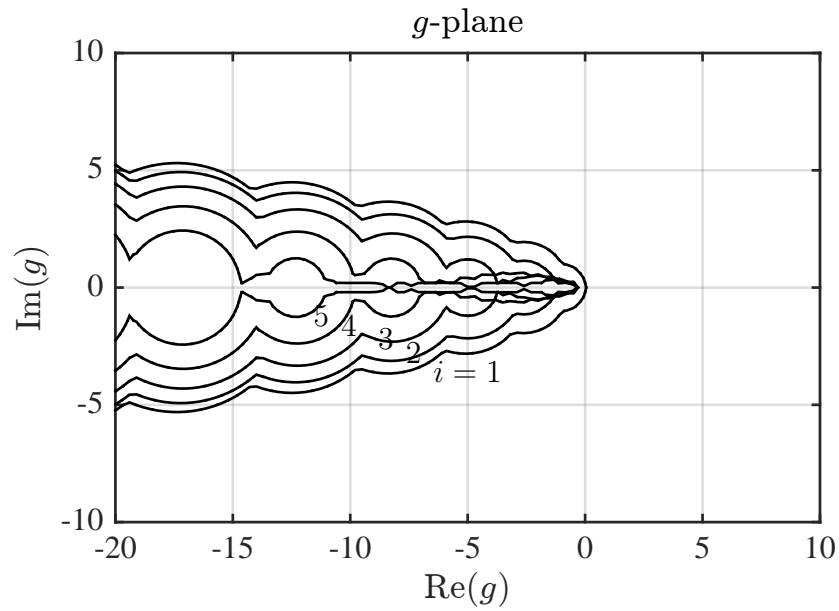


Fig. 4.7 Curves representing $\max_N |F_N^{(i)}(h)| = 1$ for $i = 1, 2, \dots, 5$ where $h = g^{-1}$.

Appendix 4.A Proof of Theorem 4.1

Proof. Define

$$p(N, i) = \overbrace{(d_{N-i+1} - d_{N-i})(d_{N-i} - d_{N-i-1} + d_{N-1}d_i)} - d_N d_{i-2}(d_{N-i} - d_{N-i-1}) - h d_{N-1} d_N. \quad (4.16)$$

From (3.5) and the recursion of $F_N^{(i)}$ in (4.3), it may be seen that the theorem is equivalent to $p(N, i) = 0$ for all $i \in \mathbb{N}$ and $i \leq N \in \mathbb{N}$. The proof will follow by induction after establishing the following facts:

1. $p(N, 1) = 0$ for all $N \geq 1$.
2. $p(N, 2) = 0$ for all $N \geq 2$.
3. $p(N, i) = p(N, i-1) + p(N-1, i-1) - p(N-1, i-2)$ for any $i \geq 3, N \geq i$.

Now these facts are established in turn.

$$\begin{aligned} 1. \quad p(N, 1) &= (d_N - d_{N-1} - d_N d_{-1})(d_{N-1} - d_{N-2}) \\ &\quad + d_{N-1}(d_1(d_N - d_{N-1}) - h d_N) \\ &= d_{N-1}(d_N - (h+2)d_{N-1} + d_{N-2}) \\ &= 0, \end{aligned}$$

where the second step uses $d_{-1} = 1$ and $d_1 = h+1$, and the third step follows from (4.2).

$$\begin{aligned} 2. \quad p(N, 2) &= (d_{N-1} - d_{N-2} - d_N d_0)(d_{N-2} - d_{N-3}) \\ &\quad + d_{N-1} d_2(d_{N-1} - d_{N-2}) - h d_{N-1} d_N \\ &= -(h+1)d_{N-1}(d_{N-1} - (h+1)d_{N-2}) \\ &\quad + d_{N-1}(h^2 + 3h + 1)(d_{N-1} - d_{N-2}) \\ &\quad - h d_{N-1} d_N \\ &= -h d_{N-1}(d_N - (h+2)d_{N-1} + d_{N-2}) \\ &= 0, \end{aligned}$$

where the second step follows from $d_{N-2} - d_{N-3} = d_{N-2} - ((h+2)d_{N-2} - d_{N-1})$, $d_{N-1} - d_{N-2} - d_N d_0 = d_{N-1} - ((h+2)d_{N-1} - d_N) - d_N$ and $d_2 = h^2 + 3h + 1$ using (4.2).

3. Consider the expression

$$\begin{aligned} X(N, i) &= p(N, i) - p(N, i-1) \\ &\quad - p(N-1, i-1) + p(N-1, i-2). \end{aligned} \quad (4.17)$$

It may be observed that the four terms in (4.17) corresponding to the overbrace in (4.16) cancel pairwise. Also the four terms in (4.17) of the form $-hd_{N-1}d_N$ cancel pairwise. Thus

$$\begin{aligned} X(N, i) &= (d_{N-i} - d_{N-i-1})(d_{N-1}d_{i-3} - d_Nd_{i-2}) \\ &\quad + (d_{N-i+1} - d_{N-i})(d_{N-1}d_i + d_Nd_{i-3} \\ &\quad \quad \quad - d_{N-2}d_{i-1} - d_{N-1}d_{i-4}) \\ &\quad + (d_{N-i+2} - d_{N-i+1})(d_{N-2}d_{i-2} - d_{N-1}d_{i-1}). \end{aligned} \quad (4.18)$$

Using the following substitution

$$\begin{aligned} d_i &= (h+2)d_{i-1} - d_{i-2} \\ d_N &= (h+2)d_{N-1} - d_{N-2} \\ d_{i-1} &= (h+2)d_{i-2} - d_{i-3} \\ d_{i-4} &= (h+2)d_{i-3} - d_{i-2} \end{aligned}$$

in the second term of (4.18) and rearranging gives

$$\begin{aligned} X(N, i) &= (d_{N-i} - d_{N-i-1})(d_{N-1}d_{i-3} - d_Nd_{i-2}) \\ &\quad + (d_{N-2}d_{i-2} - d_{N-1}d_{i-1})(d_{N-i+2} - d_{N-i+1} - (h+2)(d_{N-i+1} - d_{N-i})). \end{aligned}$$

Now note that

$$\begin{aligned} d_{N-i+2} - d_{N-i+1} - (h+2)(d_{N-i+1} - d_{N-i}) &= (h+1)d_{N-i} - d_{N-i+1} \\ &= -(d_{N-i} - d_{N-i-1}). \end{aligned}$$

Hence

$$\begin{aligned}
X(N, i) &= (d_{N-i} - d_{N-i-1})(d_{N-1}d_{i-3} - d_N d_{i-2} - d_{N-2}d_{i-2} + d_{N-1}d_{i-1}) \\
&= (d_{N-i} - d_{N-i-1})(d_{N-1}d_{i-3} - (h+2)d_{N-1}d_{i-2} \\
&\quad + d_{N-2}d_{i-2} - d_{N-2}d_{i-2} + (h+2)d_{N-1}d_{i-2} - d_{N-1}d_{i-3}) \\
&= 0.
\end{aligned}$$

■

Appendix 4.B Proof of (4.10b) and (4.10d)

Proof. First (4.10b) is shown.

$$\begin{aligned}
\frac{d_{i-2} - \mu_+^{(i)}}{d_{i-2} - \mu_-^{(i)}} &= \frac{d_{i-2} - \mu_+^{(i)}}{d_{i-2} - \mu_-^{(i)}} \times \frac{d_{i-2} - \mu_+^{(i)}}{d_{i-2} - \mu_+^{(i)}} \\
&= \frac{(d_{i-2} - \mu_+^{(i)})^2}{d_{i-2}^2 - d_{i-2}(\mu_+^{(i)} + \mu_-^{(i)}) + \mu_+^{(i)}\mu_-^{(i)}} \\
&= \frac{(d_{i-2} - \mu_+^{(i)})^2}{d_{i-2}d_i - h} \\
&= \left(\frac{d_{i-2} - \mu_+^{(i)}}{d_i} \right)^2 \\
&= \zeta^2
\end{aligned}$$

where the third step follows from $\mu_+^{(i)} + \mu_-^{(i)} = -(d_i - d_{i-2})$ and $\mu_+^{(i)}\mu_-^{(i)} = -h$ (see (4.5)) and the fourth step follows from (4.7).

To show (4.10d), note that

$$\begin{aligned}
 \zeta + \frac{1}{\zeta} &= \frac{d_{i-2} - \mu_+^{(i)}}{d_{i-1}} + \frac{d_{i-1}}{d_{i-2} - \mu_+^{(i)}} \\
 &= \frac{d_{i-2}^2 - 2d_{i-2}\mu_+^{(i)} + \mu_+^{(i)2} + d_{i-1}^2}{d_{i-1}(d_{i-2} - \mu_+^{(i)})} \\
 &= \frac{(d_{i-2} + d_{i-1})(d_{i-2} - \mu_+^{(i)})}{d_{i-1}(d_{i-2} - \mu_+^{(i)})} \\
 &= h + 2
 \end{aligned}$$

where the third step substitutes for $\mu_+^{(i)2}$ and d_{i-1}^2 from (4.5) and (4.7) and the fourth step uses (4.2). ■

Appendix 4.C Proof of (4.14)

Proof. Since $\mu_{\pm}^{(i)}$ are the solutions of (4.5), $\mu_+^{(i)} \mu_-^{(i)} = -h$. Therefore,

$$\begin{aligned}
 \frac{\mu_+^{(i)}}{\mu_-^{(i)}} &= -\frac{\mu_+^{(i)2}}{h} \\
 &= -\frac{\left(\zeta^{i-1} \mu_+^{(1)}\right)^2}{h} \\
 &= -\zeta^{2i-2} \left(1 - \mu_+^{(1)}\right) \\
 &= -\zeta^{2i-1},
 \end{aligned}$$

where (4.11), (4.5) and (4.10c) are used in the second, third and fourth steps above. ■

Appendix 4.D Proof of Theorem 4.5

Two lemmas are first established which are needed in the proof of this theorem. The first lemma gives a relatively straightforward bound on $\sup_{N \geq i} |F_N^{(i)}(h)|$ for h bounded away from the interval $[-4, 0]$. The second lemma is significantly more delicate and deals with the fact that $h(j\omega) \rightarrow 0$ as $\omega \rightarrow 0$. The manner in which this convergence occurs is critical to establish an upper bound.

Lemma 4.1. *Let $h \in \mathbb{C}$ lie on an ellipse with foci $(-4, 0)$ and $(0, 0)$, and semi-major axis A . Then*

$$\sup_{N \geq i} |F_N^{(i)}| \leq \frac{(1 + |\zeta|)(1 + |\zeta|^2)}{1 - |\zeta|^3}$$

where ζ is defined by (4.10c). Moreover

$$|\zeta| = \frac{A - \sqrt{A^2 - 4}}{2}, \quad A = \frac{|h| + |h + 4|}{2}.$$

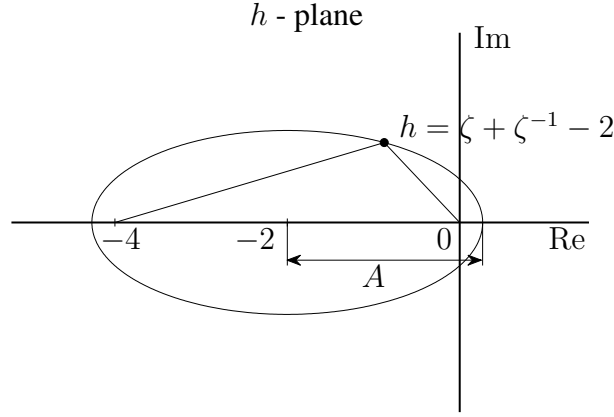


Fig. 4.8 The ellipse defined by $h = \zeta + \zeta^{-1} - 2$ for $|\zeta|$ fixed and $\arg(\zeta)$ varying.

Proof. From (4.10d), $\zeta + \zeta^{-1} = h + 2$. Letting $\zeta = |\zeta|e^{j\theta}$, $-\pi \leq \theta \leq \pi$,

$$\left(|\zeta| + \frac{1}{|\zeta|}\right) \cos \theta + j \left(|\zeta| - \frac{1}{|\zeta|}\right) \sin \theta = h + 2. \quad (4.19)$$

Keeping $|\zeta|$ fixed and solving (4.19) for h as a function of θ gives an ellipse in the h -plane with centre $(-2, 0)$, foci $(-4, 0)$, $(0, 0)$ and semi-major axis $A = |\zeta| + 1/|\zeta|$ (Fig. 4.8). Therefore $|\zeta| = (A - \sqrt{A^2 - 4})/2$ where $A > 2$ and $|\zeta| < 1$. Since the sum of the distances from the two foci and to a point on the ellipse is constant and equal to the major axis,

$$A = \frac{|h| + |h + 4|}{2}. \quad (4.20)$$

Then from (4.13), for all $N \geq i \geq 1$,

$$\begin{aligned} \sup_{N \geq i} |F_N^{(i)}| &\leq |\mu_+^{(1)}| \frac{1 + |\zeta|^2}{1 - |\zeta|^3} \\ &\leq \frac{(1 + |\zeta|)(1 + |\zeta|^2)}{1 - |\zeta|^3} \end{aligned}$$

since $|\mu_+^{(i)}| < |\mu_+^{(1)}|$ as shown in Theorem 4.4 and $\mu_+^{(1)} = 1 - \zeta$. ■

Lemma 4.2. *Let $h(s)$ be defined as in Theorem 4.5. Then $h(j\omega) = -c_1\omega^2 + jc_2\omega^3 + \omega^4 h_1(j\omega)$ for $\omega \geq 0$ where c_1 and c_2 are positive constants and $|h_1(j\omega)| \leq c_3 \in \mathbb{R}_+$ for $0 \leq \omega \leq \omega_1$. Furthermore there exists ω_0 with $0 < \omega_0 \leq \omega_1$ such that*

$$\sup_{N \geq i} |F_N^{(i)}(h(j\omega))| < \frac{2\sqrt{c_1 + c_2 + c_3\omega_0}}{1 - \exp\left(-\frac{(c_2 - \omega_0 c_3)\pi\omega_0}{8c_4^2}\right)}$$

for $0 \leq \omega < \omega_0$ where $c_4 = \sqrt{2(2c_1 + c_2 + 2c_3)}$.

Proof. First note that when $\omega = 0$, $h(j\omega) = 0$ and $|F_N^{(i)}| = 0$ for any $N \geq i$ from (4.3).

When $\omega \neq 0$, $h \notin [-4, 0]$ and therefore ζ as defined in (4.10c) is nonreal and $|\zeta| < 1$. Hence $|1 - \zeta^{2(N-i+1)}| < 1 + |\zeta|^2$. The magnitude of the denominator in (4.13) takes its smallest value when ζ^{2N+1} is at the closest point to -1 . Let p be the positive real number such that ζ^p has the minimum real part. With p defined in this way, the smallest value is always larger than $1 - |\zeta|^p$. Therefore,

$$\sup_{N \geq i} |F_N^{(i)}| \leq |\mu_+^{(1)}| \frac{1 + |\zeta|^2}{1 - |\zeta|^p}. \quad (4.21)$$

Since $\mu_+^{(1)2} = h(1 - \mu_+^{(1)}) = h\zeta$ from (4.5) and (4.10c), for $0 < \omega \leq \min\{1, \omega_1\}$,

$$\begin{aligned} |\mu_+^{(1)}|^2 &< |h| \\ &\leq |-c_1\omega^2 + jc_2\omega^3| + |\omega^4 h_1(j\omega)| \\ &\leq \sqrt{(c_1^2 + c_2^2)\omega^4} + |h_1(j\omega)|\omega^2 \\ &\leq (c_1 + c_2 + c_3)\omega^2. \end{aligned} \quad (4.22)$$

Therefore, the numerator in (4.21) is bounded above:

$$|\mu_+^{(1)}|(1 + |\zeta|^2) < 2\sqrt{c_1 + c_2 + c_3}\omega.$$

Next, a lower bound on the denominator in (4.21) is shown. First note the general inequality

$$|\zeta| + \frac{1}{|\zeta|} > 2. \quad (4.23)$$

Defining A as in (4.20), $A \leq 2 + |h|$ is obtained. Writing $\zeta = |\zeta|e^{j\theta}$, from (4.10d), $A \cos \theta = \operatorname{Re}(h + 2) = 2 - (c_1 - \omega^2 \operatorname{Re}(h_1(j\omega)))\omega^2 \geq 2 - (c_1 + c_3)\omega^2$. Hence,

$$\begin{aligned} \cos \theta &= \frac{\operatorname{Re}(h + 2)}{A} \\ &\geq \frac{2 - (c_1 + c_3)\omega^2}{2 + |h|} = 1 - \frac{(c_1 + c_3)\omega^2 + |h|}{2 + |h|} \end{aligned}$$

and if $\omega \leq \sqrt{2/(c_1 + c_3)}$, $-\pi/2 \leq \theta \leq \pi/2$. On the other hand, $\cos \theta \leq 1 - \theta^2/4$ when $-\pi/2 \leq \theta \leq \pi/2$. Therefore, for $0 < \omega \leq \min\{1, \omega_1, \sqrt{2/(c_1 + c_3)}\}$,

$$\begin{aligned} |\theta| &\leq 2\sqrt{\frac{(c_1 + c_3)\omega^2 + |h|}{2 + |h|}} \\ &\leq 2\sqrt{\frac{(c_1 + c_3)\omega^2 + (c_1 + c_2 + c_3)\omega^2}{2}} \\ &= \sqrt{2(2c_1 + c_2 + 2c_3)}\omega \\ &=: c_4\omega \end{aligned}$$

using (4.22). Also, $\operatorname{Im}(h + 2) = (c_2 + \omega \operatorname{Im}(h_1(j\omega)))\omega^3 \geq (c_2 - \omega c_3)\omega^3 > 0$ when $\omega < c_2/c_3$. Hence

$$\frac{1}{|\zeta|} - |\zeta| = \left| \frac{\operatorname{Im}(h + 2)}{\sin \theta} \right| \geq \frac{(c_2 - \omega c_3)\omega^2}{c_4} \quad (4.24)$$

for $0 < \omega < \min\{1, \omega_1, \sqrt{2/(c_1 + c_3)}, c_2/c_3\}$. Also note that $-\pi < \theta < 0$ follows from (4.19) when $\operatorname{Im}(h + 2) > 0$. Adding (4.24) to (4.23) gives

$$\frac{2}{|\zeta|} > 2 + \frac{(c_2 - \omega c_3)\omega^2}{c_4}$$

and therefore,

$$\begin{aligned} |\zeta| &< \frac{2c_4}{2c_4 + (c_2 - \omega c_3)\omega^2} \\ &\leq 1 - \frac{(c_2 - \omega c_3)\omega^2}{4c_4} \end{aligned} \quad (4.25)$$

if $0 \leq (c_2 - \omega c_3)\omega^2 / 2c_4 \leq 1$. This condition is satisfied if $\omega \leq c_2/c_3$ and $\omega \leq \sqrt{2c_4/c_2}$.

Now let $\omega_0 = \min\{1, \omega_1, \sqrt{2/(c_1 + c_3)}, c_2/c_3, \sqrt{2c_4/c_2}\}$. Since p is the positive real number such that ζ^p has minimum real part, it is shown that $-\pi \leq p\theta < 0$ on noting that $-\pi/2 \leq \theta < 0$ for $\omega < \omega_0$. Further observe that $-\pi \leq p\theta \leq -\pi/2$, which gives

$$p \geq \frac{\pi}{2|\theta|} > \frac{\pi}{2c_4\omega}. \quad (4.26)$$

Using (4.25) and (4.26), since $(1 - x/n)^n < e^{-x}$ for $x/n \leq 1$,

$$\begin{aligned} |\zeta|^p &< \left(1 - \frac{(c_2 - \omega c_3)\omega^2}{4c_4}\right)^{\frac{\pi}{2c_4\omega}} \\ &< \exp\left(-\frac{(c_2 - \omega c_3)\pi\omega}{8c_4^2}\right) \\ &< \exp\left(-\frac{(c_2 - \omega_0 c_3)\pi\omega}{8c_4^2}\right) \end{aligned}$$

for $\omega < \omega_0$ which establishes the required lower bound on the denominator in (4.21).

The proof is now complete since $ax/(1 - e^{-bx})$ is a monotonically increasing function with a and b positive. ■

Theorem 4.5 will be now proven.

Proof of Theorem 4.5. For $h(j\omega) = mj\omega Z(j\omega)$, from Lemma 4.2, there exists $\omega_0 > 0$ such that

$$\sup_{N \geq i} |F_N^{(i)}(h(j\omega))| < \frac{2\sqrt{c_1 + c_2 + c_3}\omega_0}{1 - \exp\left(-\frac{(c_2 - \omega_0 c_3)\pi\omega_0}{8c_4^2}\right)}$$

for $0 \leq \omega < \omega_0$ where c_1, c_2, c_3 and c_4 are positive constants defined in Lemma 4.2. For $\omega_0 \leq \omega \leq \infty$, since $h(j\omega)$ is bounded away from $[-4, 0]$, from Lemma 4.1,

$$\sup_{N \geq i} |F_N^{(i)}(h(j\omega))| \leq \frac{(1 + |\zeta_0|)(1 + |\zeta_0|^2)}{1 - |\zeta_0|^3}$$

where

$$|\zeta_0| = \frac{A_0 - \sqrt{A_0^2 - 4}}{2}, \quad A_0 = \min_{\omega \geq \omega_0} \left(\frac{|h(j\omega)| + |h(j\omega) + 4|}{2} \right).$$

From Theorem 3.2, $T_{\hat{x}_0 \rightarrow \hat{\delta}_i}(= -F_N^{(i)})$ is a stable transfer function under the condition of Theorem 4.5. Therefore the maximum modulus principle can be applied to complete the proof. ■

DESIGN OF PASSIVE INTERCONNECTION

5.1 Overview

In the previous chapter, a graphical approach has been introduced to design a passive interconnection which achieves a good disturbance rejection performance in an arbitrary length of the mass chain. From a practical point of view, it is equally important to build a design methodology for a specific length of the mass chain. For this aim, this chapter introduces a systematic design method. The essential technique is the same as the one used for the uniform boundedness in the previous chapter; contour plots of the magnitude of the transfer functions. The chapter demonstrates the design methodology in the context of seismic design of a multi-storey building.

The chapter first poses the control problem for a homogeneous mass chain model representing a multi-storey building with base excitation. The graphical technique to design the interconnection is then introduced. A dominant frequency range of the ground displacement due to earthquake is considered for design. The technique is demonstrated using a 10-storey homogeneous building model and some simple configurations for the interconnection. Frequency responses and time responses against historical earthquakes are presented to verify the validity of the proposed design method. The disturbance suppression performance of the designed interconnection is also verified for a 10-storey building model which has a different stiffness distribution but with the same undamped first natural frequency as the homogeneous model.

5.2 Disturbance Rejection and Design Objectives

Consider again the homogeneous mass chain introduced in Chapter 3. For convenience, the system is depicted again in Fig. 5.1a. The transfer function from a movable point x_0

and the i th intermass displacement δ_i in a chain of N masses is again denoted as $-F_N^{(i)}$ for $i = 1, 2, \dots, N$. As shown in Chapter 3, this can be described as a function of a dimensionless parameter $h = sZ(s)m$. In particular for a multi-storey building model, the interconnection is modelled as Fig. 5.1b where k_s , c_s represent the storey stiffness and the structural damping. A passive interconnection $Z_a(s)$ is to be designed to achieve good disturbance rejection from x_0 . For this aim, it would be required that the magnitude of the transfer function from x_0 to δ_i for all i be made small in the frequency range where x_0 is significant. The design task is therefore to make the maximum value of $|F_N^{(i)}(j\omega)|$ over i small by choosing a suitable interconnection $Z_a(s)$.

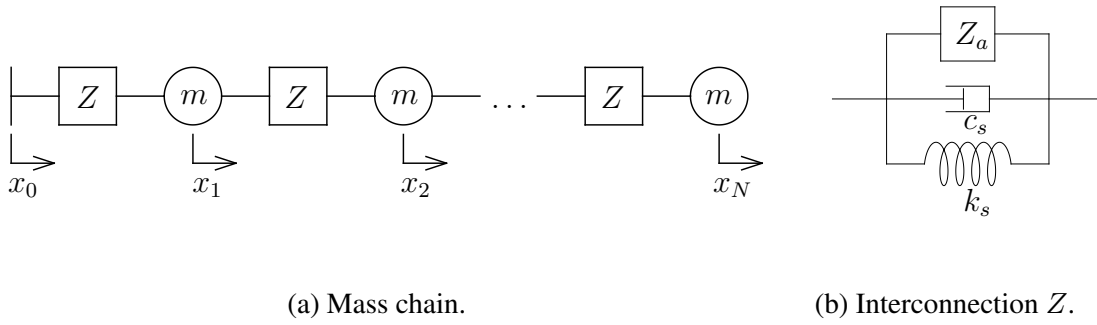


Fig. 5.1 Chain of N masses m connected by a passive mechanical impedance $Z(s)$ (admittance $Y(s) = Z(s)^{-1}$), and connected to a movable point x_0 . Each interconnection is depicted in (b) where its admittance $Y(s) = k_s/s + c_s + Y_a(s)$ ($Y_a(s) = Z_a(s)^{-1}$).

5.2.1 Graphical design method

Let us revisit the recursions given in Theorem 4.1 of the form:

$$F_N^{(i)} = \frac{d_{i-2}F_{N-1}^{(i)} + h}{F_{N-1}^{(i)} + d_i}$$

where $F_{i-1}^{(i)} = 0$ and

$$d_i(h) = (h + 2)d_{i-1}(h) - d_{i-2}(h)$$

supposing $d_{-1} = 1$ and $d_0 = 1$ for $i = 1, 2, \dots, N$. Using these recursions, one can compute the value of $\max_i |F_N^{(i)}(h)|$ at each complex value h for each N . The contour plot of $\max_i |F_N^{(i)}(h)|$ in Fig. 5.2 is illustrated for $N = 10$ in the g -plane where g is again the inverse of h , i.e., $g = Y(s)/(sm)$. The spacing of the contours is 0.2 where $\ln(\gamma)$ takes the value $-3, -2.8, -2.6, \dots$. The proposed design method involves essentially finding an interconnection $Y_a = Z_a^{-1}$ that moves the locus $g(j\omega)$ away from the dark region in the

contour map. Since $g(s) = Y(s)/(sm) = (k_s/s + c_s + Y_a(s))/(sm)$, a large gain of $Y_a(j\omega)$ would be required especially in the frequency range where the disturbance x_0 is significant.

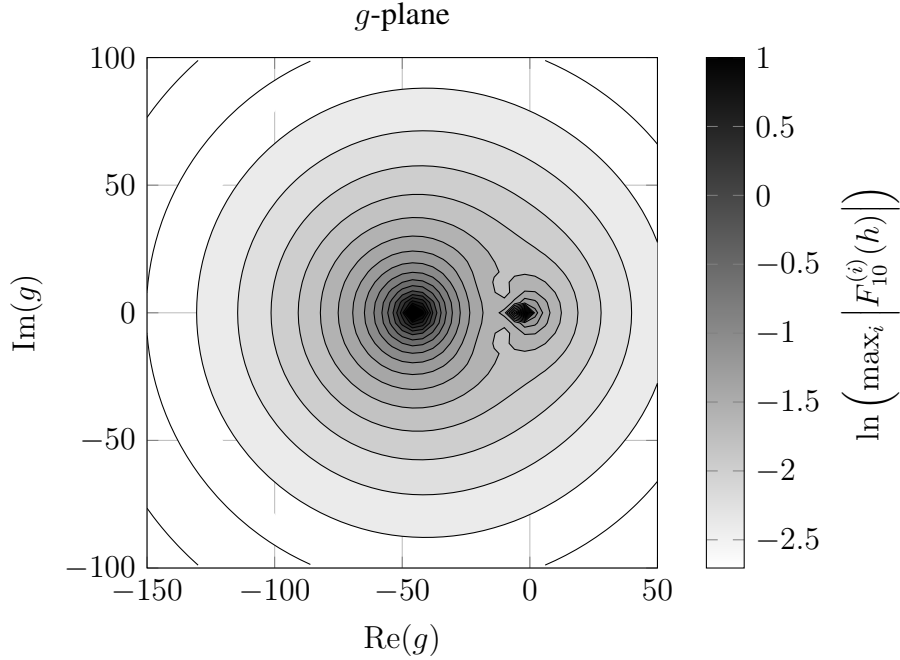


Fig. 5.2 Contour plot of $\max_i |F_{10}^{(i)}(h)|$ where $h = g^{-1}$.

5.2.2 Frequency content of ground displacements

Any information on the disturbance normally helps to improve a design. Although each earthquake has a different characteristic, there are some tendencies as described in Chapter 2. The weighting function $W(s)$ based on Clough-Penzien-Kanai-Tajimi acceleration filter $W_{CP}(s)W_{KT}(s)$ is a commonly used model for the frequency content of strong ground motions:

$$W(s) = \frac{W_0(s)}{\|W_0(s)\|_\infty}$$

where

$$W_0(s) = \frac{1}{s^2} W_{CP}(s) W_{KT}(s) = \frac{1}{s^2} \frac{-s^2}{s^2 + 2\eta_f \omega_f s + \omega_f^2} \frac{2\eta_g \omega_g s + \omega_g^2}{s^2 + 2\eta_g \omega_g s + \omega_g^2}.$$

The typical parameters in $W_{CP}(s)W_{KT}(s)$ for three different soil conditions are listed in Chapter 2 and Fig. 5.3 shows the log-log plot of the magnitude of $W(j\omega)$ using those parameters. As can be seen from the figure, \hat{x}_0 dominates in the low frequency range. Hence,

$|F_N^{(i)}|$ needs to be made small in this frequency range. Throughout this chapter, the weighting function for rock or stiff soil conditions is used for numerical examples:

$$W(s) = \frac{-30.16s - 631.7}{0.1654(s^2 + 3.016s + 6.317)(s^2 + 30.16s + 631.7)}. \quad (5.1)$$

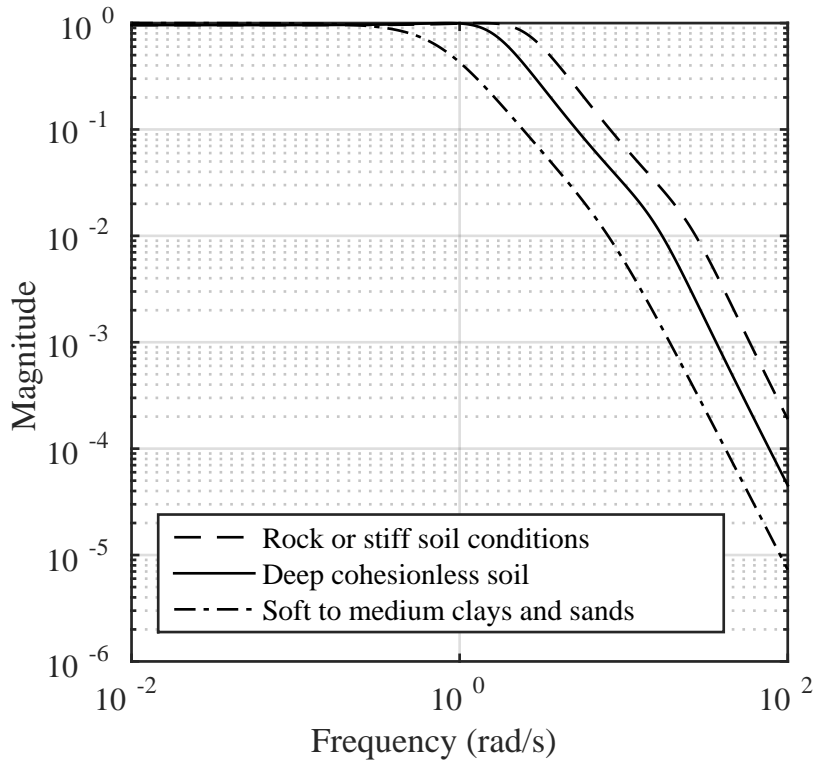


Fig. 5.3 A log-log plot of weighting functions $W(j\omega)$ for three different soil conditions: rock or stiff soil conditions, deep cohesionless soils and soft to medium clays and sands.

5.3 Case Study

This section shows the design procedure proposed in the last section using a benchmark model for a 10-storey building.

5.3.1 Multi-storey homogeneous building model

Consider a 10-storey building model depicted in Fig. 5.1 ($N = 10$). The structural parameters are shown in Table 5.1. The floor mass m and the storey stiffness k_s are fixed as

Table 5.1 Structural parameters of the homogeneous building model.

Parameter	Value	Description
N	10	Number of storeys
m	1.00×10^5 kg	Floor mass
k_s	1.77×10^5 kN/m	Storey stiffness
c_s	1.12×10^3 kNs/m	Structural damping
T_1	1.00 s	Undamped first natural period
ω_1	6.28 rad/s	Undamped first natural frequency

1.00×10^5 kg and 1.77×10^5 kN/m and a period T_1 equal to $0.1N$ seconds is assumed for the first natural frequency ω_1 [Shibata, 2003]. The structural damping is assumed to be stiffness-proportional damping with the damping ratio being 0.02, that is, $c_s = 2 \times 0.02k_s/\omega_1$. The frequency domain plot of $\max_i |F_N^{(i)}(j\omega)W(j\omega)|$ for the uncontrolled model, i.e., $Y_a(s) = 0$ is shown in Fig. 5.4 where $W(s)$ is defined in (5.1).

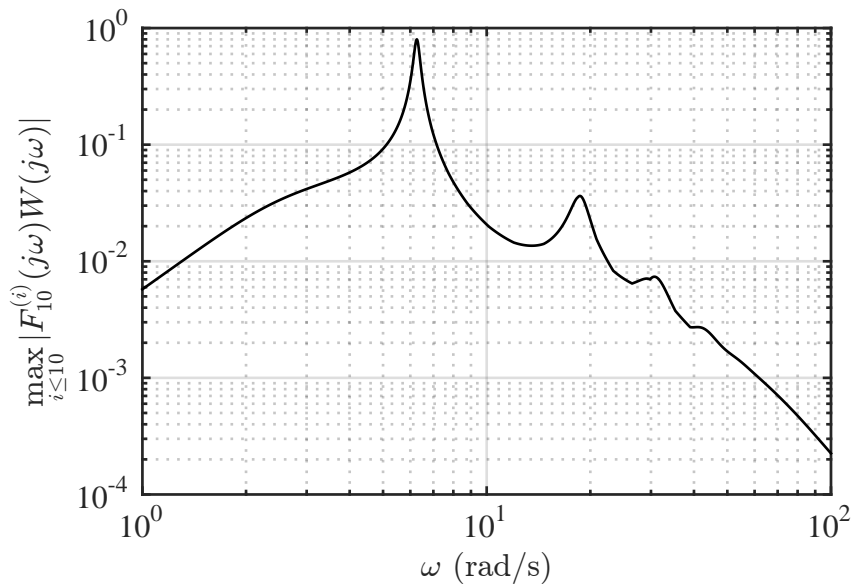
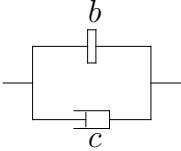
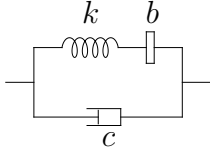
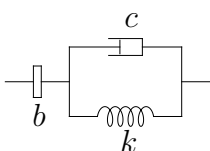
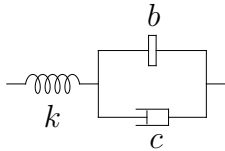


Fig. 5.4 A log-log plot of $\max_i |F_{10}^{(i)}(j\omega)W(j\omega)|$ for the uncontrolled homogeneous building model, i.e., $Y_a(s) = 0$.

5.3.2 Interconnection design

For this case study, the impedance Z as in Fig. 5.1b is considered with Y_a being the simple interconnection configurations listed in Table 5.2. Note that layout L3 is called a tuned-inerter-damper (TID) in [Lazar et al., 2014] and layout L4 is called a tuned viscous mass damper (TVMD) in [Ikago et al., 2012a,b]. The parameters of each element are selected making use of the contour plot of Fig. 5.2. For layout L1, it is clear that larger values

Table 5.2 Interconnection configuration and corresponding admittance $Y_a(s)$.

L1	L2	L3	L4
$bs + c$	$c + \frac{bks}{bs^2 + k}$	$\frac{bcs^2 + bks}{bs^2 + cs + k}$	$\frac{bks + ck}{bs^2 + cs + k}$
			

of c push $g(j\omega)$ away from the dark region in Fig. 5.2. Here the value is fixed as $c = 2 \times 0.2k_s/\omega_1 = 1.12 \times 10^4$ kNs/m assuming 20 % of critical damping. As can be seen from Fig. 5.5a, although the inerter improves the performance in the mid to high frequency range (see the white markers \circ), it makes the low frequency performance worse (see the black markers \bullet). This is confirmed by the frequency domain plots of $\max_i |F_{10}^{(i)}(j\omega)W(j\omega)|$ in Fig. 5.5b.

The admittance $Y_a(s)$ of layout L2 has infinite gain at $\omega = \sqrt{k/b}$. Here this frequency is set to be the same frequency as the undamped first natural frequency of the building ω_1 . The damping coefficient is again fixed as 1.12×10^4 kNs/m. The Nyquist diagrams of $g(j\omega)$ for three values of inertance and $k = b\omega_1^2$ are drawn again on the contour plot in Fig. 5.6a. The larger inerter is beneficial in a broad frequency range around ω_1 which can be also seen from the frequency domain plots of $\max_i |F_{10}^{(i)}(j\omega)W(j\omega)|$ in Fig. 5.6b.

Similarly, layouts L3 and L4 can be designed using the contour plot of $\max_i |F_{10}^{(i)}(h)|$. The parameters given in Table 5.3 are an example of good design with respect to the proposed design method. Note that the inertance $b = 0$ for L1 which means L1 is just a damper with no inerter in parallel. The Nyquist diagrams of $g(j\omega)$ for each layout are illustrated in Fig. 5.7a. The frequency domain plots of $\max_i |F_{10}^{(i)}(j\omega)W(j\omega)|$ are also shown in Fig. 5.7b. Layout L1 can suppress the disturbance amplification well for the entire frequency range.

Table 5.3 Parameters of vibration control devices.

Layout	c (kNs/m)	b (kg)	k (kN/m)
L1	1.12×10^4	0	–
L2	1.12×10^4	5.0×10^6	1.97×10^5
L3	1.12×10^4	5.0×10^6	1.00×10^5
L4	1.12×10^4	1.5×10^6	1.06×10^5

The other layouts L2 – L4 improve the disturbance rejection performance around the first natural frequency ω_1 but mild peaks appear at some other frequencies.

5.3.3 Time response

To verify the validity of the proposed design method, this section shows the time response of the system of Fig. 5.1 against historical earthquakes. The interconnection configurations and their parameters for $Y_a(s)$ designed in the previous section are listed in Table 5.2 and 5.3. The system with $Y_a(s) = 0$ is again referred to as the uncontrolled model.

Figure 5.8 illustrates the time response of the first interstorey drift for these four configurations against JMA Kobe 1995 NS earthquake. All the devices L1 – L4 suppress the vibration well. The interstorey drifts are under 4 cm while the uncontrolled model experiences an interstorey drift as large as 8 cm. The vibration also attenuates much quicker than the uncontrolled model. The maximum interstorey drifts of each floor during the earthquake are shown in Fig. 5.9 against JMA Kobe 1995 NS earthquake and El Centro 1940 NS earthquake. These figures confirm that the proposed designs reduce the interstorey drifts for all the floors.

5.3.4 Heterogeneous mass chain model

In the previous sections in this chapter, a graphical technique to design the interconnection when a multi-storey building is modelled as a homogeneous mass chain depicted in Fig. 5.1. However, for many tall buildings, the storey stiffness is smaller in the higher storeys. The aim of this section is to demonstrate the effectiveness of the proposed design in Table 5.3 for such a building when the undamped natural frequency ω_1 is the same. Hence, the model considered here is a heterogeneous mass chain depicted in Fig. 5.10 where the number of masses $N = 10$, all the masses have the same value as the homogeneous building model,

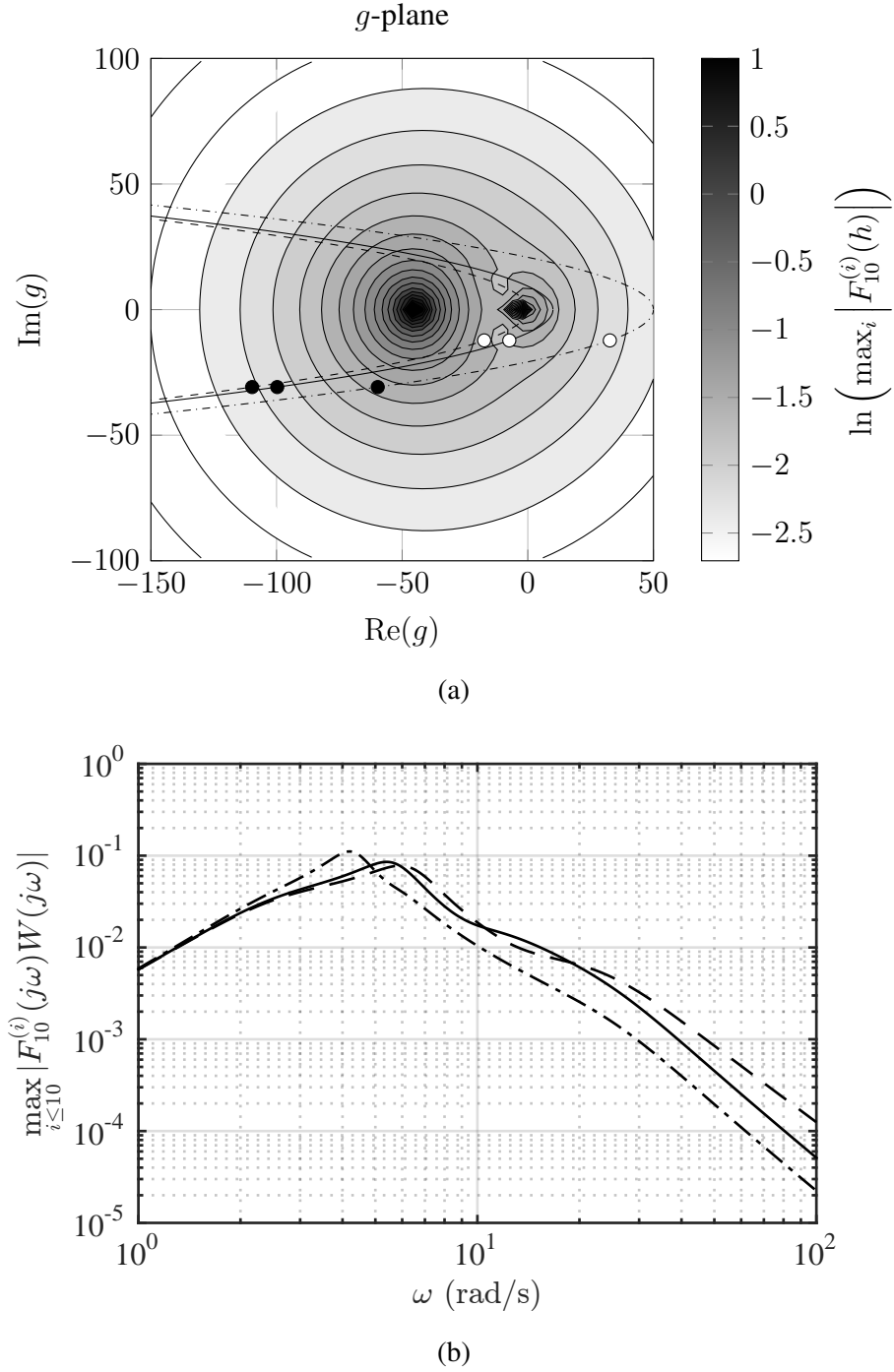


Fig. 5.5 Design of layout L1. The parameters are: $-- c = 1.12 \times 10^4$ kNs/m, $b = 0$ kg, $— c = 1.12 \times 10^4$ kNs/m, $b = 1.0 \times 10^6$ kg, $- \cdot - \cdot c = 1.12 \times 10^4$ kNs/m, $b = 5.0 \times 10^6$ kg. (a) Nyquist diagrams of $g(s) = (k_s/s + c_s + Y_a(s))/(sm)$ and the contour plot of $\max_i |F_{10}^{(i)}(h)|$. The black and white markers \bullet, \circ indicate $g(4j)$ and $g(10j)$. (b) A log-log plot of $\max_i |F_{10}^{(i)}(j\omega)W(j\omega)|$.

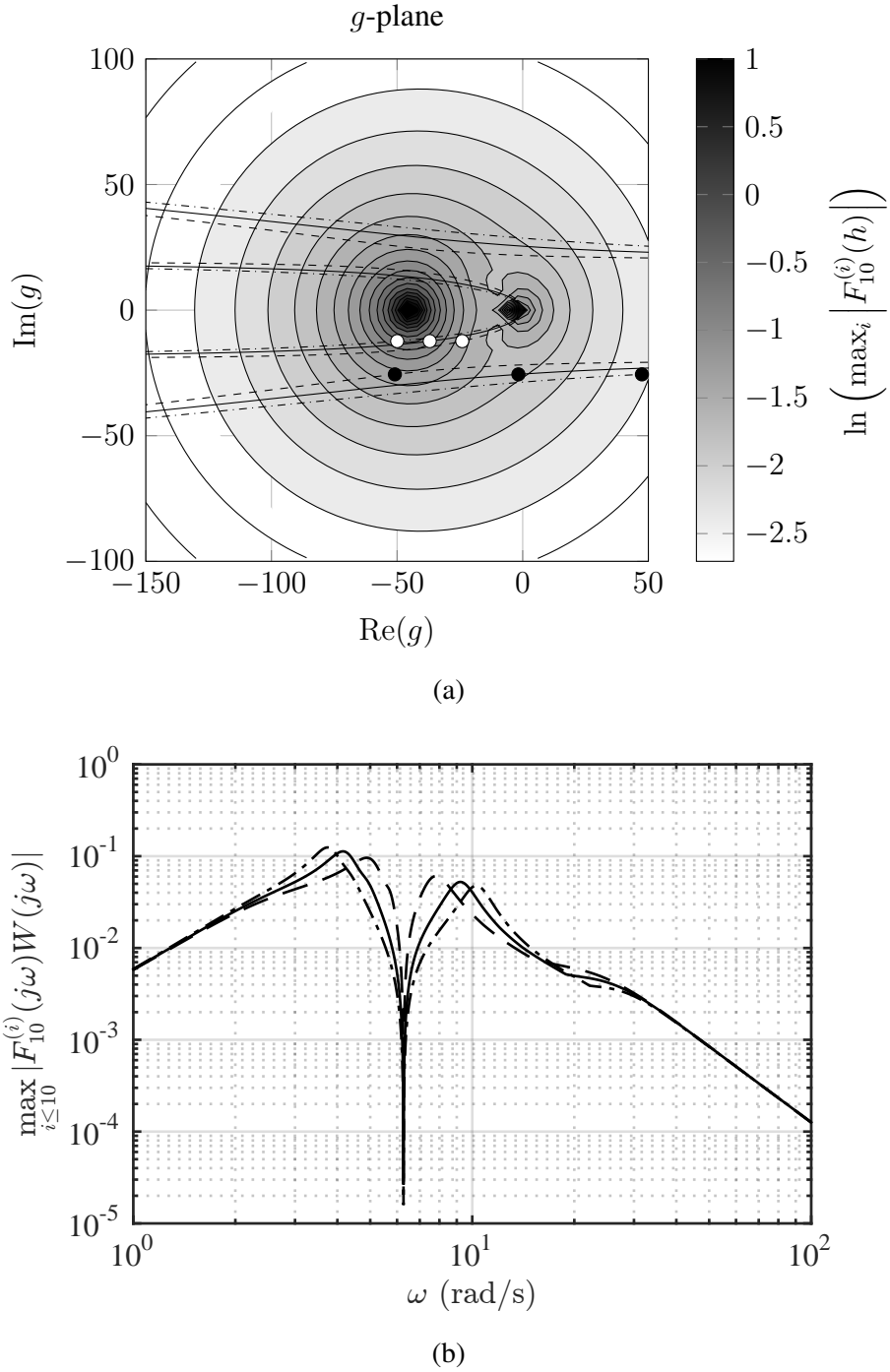


Fig. 5.6 Design of layout L2. The parameters are: $--c = 1.12 \times 10^4$ kNs/m, $b = 1.0 \times 10^6$ kg, $k = 3.93 \times 10^4$ kN/m, $—c = 1.12 \times 10^4$ kNs/m, $b = 3.0 \times 10^6$ kg, $k = 1.18 \times 10^5$ kN/m, $-\cdot-\cdot c = 1.12 \times 10^4$ kNs/m, $b = 5.0 \times 10^6$ kg, $k = 1.97 \times 10^5$ kN/m. (a) Nyquist diagrams of $g(s) = (k_s/s + c_s + Y_a(s))/(sm)$ and the contour plot of $\max_i |F_{10}^{(i)}(h)|$. The black and white markers \bullet, \circ indicate $g(4.7j)$ and $g(10j)$. (b) A log-log plot of $\max_i |F_{10}^{(i)}(j\omega)W(j\omega)|$.

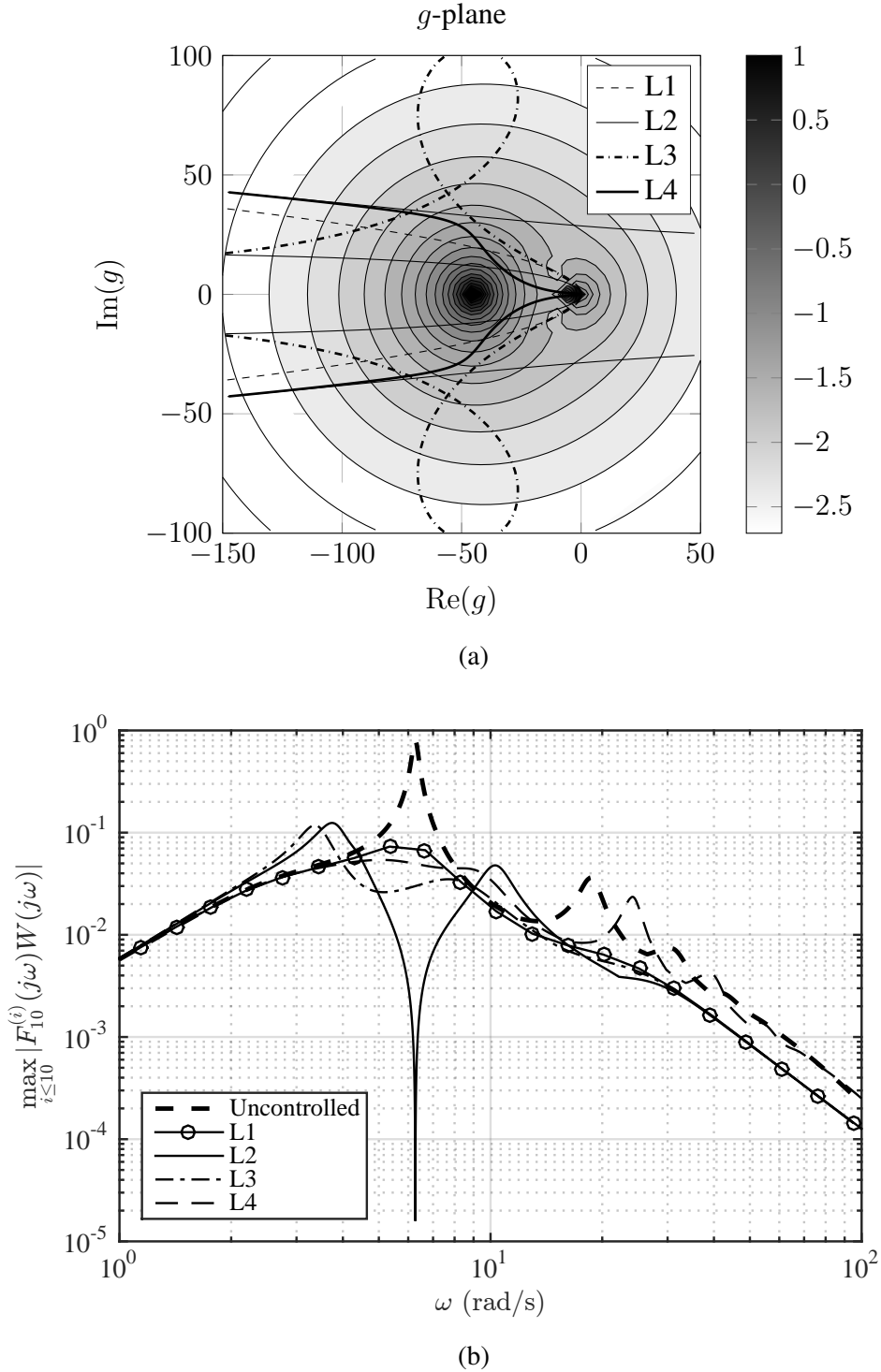
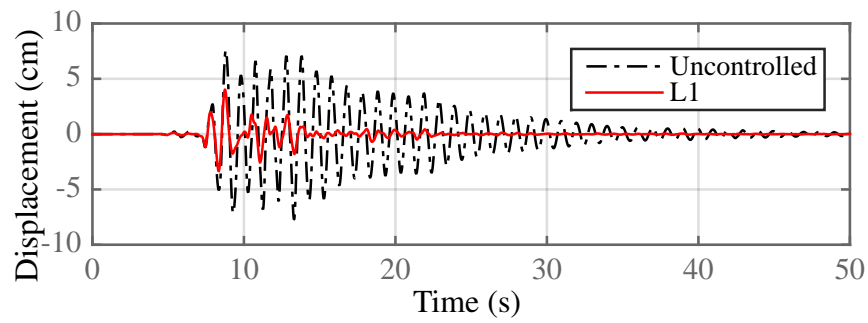
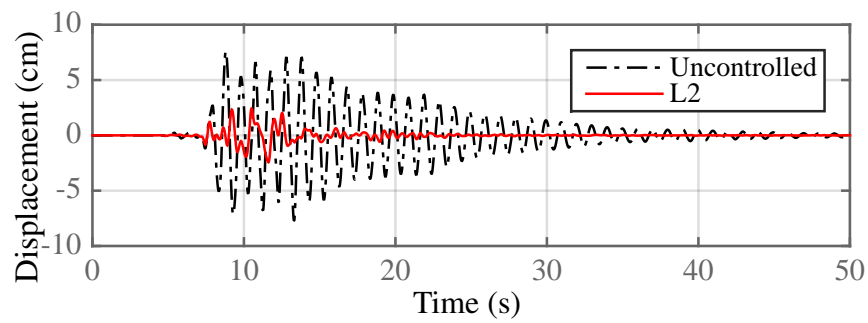


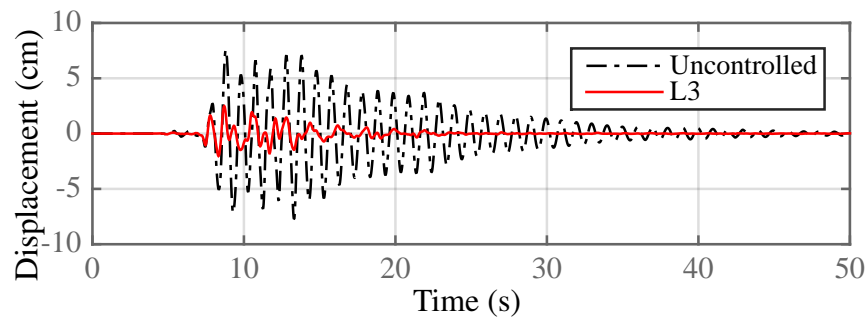
Fig. 5.7 The design of L1 – L4 in Table 5.2. The parameters are given in Table 5.3. (a) Nyquist diagrams of $g(s) = (k_s/s + c_s + Y_a(s))/(sm)$ and the contour plot of $\max_i |F_{10}^{(i)}(h)|$. (b) A log-log plot of $\max_i |F_{10}^{(i)}(j\omega)W(j\omega)|$ for the uncontrolled homogeneous building model of and the model controlled by the vibration control devices L1 – L4.



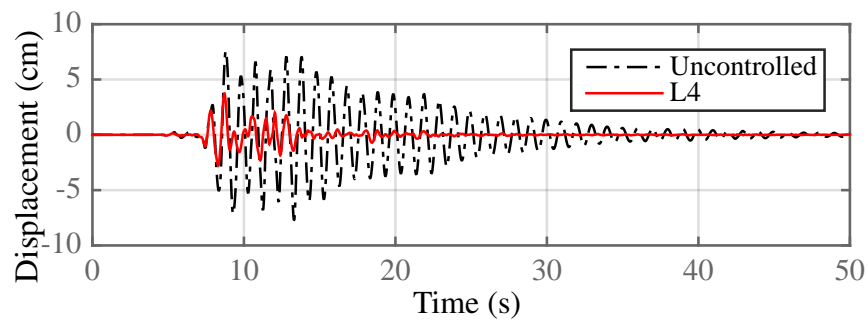
(a) L1.



(b) L2.

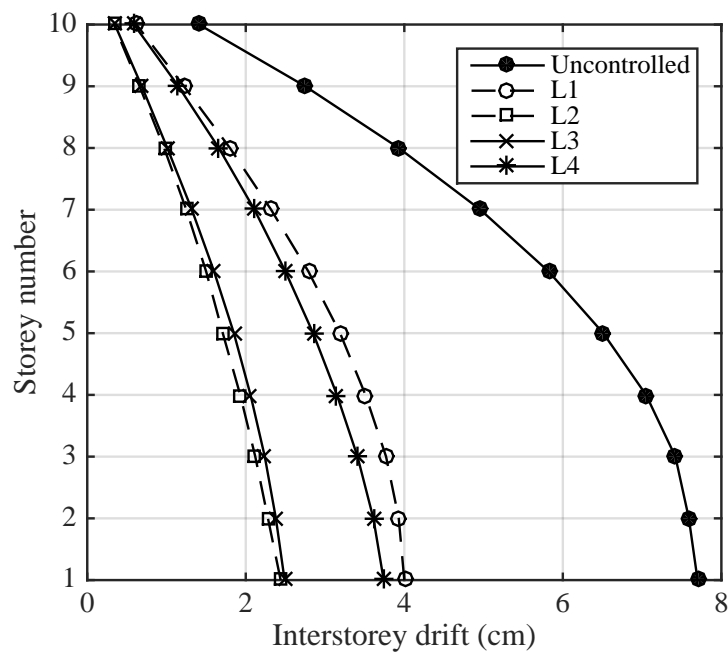


(c) L3.

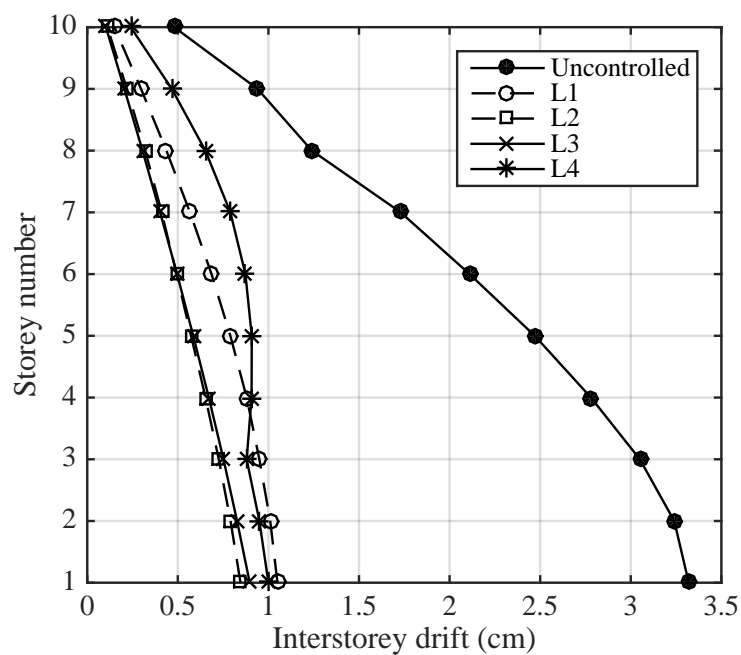


(d) L4.

Fig. 5.8 Time response of the first interstorey drift against JMA Kobe 1995 NS earthquake.



(a) JMA Kobe 1995 NS



(b) El Centro 1940 NS

Fig. 5.9 Maximum interstorey drifts against historical earthquakes for the uncontrolled homogeneous building model and the model controlled by the vibration control devices L1 – L4.

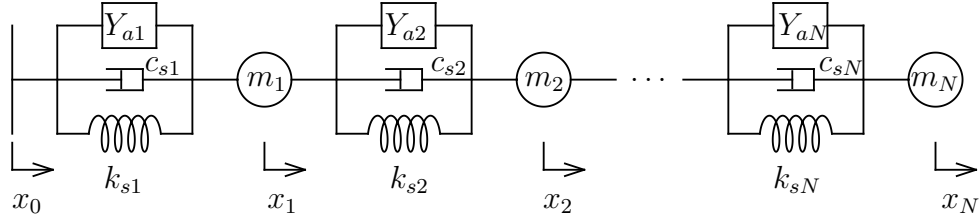


Fig. 5.10 Chain of N masses m_i and a movable point x_0 with passive interconnections corresponding to the admittance $\frac{k_{si}}{s} + c_{si} + Y_{ai}(s)$.

i.e., $m_i = 1.00 \times 10^5$ kg and the i th storey stiffness k_{si} for $i = 1, 2, \dots, 10$ is given by the following equation:

$$k_{si} = \frac{1}{2} \{N(N+1) - i(i-1)\} m \omega_1^2 \quad (5.2)$$

assuming that the shape of the fundamental eigenmode of the main frame is a straight line [Penzien, 1960; Shibata, 2003]. The structural damping is assumed to be proportional to the stiffness with the damping ratio 0.02. Hence,

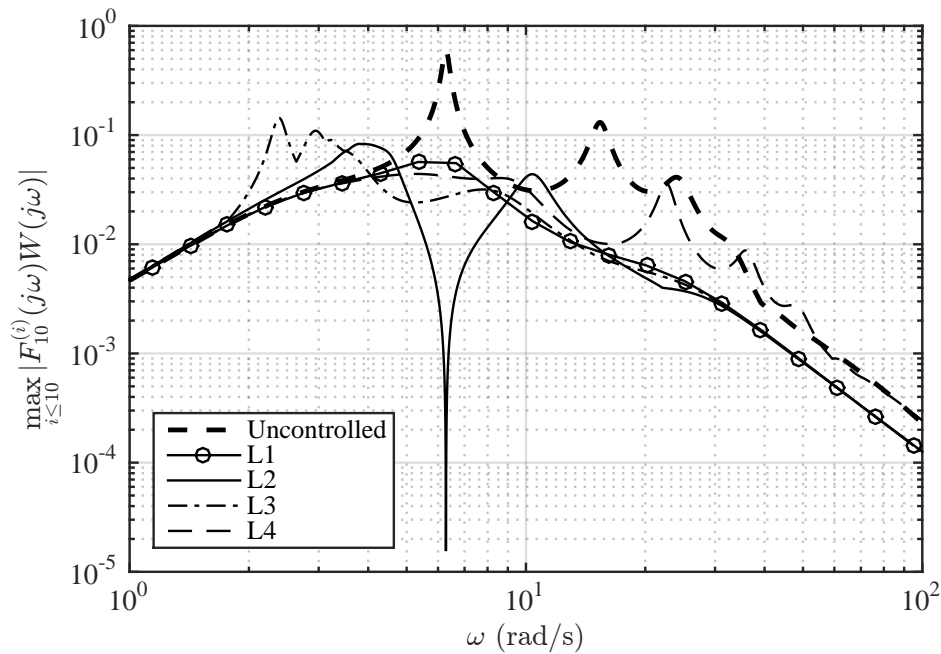
$$c_{si} = \frac{2 \times 0.02}{\omega_1} k_{si} \quad (5.3)$$

for $i = 1, 2, \dots, 10$. These structural parameters are summarised in Table 5.4. All the interconnection Y_{ai} is assumed to be identical and the layout L1 – L4 in Table 5.2 for $Y_{ai}(s)$ for the parameters given in Table 5.3 are considered here. The log-log plot of $\max_i |F_{10}^{(i)}(j\omega)W(j\omega)|$ in Fig. 5.11 and the figure of the maximum interstorey drift of the building againsts JMA Kobe 1995 earthquake in Fig. 5.12 confirm that the interconnections designed in the previous section give a good disturbance rejection/suppression performance.

The equations of motion and the system description of the heterogeneous mass chain used for the numerical examples in this section are given in Appendix 5.A. Also, it may be of interest whether there exist some recursive features in a general heterogeneous mass chain model like the ones in the homogeneous case. They indeed exist and are presented in Appendix 5.B.

Table 5.4 Structural parameters of the heterogeneous building model.

Parameter	Value	Description
N	10	Number of storeys
m	1.00×10^5 kg	Floor mass
k_{si}	Determined by (5.2).	Storey stiffness of the i th floor
c_{si}	Determined by (5.3).	Structural damping of the i th floor
T_1	1.00 s	Undamped first natural period
ω_1	6.28 rad/s	Undamped first natural frequency

Fig. 5.11 A log-log plot of $\max_i |F_{10}^{(i)}(j\omega)W(j\omega)|$ for the uncontrolled heterogeneous building model and the model controlled by the vibration control devices L1 – L4.

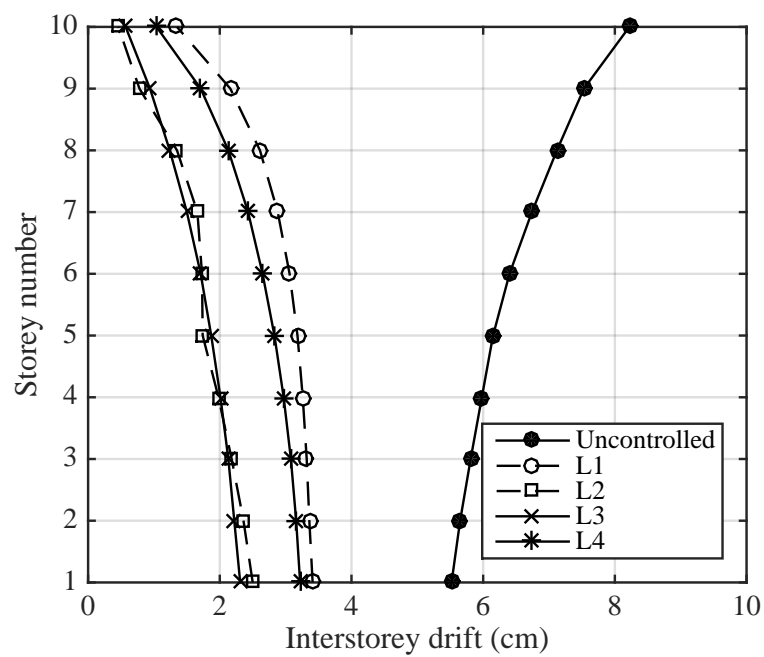


Fig. 5.12 Maximum interstorey drift against JMA Kobe 1995 NS earthquake for the uncontrolled heterogeneous building model and the model controlled by the vibration control devices L1 – L4.

Appendix 5.A Heterogeneous Mass Chains

Consider a heterogeneous mass chain depicted in Fig. 5.10. Assuming the initial conditions of the ground displacement and the mass displacements are all zero, the equations of motion in the Laplace transformed domain are given as follows:

$$\begin{aligned} s^2 m_i \hat{x}_i &= -sY_i(s)\hat{\delta}_i + sY_{i+1}(s)\hat{\delta}_{i+1} \quad \text{for } i = 1, \dots, N-1, \\ s^2 m_N \hat{x}_N &= -sY_N(s)\hat{\delta}_N \end{aligned}$$

where the i th interstorey drift $\hat{\delta}_i(s) = \hat{x}_i(s) - \hat{x}_{i-1}(s)$. Let $\hat{\delta} = [\hat{\delta}_1, \hat{\delta}_2, \dots, \hat{\delta}_N]^T$ and $\hat{u} = [\hat{u}_1, \hat{u}_2, \dots, \hat{u}_N]^T$. Then the interstorey displacement vector $\hat{\delta}$ is written as

$$\hat{\delta} = -(I + PK)^{-1}e_1\hat{x}_0$$

and the i th interstorey displacement $\hat{\delta}_i$ as

$$\begin{aligned} \hat{\delta}_i &= -e_i^T(I + PK)^{-1}e_1\hat{x}_0 \\ &=: -F_N^{(i)}\hat{x}_0 \end{aligned}$$

where I is the $N \times N$ identity matrix, where e_i is the standard basis in \mathbb{R}^N for $i = 1, 2, \dots, N$ (e.g., $e_1 = [1, 0, \dots, 0]^T$),

$$P = \begin{bmatrix} \frac{1}{s^2 m_1} & & & 0 \\ -\frac{1}{s^2 m_1} & \frac{1}{s^2 m_2} & & \\ & \ddots & \ddots & \\ 0 & & -\frac{1}{s^2 m_{N-1}} & \frac{1}{s^2 m_N} \end{bmatrix},$$

$$K = \begin{bmatrix} k_{s1} + sc_{s1} + sY_{a1}(s) & -(k_{s2} + sc_{s2} + sY_{a2}(s)) & & 0 \\ & k_{s2} + sc_{s2} + sY_{a2}(s) & \ddots & \\ & & \ddots & -(k_{sN} + sc_{sN} + sY_{aN}(s)) \\ 0 & & & k_{sN} + sc_{sN} + sY_{aN}(s) \end{bmatrix}.$$

The feedback configuration is illustrated in Fig. 5.13.

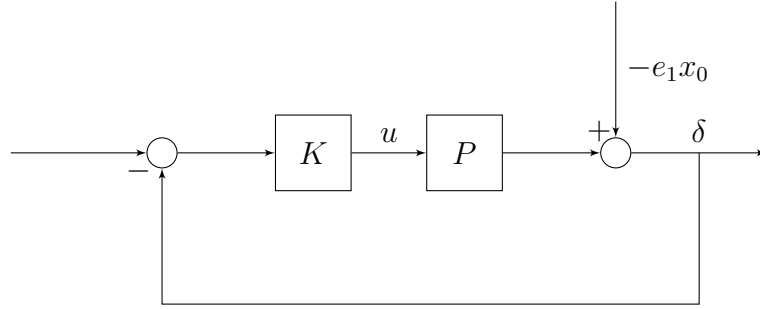


Fig. 5.13 Feedback configuration of the system of Fig. 5.10.

Appendix 5.B Recursions in Heterogeneous Mass Chains

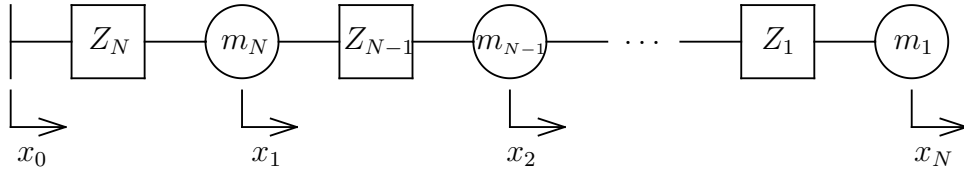


Fig. 5.14 Chain of N masses m_i connected by a passive mechanical impedance $Z_i(s)$ and connected to a movable point x_0 .

The transfer function from a movable point x_0 to a first intermass displacement $x_1 - x_0$ in a heterogeneous mass chain of Fig. 5.14 are also given recursively in the number of masses N . Note that the labelling of the indices is unusual: the first mass from the left has mass m_N and is connected to a movable point by an impedance Z_N and the indices decrease as it goes to the right in a chain of N masses of Fig. 5.14. Consider the transfer function $T_N^{(1)}$ from x_0 to the first mass displacement x_1 in a chain of N masses. It may be observed that the transfer function from x_1 to x_2 in a chain of N masses is equal to $T_{N-1}^{(1)}$. Similarly, the transfer function from x_i to x_{i+1} in a chain of N masses is equal to $T_{N-i}^{(1)}$. Therefore,

$$\hat{x}_i = \left(\prod_{j=1}^{i-1} T_{N-j}^{(1)} \right) \hat{x}_1 \quad (5.4)$$

where $\hat{}$ denotes the Laplace transform and \prod represents the product operator.

The equations of motion in the Laplace transformed domain are

$$\begin{aligned} m_N s^2 \hat{x}_1 &= -sY_N(s)(\hat{x}_1 - \hat{x}_0) + sY_{N-1}(s)(\hat{x}_2 - \hat{x}_1) \\ m_{N-1} s^2 \hat{x}_2 &= -sY_{N-1}(s)(\hat{x}_2 - \hat{x}_1) + sY_{N-2}(s)(\hat{x}_3 - \hat{x}_2) \\ &\vdots \\ m_1 s^2 \hat{x}_N &= -sY_1(s)(\hat{x}_N - \hat{x}_{N-1}). \end{aligned}$$

Summing these equations gives

$$m_N s^2 \hat{x}_1 + \left(\sum_{i=1}^{N-1} m_{N-i} s^2 \hat{x}_{i+1} \right) = -sY_N(s)(\hat{x}_1 - \hat{x}_0),$$

and hence, substituting (5.4) into the above equation gives

$$\left(h_N + \sum_{i=1}^{N-1} \frac{m_{N-i}}{m_N} h_N \prod_{j=1}^{i-1} T_{N-j}^{(1)} + 1 \right) \hat{x}_1 = \hat{x}_0$$

where $h_N = sZ_N(s)m_N$. Hence the transfer function $F_N^{(1)}$ from x_0 to the first intermass displacement $x_1 - x_0$ (with a negative sign) is equal to:

$$F_N^{(1)} := 1 - T_N^{(1)} = \frac{h_N + \sum_{i=1}^{N-1} \frac{m_{N-i}}{m_N} h_N \prod_{j=1}^{i-1} T_{N-j}^{(1)}}{h_N + \sum_{i=1}^{N-1} \frac{m_{N-i}}{m_N} h_N \prod_{j=1}^{i-1} T_{N-j}^{(1)} + 1}. \quad (5.5)$$

Further,

$$\begin{aligned} &h_N + \sum_{i=1}^{N-1} \frac{m_{N-i}}{m_N} h_N \prod_{j=1}^{i-1} T_{N-j}^{(1)} \\ &= h_N + \frac{h_N}{h_{N-1}} \frac{m_{N-1}}{m_N} T_{N-1}^{(1)} \left(h_{N-1} + \sum_{i=1}^{N-2} \frac{m_{N-i-1}}{m_{N-1}} h_N \prod_{j=1}^{i-1} T_{N-j-1}^{(1)} \right) \\ &= h_N + \frac{h_N}{h_{N-1}} \frac{m_{N-1}}{m_N} F_{N-1}^{(1)}. \end{aligned}$$

Substituting this to (5.5) gives the recursion:

$$F_N^{(1)} = \frac{h_N + \alpha_{N-1} F_{N-1}^{(1)}}{h_N + \alpha_{N-1} F_{N-1}^{(1)} + 1} \quad (5.6)$$

for $N = 1, 2, \dots$, where $F_0^{(1)} = 0$, $\alpha_0 = 0$ and

$$\alpha_i = \frac{h_{i+1}}{h_i} \frac{m_i}{m_{i+1}} = \frac{Z_{i+1}}{Z_i}$$

for $i = 1, 2, \dots, N - 1$.

The transfer functions for higher intermass displacements $F_N^{(i)}$ in a chain of N masses are given by

$$\begin{aligned} F_N^{(i)} &= -\frac{\hat{x}_i - \hat{x}_{i-1}}{\hat{x}_0} \\ &= -\frac{\hat{x}_i - \hat{x}_{i-1}}{\hat{x}_{i-1}} \frac{\hat{x}_{i-1}}{\hat{x}_1} \frac{\hat{x}_1}{\hat{x}_0} \\ &= (1 - T_{N-i+1}^{(1)}) \left(\prod_{j=1}^{i-2} T_{N-j}^{(1)} \right) T_N^{(1)} \\ &= F_{N-i+1}^{(1)} \prod_{j=0}^{i-2} (1 - F_{N-j}^{(1)}). \end{aligned}$$

These expressions may be useful for further analysis, e.g., the analysis for uniform boundedness. This is referred to in the future work section in Chapter 7.

CHAPTER 6

TOWARDS EXACT COMPUTATION OF SUPREMAL BOUNDS AND CONJECTURES

6.1 Introduction

In Chapter 4, it has been shown that the homogeneous mass chain system is scalable with respect to the \mathcal{H}_∞ -norm of the transfer functions from disturbance to a given intermass displacement. Conditions have been derived for the \mathcal{H}_∞ norm to remain bounded by a fixed value independent of the length of the mass chain.

In this chapter, the scalability problem is further considered. In particular, a conjecture is made for a special impedance that the \mathcal{H}_∞ -norm of the transfer function from the disturbance to the first intermass displacement is smaller than one for an arbitrary length of the mass chain. Although an analytical proof has not been obtained, some heuristic justifications are given in this chapter. Several techniques introduced in this chapter are possibly useful for obtaining a rigorous uniform bound.

The chapter continues to pose conjectures on higher intermass displacements. A graphical observation suggests that the supremum magnitude of the first intermass displacement transfer function over N be bigger than that of any other intermass displacement transfer functions at any frequencies. Further, numerical observations suggest that the \mathcal{H}_∞ -norm of the transfer functions monotonically decrease along the mass chain for a fixed number of the mass chain.

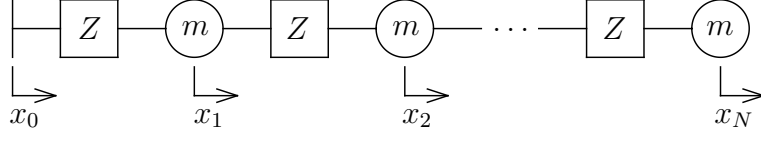


Fig. 6.1 Chain of N masses m connected by a passive mechanical impedance $Z(s)$ (admittance $Y(s) = Z(s)^{-1}$), and connected to a movable point x_0 .

6.2 Description of the Problem and Motivations

Consider again the recursions introduced in Theorem 4.1 of the form:

$$F_N^{(i)} = \frac{d_{i-2}F_{N-1}^{(i)} + h}{F_{N-1}^{(i)} + d_i} \quad (6.1)$$

for $N = i, i+1, \dots$ where $F_{i-1}^{(i)} = 0$, $h(s) = sZ(s)m$ and

$$d_i(h) = (h+2)d_{i-1}(h) - d_{i-2}(h) \quad \text{for } i = 1, \dots, N$$

with $d_{-1} = 1$ and $d_0 = 1$. For convenience, the system is depicted again in Fig. 6.1. For $i = 1$ in particular, it can be written as:

$$F_N^{(1)} = \frac{F_{N-1}^{(1)} + h}{F_{N-1}^{(1)} + h + 1} \quad (6.2)$$

for $N = 1, 2, \dots$ where $F_0^{(1)} = 0$. Then the conjecture is as follows:

Conjecture 6.1. *Suppose $h(s)$ has a normalised form $s^2/(\sqrt{2}s + 1)$. Then*

$$\left\| F_N^{(1)}(s) \right\|_{\infty} = 1 \quad \text{for all } N \in \mathbb{N}.$$

□

Graphical observations motivate the conjecture. In Fig. 6.2, the locus $g(j\omega) = h^{-1}(j\omega)$ where $h = s^2/(\sqrt{2}s + 1)$ is plotted on a contour plot of $\max_N |F_N^{(1)}(h)|$ where \mathcal{G}_1 denotes the set $\{g \in \mathbb{C} : \max_N |F_N^{(1)}(g^{-1})| \leq 1\}$. It can be observed that $g(j\omega) \in \mathcal{G}_1$ and also $g(j\omega)$ touches the boundary at $\omega = \infty$, indicating $\|F_N^{(1)}(s)\|_{\infty} = 1$ for all $N \in \mathbb{N}$. Further, as seen from Fig. 6.3, the Nyquist diagrams of $F_N^{(1)}(j\omega)$ stay inside the unit circle for $1 \leq N \leq 100$.

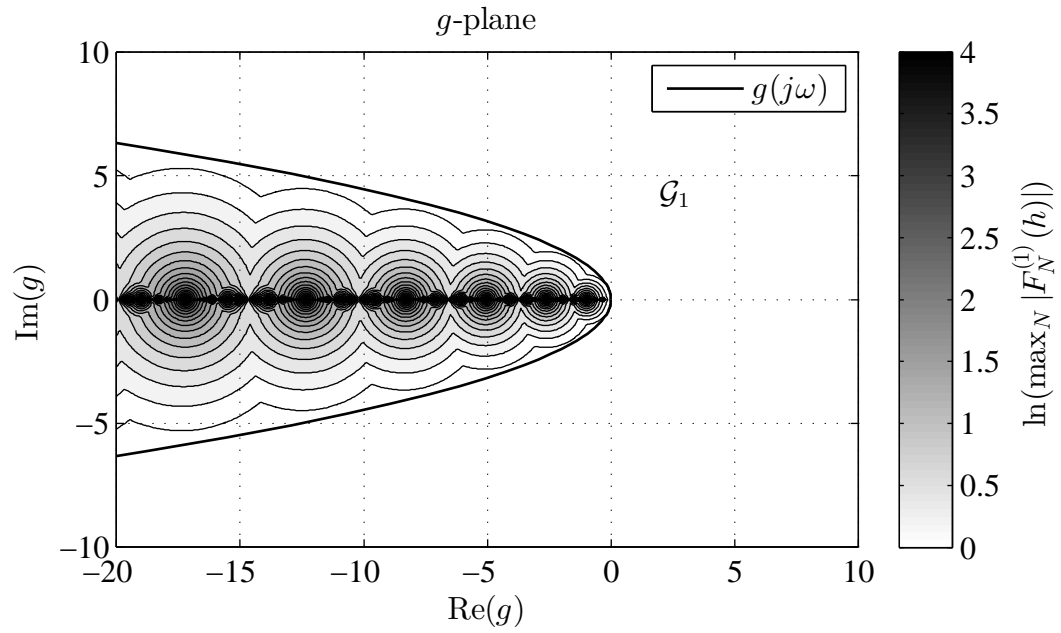


Fig. 6.2 Nyquist diagram of $g(s) = (\sqrt{2}s + 1)/s^2$ on a contour plot of $\max_N |F_N^{(1)}(h)|$ where $h = g^{-1}$.

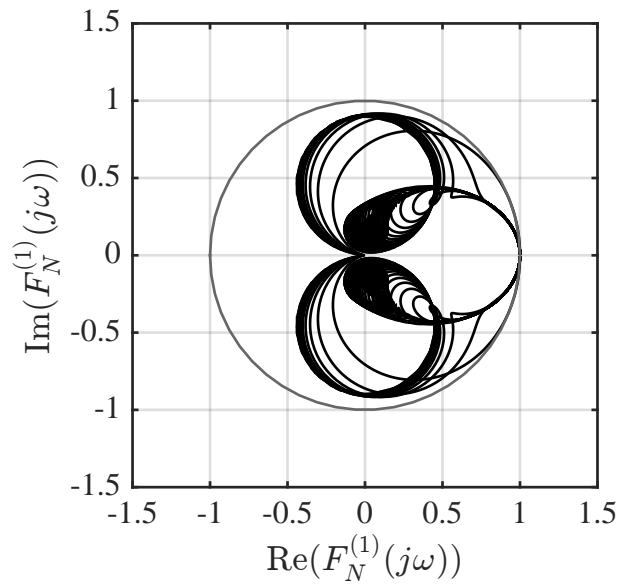


Fig. 6.3 Nyquist diagrams of $F_N^{(1)}(j\omega)$ for $N = 1, 2, \dots, 100$ and a unit circle.

Note that an interconnection arrangement of a spring and a damper in parallel gives the form

$$h(s) = \frac{ms^2}{cs + k}$$

which has the normalised form in Conjecture 6.1 when $c = \sqrt{2mk}$ and frequency is rescaled. For $N = 1$, this corresponds to a simple mass-spring-damper system of Fig. 6.4 with the damping ratio being $1/\sqrt{2}$. This value is well known in mechanical engineering as the limiting value achieving the \mathcal{H}_∞ -norm being one for the transmission from x_0 to $x_1 - x_0$. The values of $\sup_N \|F_N^{(1)}(s)\|_\infty$ with respect to the damping coefficient c is plotted in Fig. 6.5.

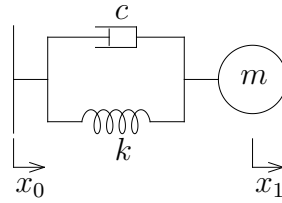


Fig. 6.4 A mass-spring-damper system.

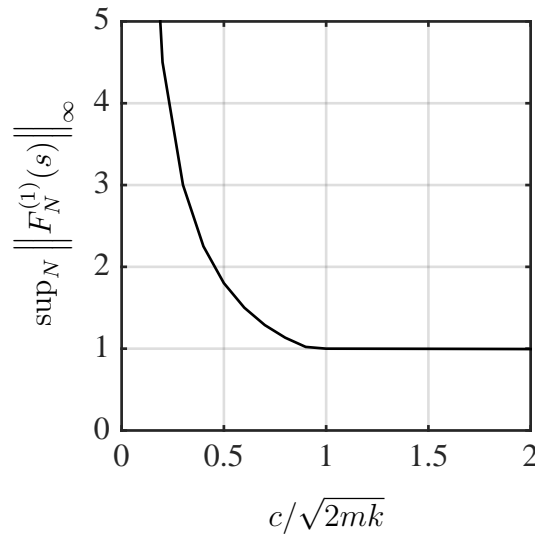


Fig. 6.5 Values of $\sup_N \|F_N^{(1)}(s)\|_\infty$ with respect to the damping coefficient c in the system of Fig. 6.4.

Available results

The closed form of the recursions (6.1) are given in (4.13). For $i = 1$, it is in the form:

$$\begin{aligned} F_N^{(1)} &= \mu_+^{(1)} \frac{1 - \zeta^{2N}}{1 + \zeta^{2N+1}} \\ &= \frac{(1 - \zeta)(1 - \zeta^{2N})}{1 + \zeta^{2N+1}} \end{aligned} \quad (6.3)$$

where ζ is the root of the quadratic equation $\zeta^2 - (h + 2)\zeta + 1 = 0$ satisfying $|\zeta| < 1$. It is clear that $\zeta(j\infty) = 0$ where $h(s) = s^2/(\sqrt{2}s + 1)$. Hence, from (6.3), $|F_N^{(1)}(j\infty)| = 1$ for all $N \in \mathbb{N}$.

The conjecture in regard to other frequencies, i.e.,

$$\sup_{N \in \mathbb{N}} |F_N^{(1)}(j\omega)| \leq 1$$

for finite ω is unsolved.

6.3 Possible Solution Paths

The following statements are all equivalent:

- 1) $\sup_{N \in \mathbb{N}} \|F_N^{(1)}(s)\|_{\infty} \leq 1$.
- 2) $1 - F_N^{(1)}(s)F_N^{(1)}(-s) \geq 0$ for all $N \in \mathbb{N}$, $s \in \mathbb{C}_+$.
- 3) $\inf_{N \in \mathbb{N}} \operatorname{Re}(F_{N-1}^{(1)}(j\omega) + h(j\omega)) + \frac{1}{2} \geq 0$ for all $\omega \in \mathbb{R}$.

It is straightforward to see the equivalence between the first and the second statements. The third statement follows from (6.2):

$$\begin{aligned} |F_N^{(1)}| \leq 1 &\Leftrightarrow \left| 1 + \frac{1}{F_{N-1}^{(1)} + h} \right| \geq 1 \\ &\Leftrightarrow \operatorname{Re}(F_{N-1}^{(1)} + h) \geq -\frac{1}{2}. \end{aligned}$$

Sturm's theorem

Proving the second statement is also equivalent to showing that there is no real root of the polynomial $1 - F_N^{(1)}(j\omega)F_N^{(1)}(-j\omega)$ in the interval $[0, \infty)$. Sturm's theorem [Gantmacher,

2000] may be suitable for the test. The algorithm implemented in the software Maple18 has been used to check that the statement is true for $N = 1, 2, \dots, 100$. However, to prove for infinitely many numbers of N , some sort of inductive relations may be needed. Similarly, the third statement may require an inductive relation. They have not yet been discovered.

Logarithmic spiral

Another possibility is to work on the expression (6.3). It is, however, problematic to directly compute the magnitude of (6.3). In fact, $\zeta^p, p \in \mathbb{R}_+$ is shown to be a logarithmic spiral which may be useful for further analysis.

Definition 6.1 (logarithmic spiral). A logarithmic spiral is a spiral which has a polar form

$$r = ae^{b\theta}$$

where a and b are arbitrary positive real constants. ◇

Note that in parametric form, it can be written as

$$\begin{cases} x &= a \cos \theta e^{b\theta} \\ y &= a \sin \theta e^{b\theta}. \end{cases}$$

Let $\zeta = |\zeta|e^{j\phi}$. Then ζ^p is a logarithmic spiral with $\theta = p\phi$ since:

$$\begin{aligned} (|\zeta|e^{j\phi})^p &= (e^{\ln |\zeta|} e^{j\phi})^p \\ &= e^{p \ln |\zeta| + jp\phi} \\ &= e^{(\ln |\zeta|/\phi)\theta + j\theta} \\ &= e^{(\ln |\zeta|/\phi)\theta} e^{j\theta} \end{aligned}$$

where $\ln |\zeta|/\phi > 0$ since $|\zeta| < 1$ and $\phi < 0$ which is straightforward to check. The locus $\zeta(j\omega)$ where $h(s) = s^2/(\sqrt{2}s + 1)$ is shown in Fig. 6.6. Note that the spiral is clockwise since $\theta < 0$.

In particular, the logarithmic spiral expression is potentially useful to develop an upper bound of (6.3) by finding a positive real number p_1 which maximises the modulus of the numerator and p_2 which minimises the modulus of the denominator for a fixed ζ , i.e.,

$$\frac{\max_p |(1 - \zeta)(1 - \zeta^p)|}{\min_p |1 + \zeta^p|}. \quad (6.4)$$

Figure 6.7 illustrates an example of a spiral ζ^p and its closest point to $(-1, 0)$ which gives

the minimum value of the denominator in (6.3). The values of (6.4) for each frequency are plotted in Fig. 6.8. Although the bound is greater than one for some frequencies, it is less than one in the lower frequency range where the effect of the low frequency resonances make the other analysis methods difficult. Furthermore, it is observed in Fig. 6.9 that the behaviour of $|F_N^{(1)}(j\omega)|$ is simple for $\omega \geq 1$ and it may be possible to construct another upper bound for this frequency range using a different technique.

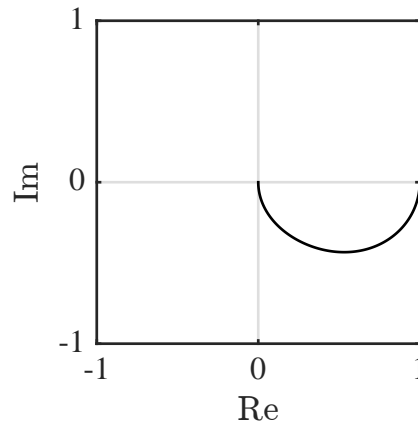


Fig. 6.6 The locus $\zeta(j\omega)$ where $h(s) = s^2/(\sqrt{2}s + 1)$.

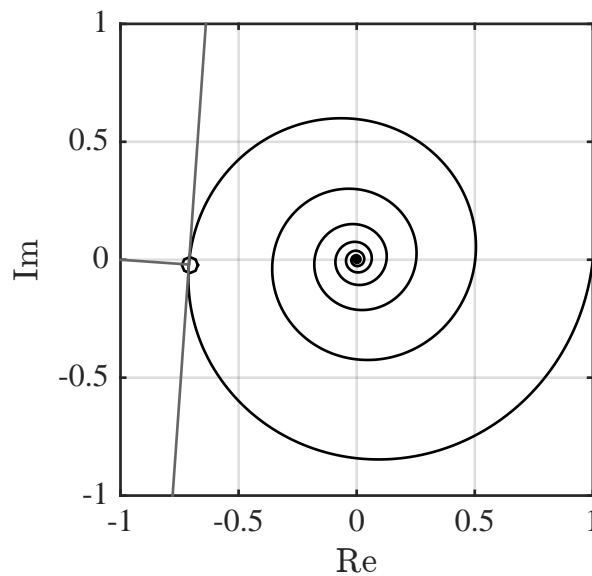


Fig. 6.7 A spiral ζ^p and its closest point to $(-1, 0)$.

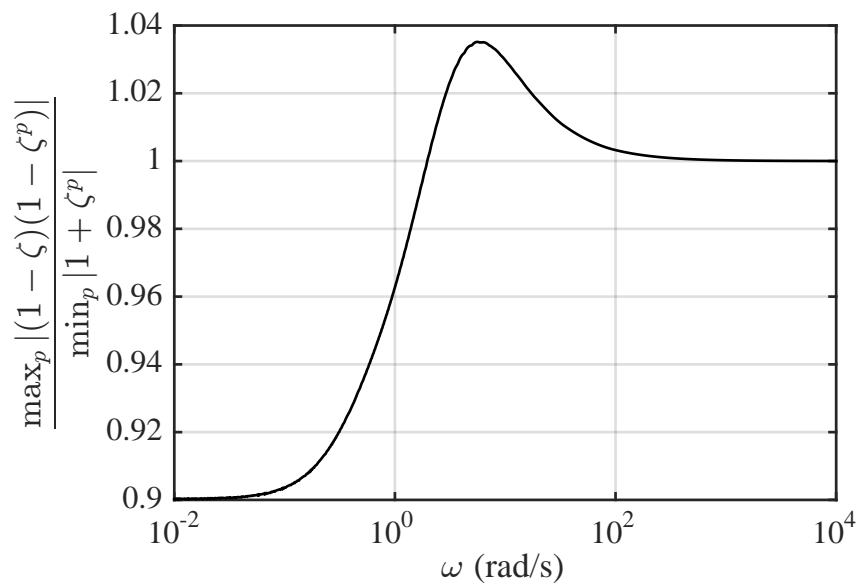


Fig. 6.8 Values of the upper bound (6.4).

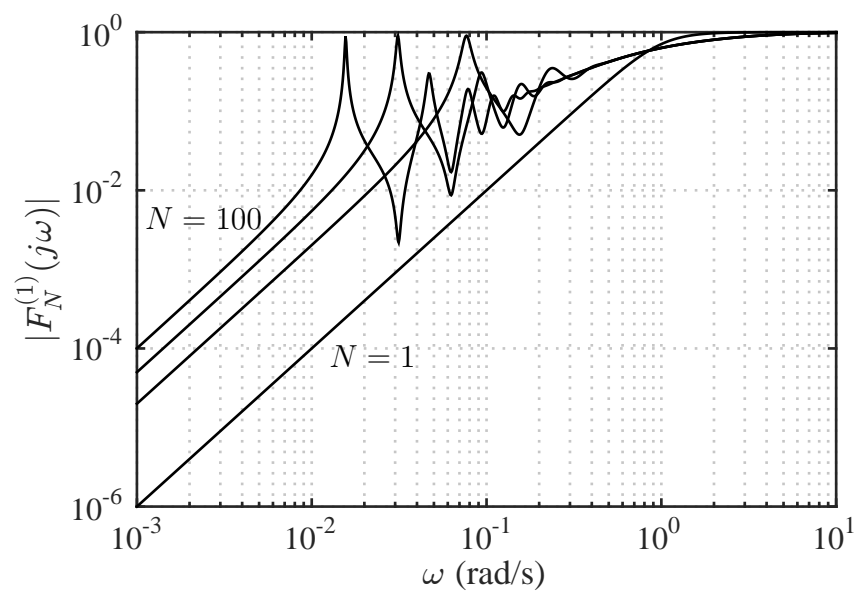


Fig. 6.9 A log-log plot of $|F_N^{(1)}(j\omega)|$ for $N = 1, 20, 50, 100$.

Redheffer's lemma

The following approach based on Redheffer's lemma or Lemma 15 in [Doyle et al., 1989] appears initially promising. Consider the system of Fig. 6.10 in which

$$P = \begin{bmatrix} P_{11} & P_{12} \\ P_{21} & P_{22} \end{bmatrix} \in \mathcal{RH}_\infty,$$

$$Q \in \mathcal{RH}_\infty.$$

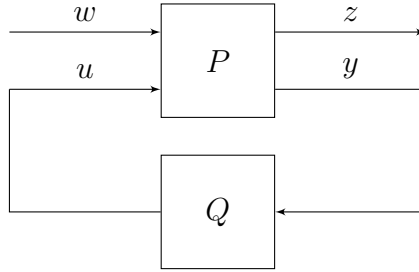


Fig. 6.10 A lower linear fractional transformation in Redheffer's lemma.

Suppose $\|P\| \leq 1$ and P_{21} is invertible. Then $\|Q\| \leq 1$ implies $\|T_{w \rightarrow z}\| \leq 1$ where $\|T_{w \rightarrow z}\|$ denotes the transfer function from w to z . This is shown since $\|P\| \leq 1$ implies $\|z\|^2 + \|y\|^2 \leq \|w\|^2 + \|u\|^2$, and therefore $\|z\|^2 - \|w\|^2 \leq \|u\|^2 - \|y\|^2 = \|Qy\|^2 - \|y\|^2$. $\|Q\| \leq 1$ then implies $\|z\|^2 - \|w\|^2 \leq 0$ and hence $\|T_{w \rightarrow z}\| \leq 1$.

To see how the conjecture can be posed in the setup of Fig. 6.10, let

$$Q = F_{N-1}^{(1)}$$

$$P = \begin{bmatrix} \frac{h}{h+1} & P_{12} \\ P_{21} & \frac{-1}{h+1} \end{bmatrix} \quad (6.5)$$

where $P_{12}P_{21} = 1/(h+1)^2$ and $h = s^2/(\sqrt{2}s+1)$, and note that $T_{w \rightarrow z} = F_N^{(1)}$. This block diagram generates the recursion (6.2). Although it may look promising at first sight, it turns out that a P with $\|P\| \leq 1$ cannot be found. An explanation for this can be seen by noting that the above argument is equally applicable frequency by frequency, whereas the maximum value of $|F_N^{(1)}(j\omega)|$ is not monotonically decreasing with N as can be seen in Fig. 6.9. The frequency plot of the largest singular values of P is shown in Fig. 6.11

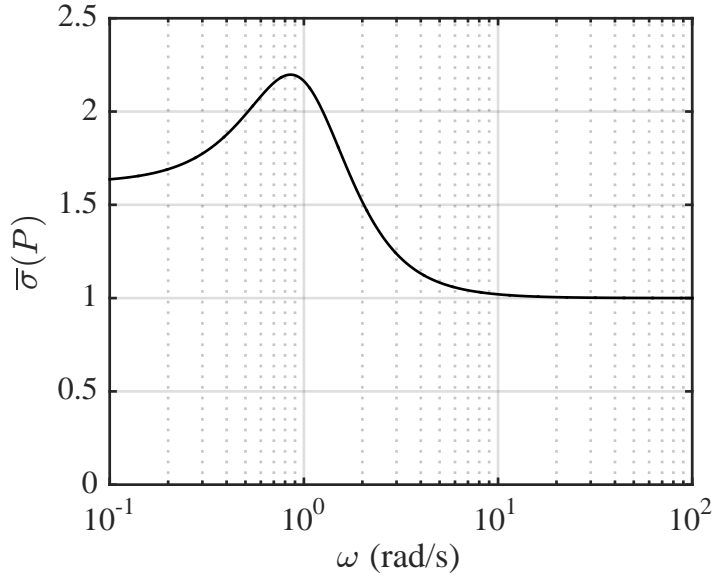


Fig. 6.11 Frequency plot of the largest singular values of P defined in (6.5) with $P_{12} = P_{21} = 1/(h+1)$ where $h = s^2/(\sqrt{2}s+1)$

where $P_{12} = P_{21} = 1/(h+1)$. It may be observed the values are greater than one for any frequency.

6.4 Conjectures on Higher Intermass Displacements

It has been pointed out in Chapter 4 that the set $\{g \in \mathbb{C} : \max_N |F_N^{(1)}(g^{-1})| \leq 1\}$ contains the sets $\{g \in \mathbb{C} : \max_N |F_N^{(i)}(g^{-1})| \leq 1\}$, for $i = 2, \dots, 5$ in Fig. 4.7. This observation leads to the following conjecture:

Conjecture 6.2. For $F_N^{(i)}$ described in (6.1),

$$\sup_{N \in \mathbb{N}} |F_N^{(i)}(h)| \leq \sup_{N \in \mathbb{N}} |F_N^{(1)}(h)|$$

for any $h \in \mathbb{C} \setminus [-4, 0)$. □

Further, another conjecture follows from numerical studies shown in Table 6.1:

Conjecture 6.3. Suppose $h(j\omega)$ does not intersect the interval $[-4, 0)$ for any $\omega \geq 0$. Then for $F_N^{(i)}$ described in (6.1),

$$\|F_N^{(N)}(h(s))\|_{\infty} \leq \|F_N^{(N-1)}(h(s))\|_{\infty} \leq \dots \leq \|F_N^{(1)}(h(s))\|_{\infty}$$

Table 6.1 Values of $\|F_{10}^{(i)}(h(s))\|_\infty$.

i	$h(s) = \frac{s^2}{\sqrt{2}s + 1}$	$h(s) = \frac{s^2}{s^2 + s + 1}$	$h(s) = \frac{s^2}{s + 1}$
1	1.00	0.87	1.27
2	0.88	0.85	1.24
3	0.84	0.80	1.18
4	0.78	0.75	1.10
5	0.70	0.67	0.99
6	0.61	0.58	0.86
7	0.51	0.49	0.71
8	0.39	0.38	0.55
9	0.27	0.25	0.37
10	0.13	0.13	0.19

for a fixed $N \in \mathbb{N}$. □

If Conjecture 6.1 is true and at least one of the Conjectures 6.2 and 6.3 is true, it can be shown that the transfer functions from x_0 to the i th intermass displacement are uniformly bounded by one in N for any i :

Conjecture 6.4. Suppose $h(s)$ has a normalised form $s^2/(\sqrt{2}s + 1)$. Then

$$\left\| F_N^{(i)}(s) \right\|_\infty = 1 \quad \text{for all } i \in \mathbb{N} \text{ and } N \geq i.$$

□

CONCLUSIONS

This thesis has studied the interconnection of a chain of N identical masses in which neighbouring masses are connected by identical two-terminal passive mechanical impedances, and where the first mass is also connected by the same impedance to a movable point. The motivation of the problem is vibration suppression in multi-storey buildings subjected to earthquake disturbances. The problem is similar to that of symmetric bidirectional control of a vehicle string, albeit with a passivity constraint.

7.1 Contributions

The principal contributions of this thesis are summarised below.

Recursive features in mass chains. Formulae for the transfer functions from the movable point displacement to a given intermass displacement have been derived in the form of complex iterative maps as a function of a dimensionless parameter h depending on the impedance and mass. The maps take the form of an iterated Möbius transformation. It is shown that the fixed points of the mappings provide information on the asymptotic behaviour of the disturbance transfer functions. Similar recurrence relations have been found in a heterogeneous mass chain, i.e., a chain of N non-identical masses with non-identical passive interconnections.

Scalability. The scalar transfer functions from the movable point displacement to a given intermass displacement have been employed as a scalability measure. They have been shown to be uniformly bounded with respect to the size of the chain of masses for a suitable choice of the interconnection. The recursive features in these transfer functions have been used for an analytical proof: the use of a conjugacy transformation allows the iterative map to be written in a convenient form to derive formal upper

bounds on the infinity norm of the individual transfer functions from the movable point displacement to a given intermass displacement. In particular they are shown to be uniformly bounded with respect to N for a suitable choice of h . This boundedness result was illustrated graphically. The graph can be used to design a suitable interconnection impedance so that the supremum of the \mathcal{H}_∞ -norm over N is no greater than a pre-specified value.

Passive interconnection design. A systematic approach to design a passive interconnection which achieves good disturbance rejection has been proposed. The method makes use of contour maps of the magnitude of the transfer functions and is applicable to any layouts for the passive interconnection.

Case study. The design methodology for the interconnections developed in this thesis has been demonstrated using a 10-storey homogeneous building model. Numerical evaluations for the disturbance suppression performance under several historical earthquakes have shown the efficacy of the proposed method. The validity of the designed interconnection has also been verified for a 10-storey building model which has a different stiffness distribution but with the same undamped first natural frequency as the homogeneous model.

7.2 Future Research Directions

The following can be thought of as future research directions.

Exact computation of uniform bound. The upper bound given in the thesis for the \mathcal{H}_∞ -norm of the transfer functions may not be a tight bound. However, some observations suggest that the norm be bounded by one for a certain class of interconnection impedances. Several conjectures have been made in Chapter 6 for this problem. The techniques introduced in this chapter also have a possibility to find a rigorous upper bound not only for the specific interconnection impedance discussed in the chapter but also other impedances.

Conjectures on higher intermass displacements. If Conjecture 6.2 based on a graphical observation is true, the supremum value of the magnitude of the transfer function for the first intermass displacement is always greater than that of the higher ones, with respect to the size of the mass chain. This means that the upper bound for the first intermass displacement is only needed to consider for the uniform bound of the disturbance amplification to any given intermass displacement.

Disturbance propagation along the mass chain. Numerical observations suggest that the \mathcal{H}_∞ -norm of the transfer function from the disturbance to a given intermass displacement be monotonically decreasing along a fixed length of the mass chain (Conjecture 6.3).

Scalability in heterogeneous mass chains. The recurrence relations in heterogeneous mass chains has been derived in Appendix 5.B in Chapter 5. They could be used for deriving conditions on the heterogeneous interconnections for achieving the uniform boundedness.

Different topology. The extension of the proposed analysis method to different topologies could be considered. This will enable to investigate many different applications such as power networks and internet congestion problems.

H_2 -norm of the transfer functions. The vibration due to the disturbance at the movable point in the mass chain propagates to the higher masses and comes back down to the lower masses. Therefore, the vibration may continue for a very long time when the mass chain is infinitely long, even though the H_∞ -norm is small. To analyse this effect, the H_2 -norm might be suitable.

REFERENCES

- Alam, A. (2014). *Fuel-efficient heavy-duty vehicle platooning*. PhD thesis, KTH Royal Institute of Technology.
- Anderson, B. D. O. and Vongpanitlerd, S. (2006). *Network Analysis and Synthesis: A Modern Systems Theory Approach (Dover Books on Engineering)*. Dover Publications.
- Arakaki, T., Kuroda, H., Arima, F., Inoue, Y., and Baba, K. (1999a). Development of seismic devices applied to ball screw : Part 1 basic performance test of RD-series (in Japanese). *Journal of architecture and building science*, (8):239–244.
- Arakaki, T., Kuroda, H., Arima, F., Inoue, Y., and Baba, K. (1999b). Development of seismic devices applied to ball screw : Part 2 performance test and evaluation of RD-series (in Japanese). *Journal of architecture and building science*, (9):265–270.
- Bamieh, B., Jovanovic, M., Mitra, P., and Patterson, S. (2012). Coherence in large-scale networks: dimension-dependent limitations of local feedback. *IEEE Transactions on Automatic Control*, 57(9):2235–2249.
- Barooah, P. and Hespanha, J. P. (2005). Error amplification and disturbance propagation in vehicle strings with decentralized linear control. In *Proceedings of the 44th IEEE Conference on Decision and Control*, pages 4964–4969, Seville, Spain.
- Barooah, P., Mehta, P. G., and Hespanha, J. P. (2009). Mistuning-based control design to improve closed-loop stability margin of vehicular platoons. *IEEE Transactions on Automatic Control*, 54(9):2100–2113.
- Beardon, A. F. (2001). Continued fractions, discrete groups and complex dynamics. *Computational Methods and Function Theory*, 1(2):535–594.
- Bott, R. and Duffin, R. J. (1949). Impedance synthesis without use of transformers. *Journal of Applied Physics*, 20(8):816.
- Brune, O. (1931). Synthesis of a finite two-terminal network whose driving-point impedance is a prescribed function of frequency. *Journal of Mathematical Physics*, 10:191–236.
- Chien, C. and Ioannou, P. (1992). Automatic vehicle-following. In *Proceedings of the 1992 American Control Conference*, pages 1748–1752.
- Clough, R. W. and Penzien, J. (1975). *Dynamics of Structures*. McGraw-Hill, Inc.

- Constantinou, M. C., Soong, T. T., and Dargush, G. F. (1998). *Passive Energy Dissipation Systems for Structural Design and Retrofit*. Multidisciplinary Center for Earthquake Engineering Research Buffalo, New York.
- Deodatis, G. (1996). Non-stationary stochastic vector processes: seismic ground motion applications. *Probabilistic Engineering Mechanics*, 11(3):149–167.
- Devaney, R. (1989). *An Introduction To Chaotic Dynamical Systems, Second Edition (Addison-Wesley Studies in Nonlinearity)*. Westview Press.
- Doyle, J., Glover, K., Khargonekar, P., and Francis, B. (1989). State-space solutions to standard H_2 and H_∞ control problems. *IEEE Transactions on Automatic Control*, 34(8):831–847.
- Evangelou, S., Limebeer, D. J. N., Sharp, R. S., and Smith, M. C. (2007). Mechanical steering compensators for high-performance motorcycles. *Journal of Applied Mechanics*, 74(2):332.
- Firestone, F. A. (1933). A new analogy between mechanical and electrical systems. *Journal of Acoustical Society of America*, 4:249–267.
- Furuhashi, T. and Ishimaru, S. (2004). Mode isolation by inertial mass: study on response control by inertial mass No. 1 (in Japanese). *Journal of Structural and Construction Engineering, AIJ*, (576):55–62.
- Furuhashi, T. and Ishimaru, S. (2006). Response control of multi-degree system by inertial mass: study on response control by inertial mass No. 2 (in Japanese). *Journal of Structural and Construction Engineering, AIJ*, (601):83–90.
- Gantmacher, F. R. (2000). *Matrix Theory*, volume 2. American Mathematical Society.
- Giaralis, A. and Taflanidis, A. A. (2015). Reliability-based design of tuned mass-damper-inerter (tmd) equipped multi-storey frame buildings under seismic excitation. In *Proceedings of the 12th International Conference on Applications of Statistics and Probability in Civil Engineering*, Vancouver, Canada.
- Hara, S., Tanaka, H., and Iwasaki, T. (2014). Stability analysis of systems with generalized frequency variables. *IEEE Transactions on Automatic Control*, 59(2):313–326.
- Hartog, J. P. D. (1985). *Mechanical Vibrations*. Dover Publications (Reprint. Republication of the 4th edition (1956), McGraw-Hill).
- Hedrick, J., Tomizuka, M., and Varaiya, P. (1994). Control issues in automated highway systems. *Control Systems, IEEE*, 14(6):21–32.
- Horn, R. A. and Johnson, C. R. (1999). *Matrix Analysis*. Cambridge University Press, New York.
- Horowitz, R. and Varaiya, P. (2000). Control design of an automated highway system. In *Proceedings of the IEEE*, volume 88, pages 913–925.

- Ikago, K., Saito, K., and Inoue, N. (2012a). Seismic control of single-degree-of-freedom structure using tuned viscous mass damper. *Earthquake Engineering & Structural Dynamics*, 41(3):453–474.
- Ikago, K., Sugimura, Y., Saito, K., and Inoue, N. (2012b). Modal response characteristics of a multiple-degree-of-freedom structure incorporated with tuned viscous mass dampers. *Journal of Asian Architecture and Building Engineering*, 11(2):375–382.
- Ioannou, P., Chien, C.-C., et al. (1993). Autonomous intelligent cruise control. *IEEE Transactions on Vehicular Technology*, 42(4):657–672.
- Jiang, J. Z., Matamoros-Sanchez, A. Z., Goodall, R. M., and Smith, M. C. (2012). Passive suspensions incorporating inerters for railway vehicles. *Vehicle System Dynamics*, 50(sup1):263–276.
- Jovanovic, M. and Bamieh, B. (2005). On the ill-posedness of certain vehicular platoon control problems. *IEEE Transactions on Automatic Control*, 50(9):1307–1321.
- Kanai, K. (1957). Semi-empirical formula for the seismic characteristics of the ground. *Bulletin of the Earthquake Research Institute, University of Tokyo*, 35:309–325.
- Knorn, S., Donaire, A., Agüero, J. C., and Middleton, R. H. (2014). Passivity-based control for multi-vehicle systems subject to string constraints. *Automatica*, 50(12):3224 – 3230.
- Lazar, I., Neild, S., and Wagg, D. (2014). Using an inerter-based device for structural vibration suppression. *Earthquake Engineering & Structural Dynamics*, 43:1129–1147.
- Léger, P. and Dussault, S. (1992). Seismic-energy dissipation in MDOF structures. *Journal of Structural Engineering*, 118(5):1251–1269.
- Lestas, I. and Vinnicombe, G. (2007). Scalability in heterogeneous vehicle platoons. In *Proceedings of the 2007 American Control Conference*, pages 4678–4683, New York.
- Levine, W. S. and Athans, M. (1966). On the optimal error regulation of a string of moving vehicles. *IEEE Transactions on Automatic Control*, 11(3):355–361.
- Marian, L. and Giaralis, A. (2014). Optimal design of a novel tuned mass-damper-inerter (TMDI) passive vibration control configuration for stochastically support-excited structural systems. *Probabilistic Engineering Mechanics*, 38:156–164.
- Melzer, S. and Kuo, B. (1971). Optimal regulation of systems described by a countably infinite number of objects. *Automatica*, 7(3):359–366.
- Middleton, R. H. and Braslavsky, J. H. (2010). String instability in classes of linear time invariant formation control with limited communication range. *IEEE Transactions on Automatic Control*, 55(7):1519–1530.
- Needham, T. (1997). *Visual Complex Analysis*. Clarendon Press - Oxford University Press, Oxford.
- Okumura, A. (1997). *Vibration shut-off connection mechanism*. Japan Patent 09-177875, filed December 27, 1995, and issued July 11, 1997.

- Papageorgiou, C., Houghton, N. E., and Smith, M. C. (2009). Experimental testing and analysis of inerter devices. *Journal of dynamic systems, measurement, and control*, 131(1):011001.
- Papageorgiou, C. and Smith, M. C. (2005). Laboratory experimental testing of inerters. In *Proceedings of the 44th IEEE Conference on Decision and Control*, pages 3351–3356, Seville, Spain. IEEE.
- Papageorgiou, C. and Smith, M. C. (2006). Positive real synthesis using matrix inequalities for mechanical networks: Application to vehicle suspension. *IEEE Transactions on Control Systems Technology*, 14(3):423–435.
- Papageorgiou, C. and Smith, M. C. (2007). Experimental testing and modelling of a passive mechanical steering compensator for high-performance motorcycles. In *Proceedings of the European Control Conference 2007*, pages 3592–3599, Kos, Greece.
- Penzien, J. (1960). Elasto-plastic response of idealized multi-story structures subjected to a strong motion earthquake. In *Proceedings of the 2nd World Conference on Earthquake Engineering*, volume 2, pages 739–760, Tokyo and Kyoto, Japan.
- Peppard, L. (1974). String stability of relative-motion PID vehicle control systems. *IEEE Transactions on Automatic Control*, 19(5):579–581.
- Pradono, M. H., Iemura, H., Igarashi, A., and Kalantari, A. (2008). Application of angular-mass dampers to base-isolated benchmark building. *Structural Control and Health Monitoring*, 15(5):737–745.
- Rajamani, R. (2005). *Vehicle Dynamics and Control*. Springer & Mechanical Engineering Series.
- Saito, K., Kurita, S., and Inoue, N. (2007). Optimum response control of 1-DOF system using linear viscous damper with inertial mass and its Kelvin-type modeling (in Japanese). *Journal of Structural Engineering*, 53:53–66.
- Saito, K., Sugimura, Y., Nakaminami, S., Kida, H., and Inoue, N. (2008). Vibration tests of 1-story response control system using inertial mass and optimized soft spring and viscous element (in Japanese). *Journal of Structural Engineering*, 54:623–634.
- Schultz, A. E. (1992). Approximating lateral stiffness of stories in elastic frames. *Journal of Structural Engineering*, 118(1):243–263.
- Seiler, P., Pant, A., and Hedrick, J. K. (2004). Disturbance propagation in vehicle strings. *IEEE Transactions on Automatic Control*, 49(10):1835–1841.
- Shearer, J. L., Richardson, H. H., and Murphy, A. T. (1971). *Introduction to System Dynamics*. Addison Wesley.
- Shibata, A. (2003). *Dynamic Analysis of Earthquake Resistant Structures (in Japanese)*. Morikita Publishing Co., Ltd., 2nd edition.
- Smith, M. C. (2002). Synthesis of mechanical networks: the inerter. *IEEE Transactions on Automatic Control*, 47(10):1648–1662.

- Smith, M. C. (2005). *Force-controlling mechanical device*. U.S. Patent 20050034943 A1, filed July 3, 2002, and issued February 17, 2005.
- Smith, M. C. and Walker, G. W. (2000). Performance limitations and constraints for active and passive suspensions: a mechanical multi-port approach. *Vehicle System Dynamics*, 33(3):137–168.
- Smith, M. C. and Wang, F. C. (2004). Performance benefits in passive vehicle suspensions employing inerters. *Vehicle System Dynamics*, 42(4):235–257.
- Soong, T. T. and Dargush, G. F. (1997). *Passive Energy Dissipation Systems in Structural Engineering*. Wiley New York.
- Swaroop, D. and Hedrick, J. (1996). String stability of interconnected systems. *IEEE Transactions on Automatic Control*, 41(3):349–357.
- Swaroop, D. and Rajagopal, K. (2001). A review of constant time headway policy for automatic vehicle following. In *2001 IEEE Intelligent Transportation Systems Proceedings*, pages 65–69. IEEE.
- Symans, M., Charney, F., Whittaker, A., Constantinou, M., Kircher, C., Johnson, M., and McNamara, R. (2008). Energy dissipation systems for seismic applications: current practice and recent developments. *Journal of Structural Engineering*, 134(1):3–21.
- Tajimi, H. (1960). Statistical method of determining the maximum response of building structure during an earthquake. In *Proceedings of the 2nd World Conference on Earthquake Engineering*, volume 2, pages 781–798, Tokyo and Kyoto, Japan.
- Takewaki, I. (2009). *Building Control with Passive Dampers: Optimal Performance-based Design for Earthquakes*. Wiley.
- Takewaki, I., Murakami, S., Yoshitomi, S., and Tsuji, M. (2012). Fundamental mechanism of earthquake response reduction in building structures with inertial dampers. *Structural Control and Health Monitoring*, 19(6):590–608.
- Varaiya, P. (1993). Smart cars on smart roads: problems of control. *IEEE Transactions on Automatic Control*, 38(2):195–207.
- Wang, F. C., Chen, C. W., Liao, M. K., and Hong, M. F. (2007). Performance analyses of building suspension control with inerters. In *Proceedings of the 46th IEEE Conference on Decision and Control*, pages 3786–3791. IEEE.
- Wang, F. C., Hong, M. F., and Chen, C. W. (2010). Building suspensions with inerters. *Proceedings of Institution of Mechanical Engineers, Part C: Journal of Mechanical Engineering Science*, 224(8):1605–1616.
- Wang, F. C., Hong, M. F., and Lin, T. C. (2011). Designing and testing a hydraulic inerter. *Proceedings of the Institution of Mechanical Engineers, Part C: Journal of Mechanical Engineering Science*, 225(1):66–72.
- Wang, F. C., Liao, M. K., Liao, B. H., Su, W. J., and Chan, H. A. (2009). The performance improvements of train suspension systems with mechanical networks employing inerters. *Vehicle System Dynamics*, 47(7):805–830.

